International Scientific-Theoretical and Production Journal

ADVANCES IN ELECTROMETALLURGY

4, 2004

Quarterly

English translation of the quarterly «Sovremennaya Elektrometallurgiya» journal published in Russian since January 1985

Founders: *E.O. Paton Electric Welding Institute of the NAS of Ukraine*
International Association «Welding»

Publisher: *International Association «Welding»*

Editorial and advertising offices are located at PWI:
International Association «Welding»,
E.O. Paton Electric
Welding Institute
of the NAS of Ukraine,
11, Bozhenko str., 03680,
Kyiv, Ukraine
Tel.: (38044) 287 67 57,
529 26 23,
Fax: (38044) 528 04 86
E-mail: journal@paton.kiev.ua
http://www.nas.gov.ua/pwj

Subscriptions:
$184, 4 issue per year,
postage and packaging included.
Back issue available

CONTENTS

ABOUT PROSPECTS OF BIMETAL PRODUCTION USING ELECTROSLAG PROCESS

B.E. PATON, L.B. MEDOVAR and **V.Ya. SAENKO**
E.O. Paton Electric Welding Institute, NASU, Kiev, Ukraine

The role of electroslag welding process in producing bimetal ingots for manufacturing sheets and rolled sections is shown. Specifics of manufacture of bimetal section semi-products by rolling in section mills of square two-layer ingots, produced by the method of cladding using mandrels of different shapes, and also by rolling and hot pressing of composite round two-layer billets, is considered. The feasibility of use of the electroslag process with a liquid metal in the production of bimetal ingots in ESR furnaces, including also the method of a continuous electroslag casting, is evaluated.

Keywords: *bimetal ingots, bimetal sheets, bimetal rolled sections, electroslag welding process, electroslag remelting, electroslag cladding, electroslag cladding with liquid metal*

It should be recognized that, in spite of more than century history of the industrial production and application of different types of bimetals, and also the variety of known methods of their producing, they have not yet occupied the worthy place among the most important structural materials. The share of bimetals, in particular rolled sections, in the total production of structural materials remains still negligible, though in some cases they have no almost alternative owing to their unique service properties. It is noted in work [1] that one of the main reasons of this situation is their high cost which is stipulated by specific features of those technological processes which are used for their manufacture. From our side, we would like also to note that one more limiting factor of a wide application of bimetals in industry is not always high and stable quality guaranteeing the absence of laminations in the process of manufacture of bimetal products and their service.

In manufacturing bimetal semi-products (sheets, rolled sections, pipes, different types of rolled shaped sections, etc.) the most different technological processes were tested, almost all the methods of pressure shaping, casting technologies, electric arc and electroslag cladding, explosion welding, electron beam technology, electrochemical methods, plasma and other methods of spraying were applied.

A special place among numerous technologies of producing different types of bimetals and bimetal products is occupied by the methods, based on electroslag welding process, whose application guarantees a reliable bonding of cladding and base layers before the rolling of a bimetal billet. For the first time in the world practice the idea of use of electroslag welding process in producing large bimetal billets with a corrosion-resistant cladding layer, designed for rolling into sheets, was suggested at the E.O. Paton Electric Welding Institute as far back as the end of the 1950s [2, 3]. On the basis of bimetal, produced by this method, the industrial production of thick-walled (36–170 mm) stamped-welded bimetal high-pressure vessels for different branches of the national economy was organized for the first time in our county at Mariupol Plant of Heavy Machine-Building in the 1960s [4–6]. In the former USSR one of main consumers of thick-sheet bimetal was petrochemical and nuclear power machine-building, and also shipbuilding [7, 8].

At the end of the 1980s ---- in the middle of the 1990s the works on industrial implementation of production of bimetal sheets using methods based on application of the electroslag process (electroslag cladding ---- ESC ---- in an inclined position [9], electroslag cladding using ESR furnaces [10] and other technologies) found the further development owing to the new problems appeared in shipbuilding. Bimetal sheets, combining the high strength of a hull steel with the high corrosion-erosion resistance and reliability of coating, were demanded for lining the nuclear ice breakers being under construction. As a result of works carried out on the basis of ESC method in an inclined position, the industrial bimetal sheets with a base layer from steel 12KhN2MD and a cladding layer from corrosion-resistant steel were produced, which passed the full-scale trials in the composition of lining of nuclear ice breaker hulls. Results of these tests served as a basis for the construction of the entire ice girth, made from a double-layer steel, for the nuclear ice breaker «Ural» [11]. The application of high-strength two- and three-layer sheet steel of AB2P and AB2T grades of 20–60 mm thickness with a base layer of 09KhN3MD steel and a cladding layer of steel 08Kh18N10B occurred to be also effective for the construction of off-shore structures, in particular ice-resistant platforms. In this case the shear resistance of a cladding layer of bimetal produced by using ESC was > 300 N/m^2 in the entire area of manufactured bimetal sheets [12].

Round bimetal section billets are used for a long time in shipbuilding [7], in particular, for manufacture of propeller shaft of high-speed ships, which are difficult to protect from corrosion using the conventional methods (for example, rubberizing). The bi-

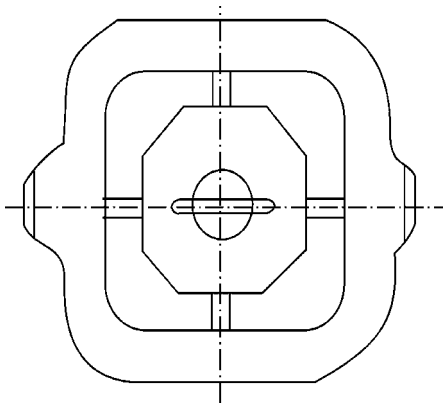

Figure 1. Scheme of octahedral bar mounting in the mould before metal pouring

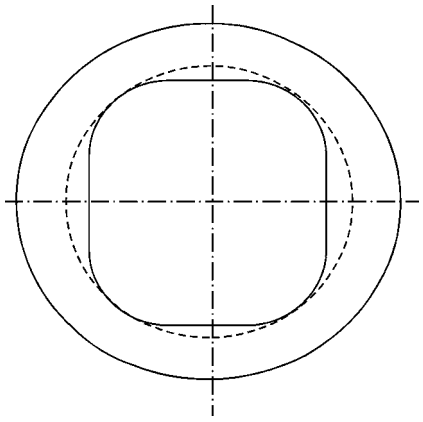

Figure 2. Shape of core in a rolled bimetal billet of 90 mm diameter in use of octahedral bar in two-layer ingot

metal rolled sections of 90, 130 and 140 mm diameter with a core from high-strength structural steel with a cladding layer from stainless steel 1Kh18N9T for the propeller shafts were produced for the first time in the former USSR in 1955 at Kuznetsk Metallurgical Works (KMW) using technology, developed in collaboration with the Research Institute of Structural Materials «Prometej» [13]. The technological process was based on the method of cladding by casting which was used at KMW for industrial production of sheet rolled bimetal.

The main task in the development and mastering of technology of production of bimetal rolled sections was to search for optimum sizes and shape of a core in a two-layer ingot, and also the conditions of deformation of the two-layer ingot in blooming mill and two-layer billet in section mill to produce a core in a ready bimetal rolled section approaching the shape of a disc of the preset diameter.

Two-layer ingots were subjected to bottom casting into square 6-ton cast iron moulds and transferred, after stripping, by a hot charge into soaking pits of the blooming mill. Ingots, heated to 1270–1280 °C, were rolled in duo-reversing mill 1100 for 310×320 mm section, and then in duo-reversing mill 900 for 180×180 and 210×210 mm section and, finally, in medium-section mill for discs of 90 and 130–140 mm diameter, respectively. To produce a round core, two types of bars were tested: of a round section and octahedral (square) section with cut edges (Figure 1).

It was established as a result of experimental works that the percent ratio of area of core section to total section area in ingot, billet and final shaped section is approximately equal. However, the core in its shape can differ greatly from the disc of a preset diameter due to the fact that the deformation in rolling is occurred only in two mutually normal directions. Even at a properly selected core in ingot the change in its shape may not correspond to the change in ingot shape due to a different degree of deformation in sides of the rolled metal being deformed. The most acceptable shape of the core is attained at maximum possible and uniform deformation in ingot sides. Therefore, the schemes recommendable for rolling of bimetal ingots envisage the maximum single and similar total reduction from one manipulation to another.

The optimum shape of a core in a round bimetal billet was produced in use of the octahedral bar. As is shown in Figure 2, the core in a round section rolled metal is arranged concentrically to the external surface and has almost right shape of octahedral with rounded corners. In case of use of round bars after rolling in reduction mills 1100 and 900 the square billet of 180×180 mm section with an oval core was produced using the conditions developed earlier, and after the rolling for a ready section (disc of 90 mm diameter) the core in the form of a square-rhomb (Figure 3) was produced, i.e. the produced bimetal section billet did not meet the preset requirements as to the core geometry.

Taking into account the difficulties in production of bimetal rolled sections, the authors of invention [14] offer to realize firstly a hot rolling in section-rolling mills of round bimetal billets by the oval–square scheme in vertical stands, and the final forming ---- by rolling using disc–disc scheme in multi-roll passes. Figure 4 shows the offered scheme of rolling of bimetal round rods using three-roll passes.

Using this technology, the double-layer cylindrical billet, consisting of a core and sheath, is used for rolling. Edges of as-assembled billet are welded around the contour. Billet, heated to the temperature

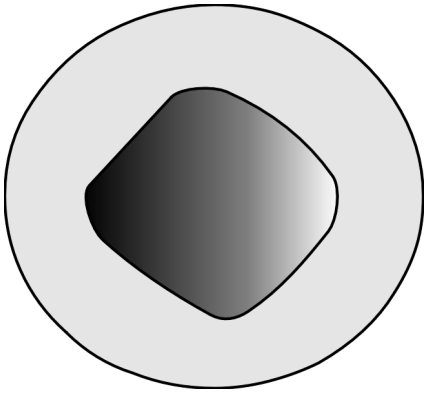

Figure 3. Shape of core in rolled bimetal billet of 90 mm diameter in use of round bar in two-layer ingot

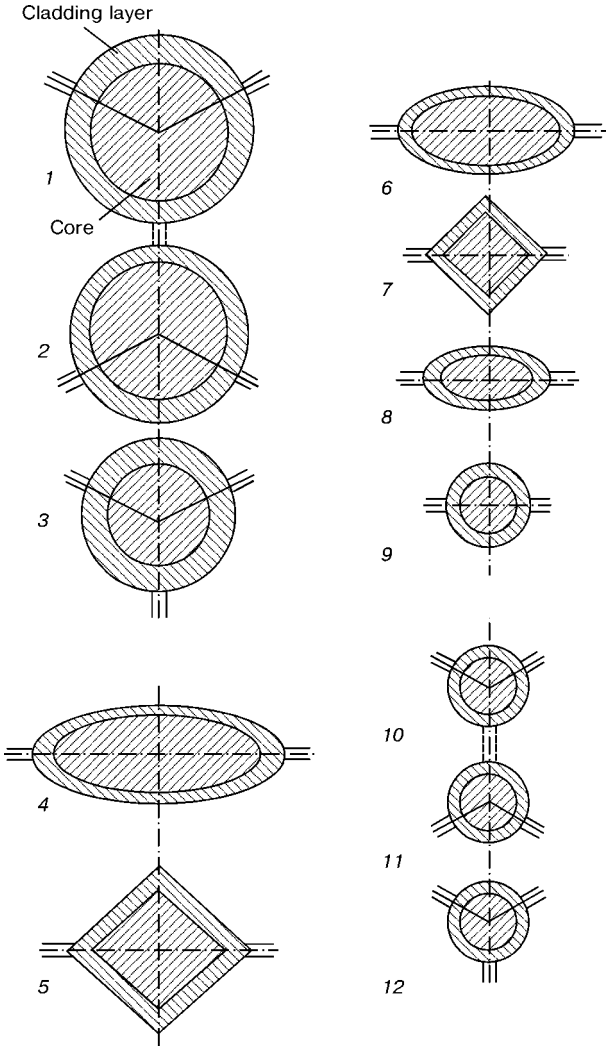

Figure 4. Rolling of bimetal round rods using three-high passes by disc–disc (*1–3*), oval–square (*4–9*), disc–disc (*10–12*) scheme

of rolling, is subjected to rolling firstly in several roughing stands with three-roll passes (positions *1–3*) using disc–disc system. When rolling in three-roll passes, closed almost around the contour, the all-sided uniform reduction of a two-layer billet is occurred without metal expansion, thus providing a reliable adhesion of metals of core and sheath over the contact surface and uniform thickness of a cladding layer in a bimetal rolled section. The number of roughing operations in three-roll passes is defined by the total value of critical reduction necessary to provide a reliable adhesion of layers in a bimetal rod and, in its turn, dependent on physical-chemical characteristics of metal of base and cladding layers. Due to a low drawing capacity of the disc–disc system of passes, the rolling in multi-roll passes for producing ready products becomes not efficient. Therefore, the further metal deforming is performed in two-roll passes (positions *4–9*) using one of known schemes, for example, applying the oval–square system of passes. To obtain the precise geometric sizes, the final formation of a ready bimetal rod after necessary drawing is made again in three-roll passes (positions *10–12*) using disc–disc system. The application of three-high rolling stands for hot grooving of a round bimetal rod makes it possible, in the opinion of authors [14], to guarantee the precision of sizes of the ready rolled metal, which is in conformity to the precision of cold-drawn shaped sections.

However, as follows from the recent work [15], the problem of producing bimetal rods with a preset uniform thickness of the cladding layer using rolling in passes remains actual. To solve it, the authors of the above-mentioned work apply the computer 3D simulation, which is supported by the results of experimental investigation of peculiarities of rolling the model bimetal specimens (steel 55 + copper M1-E) with different initial thickness of the cladding layer. Bimetal cylindrical billets of 21.7 mm diameter were subjected to rolling, whose layers were welded by the explosion method before rolling. Thickness of a cladding layer (copper) was 0.85, 1.80 and 2.85 mm in initial specimens which were subjected to hot rolling for 14 mm diameter rods.

It is known that the hot pressing, as compared with rolling, provides the more beneficial scheme of the stressed state. When pressing the round sections the deformation is axisymmetrical, thus preventing the distortion of a round core shape. In the process of hot pressing of cylindrical composite two-layer billets, the same as in rolling of two-layer packs, the adhesion of layers occurs under the action of a combined plastic deformation, and moreover, around the contour at a uniform distribution of radial compressive stresses in the deformation source, unlike the rolling. This contributes to the prevention of the core shape distortion in pressing. At the same time, at hot pressing of solid profiles of a round and shaped section the process of a plastic yielding is accompanied by a non-uniform metal deformation in section of a matrix cell, thus resulting in the more rapid yielding of the internal layers of billet metal as compared with external layers. It was established [16] that the non-uniform deformation in profile section and mode of cladding layer spreading in length in pressing of bimetal sections depend, first of all, on different strength of metals of the core and cladding layer. This effect, as compared with pressing of solid sections, becomes greater with larger scattering of values of strength properties of metals of the core and cladding layer, and in particular it is greater in case, if the there are no strong adhesion at the initial period, thus violating abruptly the initial ratio of areas of the core and cladding layer.

Thus, when producing bimetal section semi-products both by deforming the round bimetal billets in section rolling mills and also by hot pressing, the presence (or absence) of initial guaranteed adhesion between dissimilar layers of the initial two-layer billet is one of the key problems. If the permanent joining of layers over the entire contact surface is guaranteed between the core and sheath of two-layer billet before the hot deformation, the scheme of rolling of this billet can be significantly simplified. It is important

to take this into account in manufacture of shaped rolled metal.

Owing to the development of the electroslag process using liquid metal (ESR LM) at the E.O. Paton Electric Welding Institute, the new opportunities are open up for improving the technology of producing bimetal billets [17, 18], moreover, not only for the production of sheet bimetal, where the efficiency of ESR LM is out of any doubts, but also a section bimetal of a reinforcing profile. As was noted in [19], the ESR LM allows realization of a continuous electroslag process with liquid metal. The investigations [20, 21] showed that application of ESR LM provides cladding of a layer with a minimum depth of penetration of the base metal of the billet both in section and also in height. When necessary, the cladding by this method can be performed also by the scheme of braze welding, i.e. almost without guaranteed penetration of the base metal. In this case, as a result of treatment of the main billet contact surface, its purification from oxides and other contaminations is occurred, while at reaching of a definite temperature it is wetted with a metal melt, filling a mould gap, thus forming a cladding layer. This, as is known, is the obligatory condition for proceeding the process of brazing-cladding.

The important advantage of ESR LM in the production of bimetal billets for sheet and section rolled metal is the feasibility of use of operating ESR furnaces for its realization after an appropriate their modification. For this purpose, the furnaces are equipped additionally with current-carrying short moulds for electroslag cladding and units and devices for accumulation of molten metal and its dosed feeding into the zone of the cladding layer formation.

Figure 5 presents a general view of the bimetal billet of 350 mm diameter after the electroslag cladding, using ESR LM, of a corrosion-resistant austenitic layer of 35 mm thickness in ESR furnace. The investigations of metal of bimetal billet cladding layer showed that the distribution of main chemical elements in section and length of the billet is almost uniform and meets the technical requirements.

It should be noted that as far back as in the middle of the 1960s of the last century a method and design of the mould for producing bimetal billets was suggested at the E.O. Paton Electric Welding Institute. However, these suggestions did not find industrial application at that time, because it was not possible to overcome the main difficulty, such as high and non-uniform penetration of the base metal in the process of manufacture of ESR bimetal billets, that led inevitably to the undesirable dilution of the cladding layer metal with carbon steel and to inadmissible variation in its chemical composition even in the limits of one sheet. If to judge from the publications, this problem remains still actual until now in application of the canonical ESR.

We suppose that the experience in producing bimetals by ESR LM is a step to the realization of

Figure 5. Bimetal ingot of 350 mm diameter after electroslag cladding of corrosion-resistant austenitic layer of 35 mm thickness using method of ESR LM

semi-continuous and in future, probably, also continuous casting. Standard rolling mills will be still used for rolling the wide bimetal sheets and it would be necessary to roll a bimetal strip, in particular rolled sections, in planetary mills, thus combining the rolling and pressing.

As a whole, a number of problems, related to manufacturing and application of bimetals, is much wider than the problems of producing a reliable joint of dissimilar metals and reduction in cost of products by saving the expensive alloying metals. In our opinion, the existing bimetals are the prototype of structural steels and alloys of mass production in future, with a preset anisotropy of structure and properties, called by us earlier as PAS-materials of the new class [22, 23]. Here, the authors cannot but give themselves a pleasure (in hope to share it with readers) to show the known sketch from book of G.I. Pogodin-Alekseev* (Figure 6) to illustrate special properties of bimetals, PAS-steels.

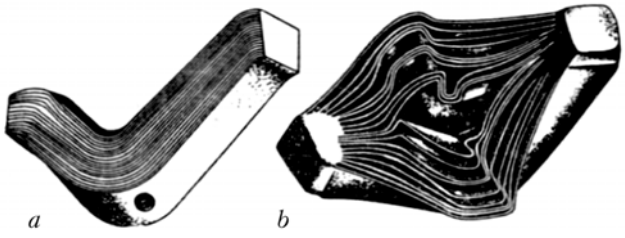

Figure 6. Behavior of multilayer specimen after impact bend test at arrangement of a plane of layers normal (*a*) and parallel (*b*) to the impact direction

*Pogodin-Alekseev, G.I. (1965) Dynamic strength and brittleness of metals. Moscow: Mashinostroenie.

It should be note in conclusion that in the ocean of steel, threatening to contain more than one billion of tons in 2004, the share of alloying steels is only 7–8 %, and the share of high-alloy steels is hardly 1 %. To provide a worthy place for the industrial production of bimetals it is necessary to develop and apply the newest technologies for producing bimetal materials using ESR, thus meeting the requirements of the century.

1. Kuznetsov, E.V. (2000) Main tendencies in development of processes of manufacturing of lamellar metallic compositions. In: *Proc. of 3rd Congress of Millmans*, Lipetsk, Oct. 19–20, 1999.
2. Paton, B.E., Medovar, B.I., Lutsyuk-Khudin, V.A. et al. *Method of manufacturing of bimetallic sheet on the base of electroslag welding*. USSR author's cert. 129473. Publ. 1980.
3. Paton, B.E., Medovar, B.I., Lutsyuk-Khudin, V.A. (1962) Manufacturing of two-layer sheets using electroslag welding. *Bull. TsNIIChM*, **6**, 15–21.
4. Medovar, B.I., Lutsyuk-Khudin, V.A., Saenko, V.Ya. et al. (1963) Manufacturing of thin-walled welded vessels of two-layer steel with corrosion-resistant austenite cladding. In: *Manufacturing, welding and application of two-layer steel.* Moscow: GOSINTI.
5. Medovar, B.I., Saenko, V.Ya., Nagaevsky, I.D. et al. (1984) *Electroslag technology in machine-building*. Ed. by B.E. Paton. Kiev: Tekhnika.
6. Paton, B.E., Chepurnoj, A.D., Saenko, V.Ya. et al. (2004) Prospects in production of welded thick-walled bimetal bodies of high-pressure vessels. *The Paton Welding J.*, **1**, 28–36.
7. Vejngarten, À. Ì ., Delle, V.A., Noskin, A.V. et al. (1962) *Shipbuilding steel.* Leningrad: Sudpromgiz.
8. (1984) *Multilayer steel in welded structures*. Ed. by B.E. Paton and B.I. Medovar. Kiev: Naukova Dumka.
9. Popov, A.V., Shejko, V.I., Kudinov, E.D. et al. (1994) Development of technology of electroslag cladding of bimetallic sheets. *Tyazh. Mashinostroenie*, **1**, 29–30.
10. Sharapov, A.A., Rodionova, I.G., Puzachev, V.I. et al. (1996) Experience of development of manufacturing technology of corrosion-resistant bimetallic billets using electroslag remelting. *Stal*, **12**, 27–29.
11. Sokolov, O.G., Malyshevsky, V.A., Legostaev, Yu.L. (1995) Current weldable shipbuilding steels in Russia and abroad. *Svarochn. Proizvodstvo*, **5**, 19–21.
12. Legostaev, Yu.L., Motovilina, G.D., Semicheva, T.G. (1998) Peculiarities of structure of heat-resistant clad steel. *Voprosy Materialovedeniya*, 15(**2**), 5.
13. Kobyzev, V.K. (1963) Manufacturing of round billet clad by stainless steel 1Kh18N10T. In: *Manufacturing, welding and application of two-layer steel*. Moscow: GOSINTI.
14. Dolzhenkov, F.E., Pisarenko, F.A., Shevchenko, Yu.T. et al. *Method of producing of multilayer rods*. USSR author's cert. 709308. Publ. 1980.
15. Dyja, H., Mroz, S., Milenin, A. et al. (2002) Experimental investigation and 3D FEM-simulation of the process of rolling of bimetallic rods. In: *Proc. of 44th Mechanical Working and Steel Processing, 8th Int. Rolling Conf. and Int. Symp. on Zinc-Coated Steels*, Orlando, Florida, Sept. 8–11, 2002.
16. Chernov, A.N., Golovanenko, S.A., Gulyaev, V.V. (1965) Special features of manufacturing of bimetallic profiles by hot pressing method. In: *Transact. of TsNIIChM on Manufacturing of Bimetals*. Moscow: Metallurgiya.
17. Medovar, B.I., Saenko, V.Ja., Medovar, L.B. (1999) Electroslag processes used in production of clad steel. *The Paton Welding J.*, Pilot Issue, July, 71–74.
18. Medovar, B.I., Saenko, V.Ya., Medovar, L.B. (2000) Producing of bimetal billets of corrosion-resistant bimetal by electroslag cladding. *Problemy Spets. Elektrometallurgii*, **2**, 3–11.
19. Paton, B.E., Medovar, L.B., Saenko, V.Ya. (2002) Improvement of efficiency in ESR metal production. *Advances in Electrometallurgy*, **3**, 2–7.
20. Paton, B.E., Medovar, L.B., Saenko, V.Ya. (2003) New possibilities of electroslag technologies in machine-building. *Metallurgiya Mashinostroeniya*, **1**, 2–5.
21. Paton, B.E., Medovar, L.B., Shevchenko, V.E. et al. (2004) Electroslag technologies in production of bimetal billets. *Advances in Electrometallurgy*, **4**, 7–10.
22. Paton, B.E., Medovar, B.I. (1980) About new class of metallic materials. *Doklady AN Ukr. SSR*, **9**, 100–102.
23. Saenko, V.Ya., Medovar, L.B., Us, V.I. et al. (1990) Steel with a preset anisotropy of structure — PAS. In: P*roblems of welding and special electrometallurgy*. Kiev: Naukova Dumka.

APPLICATION OF HARMONIC ANALYSIS OF ELECTRIC PARAMETERS FOR MONITORING AND CONTROL OF ESR PROCESS

A.A. TROYANSKY, A.D. RYABTSEV, V.Yu. MASTEPAN and **M.V. SAMBORSKY**
Donetsk National Technical University, Donetsk, Ukraine

The feasibility of application of harmonic analysis for monitoring of the process of a chamber-type ESR is shown. Values of coefficients of harmonics are given for remelting using fluxes ANF-6, ANF-1P, pure CaF_2 and CaF_2–Ca system. It was suggested to use the information, obtained by this method, in automated systems of the ESR technological process control.

Keywords: *electroslag remelting, chamber-type electroslag remelting, harmonic analysis, coefficients of harmonics, indirect methods of control*

At the present time the progress in aircraft construction, power engineering and other branches is impossible without application of structural materials possessing special properties. These materials include, first of all, highly-reactive (titanium, chromium), rare-earth metals (REM), their alloys and intermetallics. The service properties of products are defined directly by the purity level of metals and alloys used for their manufacture. To produce the initial structural billet in the form of ingots, these metals are subjected to remelting most often using vacuum-arc, electron beam or electroslag methods, which do not guarantee often the required quality of the material. Therefore, the advanced investigations are directed to searching for technological variants combining several metallurgical processes [1].

One of such promising processes is the electroslag remelting of metals and alloys under active slag systems in the chamber-type furnaces at a controllable atmosphere. This technology possesses advantages of both electroslag and also vacuum-arc remelting, and the ESR in such a variant makes it possible to solve successfully the difficult and even impossible problems for traditional methods of special electrometallurgy. They concern, first of all, the producing of high-quality ingots from highly-reactive metals (chromium, titanium), REM and their alloys [2]. The presence of the chamber and controllable atmosphere, and also the use of active components (calcium, rare-earth and other metals) in slag during remelting creates favorable conditions for effective refining, modifying and alloying of metals and alloys [3]. All this, undoubtedly, influences also all the complex of physical-chemical and electric processes of remelting. Thus, the fillers of a metallic component, in particular calcium in ESR slags, lead to significant changes in electric conditions of remelting [4], and at content of metal calcium in slag of more than 15 wt.% the electroslag process is transferred completely to arc process [5]. Therefore, when realizing the major aim of the process, i.e. the producing of quality ingots from highly-reactive metals, it is necessary to maintain the optimum concentrations of calcium in slags, close to limiting. The question arises: how to realize this using the chamber ESR process.

Sampling of slag during the melting process is connected with certain technological difficulties, and the indirect determination of calcium concentration in slag by its content in the furnace atmosphere will not give the high precision, because the calcium content in furnace atmosphere at different horizons depends on such parameters as temperature and convective gas flows, which are controlled in a complicated manner.

At the same time the electric current and voltage, which can give the precise information about a number of physical parameters of the electric circuit, are easily controllable parameters in ESR. Real electric circuits have, as a rule, non-linear elements in their composition. Thus, in ESR installation the non-linearity is typical of the slag pool resistance which depends on chemical and aggregate state, and the presence of metal calcium in slag leads to an abrupt change of its physical properties, namely electric conductivity and temperature of melting. This influences the electric characteristics of the process and can lead to exciting of arc discharges at the electrode–slag interface.

Harmonic analysis is one of the methods of obtaining information from a periodic signal. Signal harmonics occur due to separation of basic (intelligence) signal under the action of external factors. By analyzing and comparing the processes, proceeding in the technological cycle, it is possible to derive several relationships with change in a harmonic composition of signal. One of them is the content of metal calcium in a slag melt. It is possible to calculate the signal spectrum using the Fourier transformation.

It is known from the theory of electric circuits and signals [6–8] that signal at the output of a non-linear

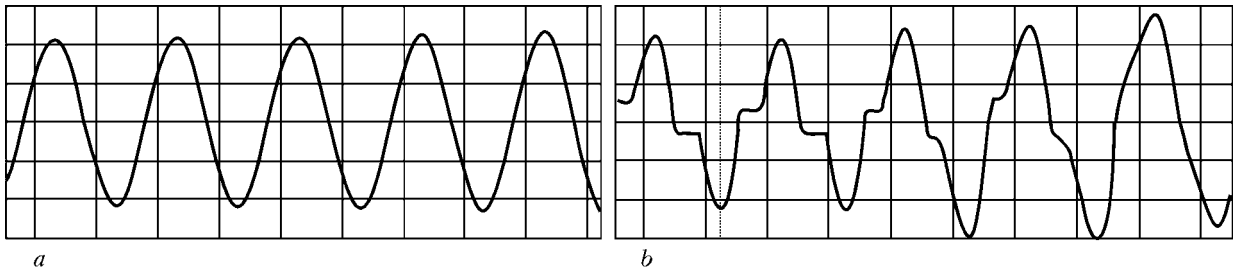

Figure 1. Curve of current in chamber ESR of steel using flux ANF-6 (*a*) and CaF_2–Ca (*b*)

element, to the input of which a periodic oscillation is supplied, contains components with frequencies, multiple of frequency of input signal. In this case, by analyzing these components it is possible to judge about the nature of non-linearity and processes proceeding in the pool.

If $x(t)$ is the periodic function from t with a period τ, then it can be presented in the form [6, 9–12]

$$x(t) = \frac{a_0}{2} + \sum_{n=1}^{\infty} \left(a_n \cos \frac{2\pi}{T} nt + b_n \sin \frac{2\pi}{\tau} nt \right)$$

or

$$x(t) = \frac{a_0}{2} + \sum_{n=1}^{\infty} (a_n \cos 2\pi\nu_0 nt + b_n \sin 2\pi\nu_0 nt),$$

where frequency $\nu_0 = 1 / \tau$.

Coefficients a_0, a_n and b_n are calculated by formulae

$$a_0 = \frac{2}{\tau} \int_{-\tau/2}^{\tau/2} x(t)dt,$$

$$a_n = \frac{2}{\tau} \int_{-\tau/2}^{\tau/2} x(t) \cos 2\pi\nu_0 nt\, dt,$$

$$b_n = \frac{2}{\tau} \int_{-\tau/2}^{\tau/2} x(t) \sin 2\pi\nu_0 nt\, dt.$$

In a general case the periodic signal contains component, not dependent on time and a finite set of harmonic oscillations, harmonics with frequencies $\nu_n = n\nu_0$ (n = 1, 2, 3, ...).

To make the quantitative evaluation of degree of a non-linearity of the signal the value of a coefficient of non-linear distortions, equal to ratio of root-mean-square level of all higher harmonics of current to amplitude of current of a useful signal, is calculated [6, 8]:

$$k_h = \frac{\sqrt{I_2^2 + I_3^2 + I_4^2 + \ldots}}{I_1}.$$

To check the assumption data a series of experiments on remelting of electrodes of steel 50 in a chamber-type ESR furnace using different fluxes was carried out. Electrodes of 50 mm diameter and 700 mm length were remelted into a copper water-cooled mould of 110 mm diameter in argon and in air. Voltage and current of remelting were kept constant (40 V and 2 kA) at 1400 g slag mass. Flux of system CaF_2–Ca was produced by mixing the calcium fluoride and metal calcium. To make the comparative melts, the chemically-pure calcium fluoride CaF_2 and mostly widely spread industrial fluxes ANF-6 and ANF-1P were used. Slag pool was set using a «solid start».

In the process of remelting the instantaneous values of current and voltage were recorded using the developed information-monitoring system [4]. A low-frequency filter of 2500 Hz suppression frequency was used in it. Frequency of discreteness was 8000 Hz, the digit capacity of quantification was 16 bits. Computer was used to record the signals, and a program

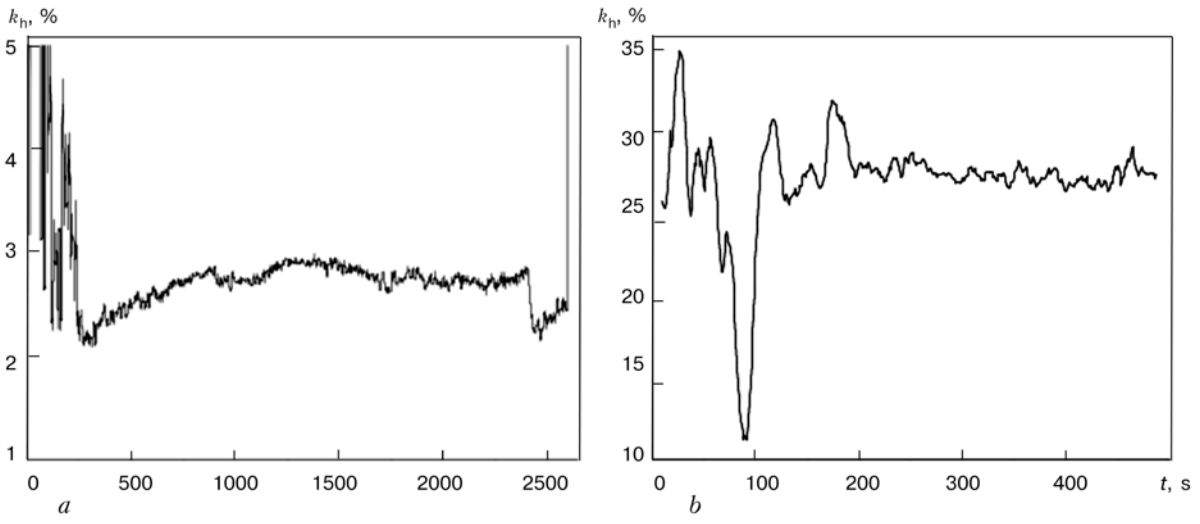

Figure 2. Coefficient of harmonics of current in chamber ESR of steel using flux ANF-6 (*a*) and CaF_2–Ca (*b*)

was developed for calculation of effective values of current and voltage, coefficient of their shape and harmonic composition to analyze and to process the information obtained.

Figures 1, *a*, *b* and 2, *a*, *b* show, respectively, the most typical sinusoids of remelting current and results of calculation of a coefficient of harmonic non-linear distortions in remelting using fluxes ANF-6 and CaF_2–Ca.

As the Figure 1, *a* shows, the remelting using flux ANF-6 is most stable from the technological point of view. In this case the noticeable distortions in the current sinusoid were not observed, and a coefficient of harmonics in a steady condition of melting has low values and lies within the ranges of 2–3 % (Figure 2, *a*).

When using flux ANF-1P the distortion of current sinusoids was almost absent, however, the increase in a coefficient of harmonics up to 5–8 % was observed. However, the use of pure CaF_2 as a slag leads to an episodic distortion of current sinusoid of remelting and to the increase in a coefficient of harmonics up to 16–18 %.

It should be noted that the use of slags ANF-6, ANF-1P and those of pure CaF_2 provides melting in a stable condition of resistance. At the same time, the transition of ESR into instable arc region at the level of a coefficient of harmonics within the 25–30 % ranges is observed when flux CaF_2–Ca is used in remelting (Figure 2, *b*).

The relationships observed between the composition of flux and a coefficient of harmonics allow the mentioned approach to be used for control of metal calcium in slag and composition of slag in the process of the on-line ESR. This information can be used as initial for realizing the automatic control of the process.

The present level in the progress of computer engineering and devices of data input–output gives opportunity to observe and analyze the rapidly proceeding processes. The study of the peculiarities of the electric condition of the chamber ESR using active slags, the finding of regularities and analysis are the basis for the creation of a determinant model of electric processes that will lead to the improvement of the process control system and allow realization of the more effective situation control than the conventional control.

Application of the automated systems for the control of the technological process of ESR can provide the required metal quality at minimum expenses.

1. *Proceedings of 7th Congress of Steelmakers* (2003) Moscow: Chermetinformatsiya.
2. Ryabtsev, A.D., Troyansky, A.A. (2001) Manufacturing of ingots of titanium, chrome and their alloys in chamber furnaces with «active» metal-containing fluxes. *Problemy Spets. Elektrometallurgii*, **4**, 6–10.
3. Ryabtsev, A.D., Troyansky, A.A., Pashinsky, V.V. (2003) On problem of possibility of producing Fe–Nd–B alloys in ESR chamber furnaces. In: *Transact. of DonDTU on Metallurgy*. Issue 66. Donetsk: DonDTU.
4. Troyansky, A.A., Ryabtsev, A.D., Samborsky, M.V. et al. (2002) Use of measurement information system to study the ESR process. *Metall i Litio Ukrainy*, **7 / 8**, 25–26.
5. Ryabtsev, A.D. (2004) *Electroslag remelting of metals and alloys using fluxes with active additions in chamber furnaces*. Syn. of Thesis for Dr. of Techn. Sci. Degree. Donetsk: DonNTU.
6. Trakhtman, A.M. (1972) *Introduction to generalized spectral theory of signals*. Moscow: Sov. Radio.
7. Vasiliev, D.V., Vitol, M.R., Gorshenkov, Yu.N. et al. (1982) *Radio circuits and signals*. Manual for institutes of higher education. Moscow: Radio i Svyaz.
8. Baskakov, S.I. (2000) *Radio engineering circuits and signals*. Manual for institutes of higher education. Moscow: Vysshaya Shkola.
9. Minami, S., Uchida, T., Kawata, S. et al. (1999) *Computer-added processing of experimental data*. Moscow: Radio i Svyaz.
10. Maxs, Zh. (1983) *Methods and technique of processing of signals in physical measurement*. Vol. 1. Moscow: Mir.
11. Vasiliev, V.N., Gurov, I.P. (1998) *Computer-added processing of signals with interferometry systems*. St-Petersburg: BKhV.
12. Hart, H. (1999) *Introduction to measurement technique*. Moscow: Mir.

SPECIFICS OF THERMAL INTERACTION BETWEEN SLAG AND METAL UNDER CONDITIONS OF ELECTROSLAG HEATING

F.K. BIKTAGIROV and **I.V. KRIKENT**
E.O. Paton Electric Welding Institute, NASU, Kiev, Ukraine

Laws of heat generation and mass transfer in slag pool at different diagrams of current supply were studied on the mathematical models relative to the non-consumable electroslag process. It is shown that to improve the heat transfer from slag to metal at a bifilar diagram of current supply, as well as at a three-phase diagram, it is necessary to keep certain geometric proportions of arrangement of electrodes in the slag melt. Experimental investigations of heat balance in electroslag heating of metal confirmed the calculated results.

Keywords: *electroslag heating, heat generation, mass transfer, mathematical modeling, heat balance*

In different technological processes, connected with use of a slag melt as a means of metal heating, the intensity of heat exchange between the contacting phases is one of main characteristics which defines in many cases the technical-economic characteristics of different technologies. This refers to a full extent to technologies of producing steel ingots using an electroslag heating to prevent the shrinkage defects.

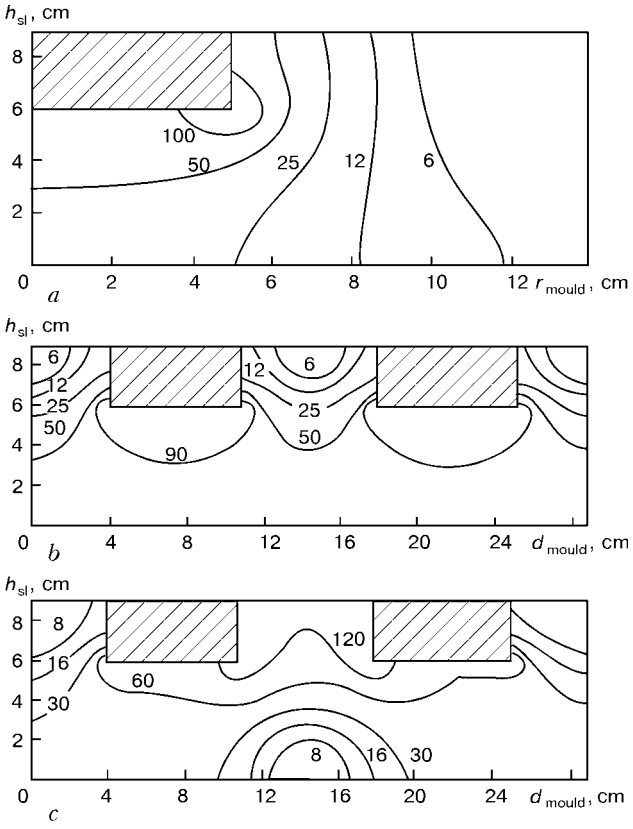

Figure 1. Density of heat sources (W / cm^3) at single-phase direct (*a*, *b*) and bifilar (*c*) diagrams of current supply

When developing the definite technology of electroslag heating it is necessary to evaluate the effect of different its parameters on intensity of heating of metal, being under the slag layer, to decrease the power consumption. Earlier, some laws of heat transfer from the overheated slag to metal were studied. It was revealed, that the coefficient of slag–metal heat transfer depends on the composition of slag used and the metal treated, specific power, generated in a slag pool, and also on a number of other factors [1, 2]. The design-technological features of electroslag installations, in particular an electric diagram of supply, are also important.

The conditions of heat exchange between the slag and metal at a single-phase direct diagram of current supply, when the electric circuit is short-circuited from electrode to metal through slag, are mostly studied. At the same time, to decrease the reactivity of a short circuit of electroslag furnaces and to increase the power factor the bifilar and three-phase supply diagrams with an arrangement of current-carrying electrodes in apexes of the equilateral triangle in the latter case are most preferable. However, the conditions of heat generation in the slag melt in this case will differ from those used at a single-phase direct (electrode–bottom plate) diagram of current supply to the slag. Our investigations were carried out to define more precisely the specifics of heat processes at single-phase, bifilar and three-phase supply diagrams relative to conditions of electroslag process with non-consumable electrodes.

Analysis of heat generation and mass transfer in a slag pool was made firstly by using the earlier developed models [3, 4]. Figure 1 gives the results of calculation of Joule heat generation in the volume of slag pool at monofilar and two-electrode (split) direct diagrams (electrode–bottom plate), and also bifilar (electrode–electrode) diagram of current supply in the case when current-carrying substrate (metal) is located under the slag melt layer. When these calculations were made the supplied power to the slag pool was about 80 kW, the electric conductivity of slag

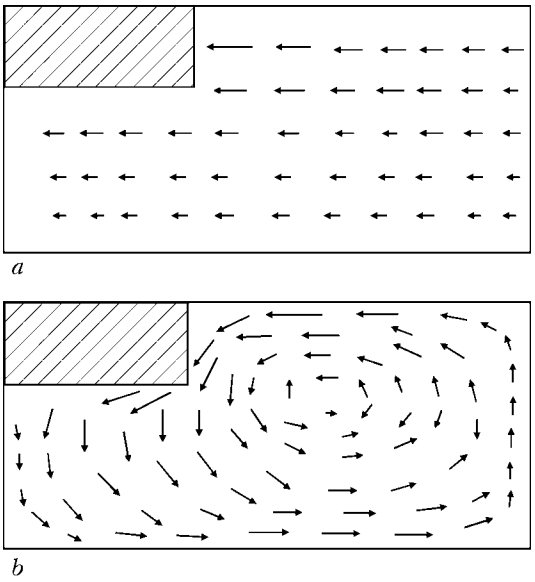

Figure 2. Direction of action of rotational constituent of electromagnetic force (*a*) and nature of slag flows caused by it (*b*)

was taken equal to 2 $Ohm^{-1} \cdot cm^{-1}$, geometric parameters (size of slag pool, diameter of electrodes, etc.) are seen in Figure.

As follows from the data obtained, the power generation in a slag pool occurs not uniformly. The density of heat sources at a direct diagram is highest under electrodes (Figure 1, *a*, *b*), and at a bifilar diagram (Figure 1, *c*) ---- near electrodes and between them, that is due to current passing mainly in the direction of electrode–metal in the first case and electrode–electrode in the second case. In spite of this non-uniform heat generation, the temperature in the slag pool is almost equalized owing to the active stirring of the slag melt under the influence of thermogravitational and electromagnetic forces. Moreover, the action of the latter is dominated usually, and they define mainly the direction and intensity of slag flows.

It may be considered in many cases during the electroslag heating by a direct diagram that electromagnetic field in a slag pool is axial-symmetric. Then, the density of electromagnetic force $\vec{F}$ can be presented in the form

$$\vec{F} = -\frac{\mu}{2}\left(\frac{2}{r} H_\varepsilon^2 \vec{e}_r + \text{grad } H_\varepsilon^2\right), \qquad (1)$$

where μ is the magnetic permeability of the slag; H_ε is the azimuth constituent of vector of magnetic field intensity; $\vec{e}_r$ is the unit vector, directed along the radial coordinate r.

In accordance with the Helmholtz theorem any vector field $\vec{A}$ can be presented in the form of a sum of two constituents: potential and eddy, i.e.

$$\vec{A} = \text{grad } \Pi + \text{rot } \vec{B}, \qquad (2)$$

where Π is some scalar function (potential).

As follows from (1), H_ε is presented as this potential, and the eddy constituent is presented in the form of a centripetal vector, directly proportional to the square of magnetic field intensity and inversely proportional to the radius.

It is known that the potential constituent of vector of force density has no influence on hydrodynamics of liquid and its action is limited by the creation of a magnetic static pressure, distributed in melt volume in a complex way. Therefore, the electromagnetic stirring of melt in the axial-symmetric electromagnetic field is realized only under the action of a rotational constituent of the electromagnetic force which has a centripetal nature.

Figure 2, *a* shows the pattern of vector field $\vec{F}_{\text{rot}} = -\mu H_\varepsilon^2 \vec{e}_r / r$ in a slag pool, calculated using the mathematical model, during the process conductance at a direct diagram of supply, while the melt flow, caused by this eddy constituent of the electromagnetic force, is shown in Figure 2, *b*.

As a result of this nature of the melt stirring, the overheated slag is transported in under-electrode zone in the direction to the metal heated. Here, the slag flows are turned to the slag pool periphery, they are lifted upward at the mould wall to the slag surface and, then, they are lowered along the lateral surface of the electrode. The slag hydrodynamics is also subjected to the effect of heat convection, which is trying to organize the eddy flow in the direction opposite to that shown in Figure 2, *b*. However, in any case the electromagnetic force exceeds the Archimedes force and favorable flow of molten slag, from the point of view of metal heating, is preserved.

The calculations show also that the electromagnetic field in the slag pool is plane-parallel in conductance of the electroslag process by a single-phase direct diagram using two wide plate electrodes, except areas adjacent to narrow faces. In this case, the vector $\vec{F}$ has only potential constituent and the slag movement under the action of electromagnetic force is possible only near the narrow faces of electrodes where the magnetic field becomes not to be plane-parallel. Here, the movement of the slag melt will occur mainly under the action of thermogravitational forces, that should be taken into account in realization of this type of the electroslag process.

At a bifilar connection of electrodes the slag movement acquires nature which differs from that of a direct diagram. Thus, according to investigations using the physical models [5] the most intensive slag movement at a comparatively small immersion of electrodes into the slag melt is occurred in the upper part of the slag pool, while the slag flows are much weaker in the lower its part near the boundary with metal.

The described difference in heat generation and mass transfer in the slag pool at connection of electrodes to the power source using different diagrams should also influence the heat exchange between the contacting phases. At a direct diagram of current supply the conditions of heat transfer from slag to metal are more favorable than at the bifilar diagram. This is due both to the higher density of heat source near the slag–metal interface (in the given case 90 W / cm^3 against 60 W / cm^3), and also to the more intensive

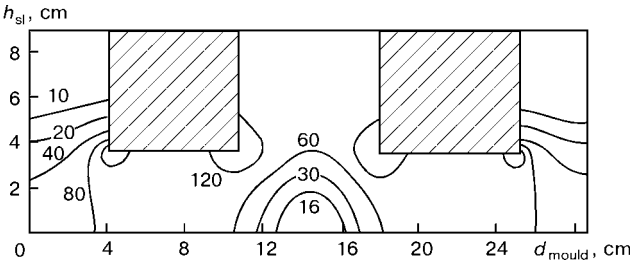

Figure 3. Density of heat sources (W / cm^3) at bifilar diagram of current supply in change of depth of immersion of electrodes

movement of slag melt here. The latter is important, as the condition of liquid movement is very important for the processes of heat transfer between the liquid and solid body (in our case between the slag melt and metal located under it). Thickness of a transition layer at the interface with a solid surface and thermal resistance to heat dissipation are depended on this.

To improve the conditions of metal heating with slag, when the latter is not connected directly to the power source, it is necessary, first of all, to bring the zone of maximum heat generation nearer to the slag–metal interface. According to model experiments (Figure 3), to realize this at interelectrode gap equal to the diameter of electrodes, the distance from the lower edge of electrodes to metal should be not more than a half of diameter of these electrodes. At such conditions, as follows from the data of physical modeling at a bifilar diagram of current supply [5], the nature of slag flows is also changed. The significant their part occurs to be directed from the under-electrode regions downward the boundary with metal, that leads to the intensification of slag movement here and should contribute to the intensification of heat exchange processes.

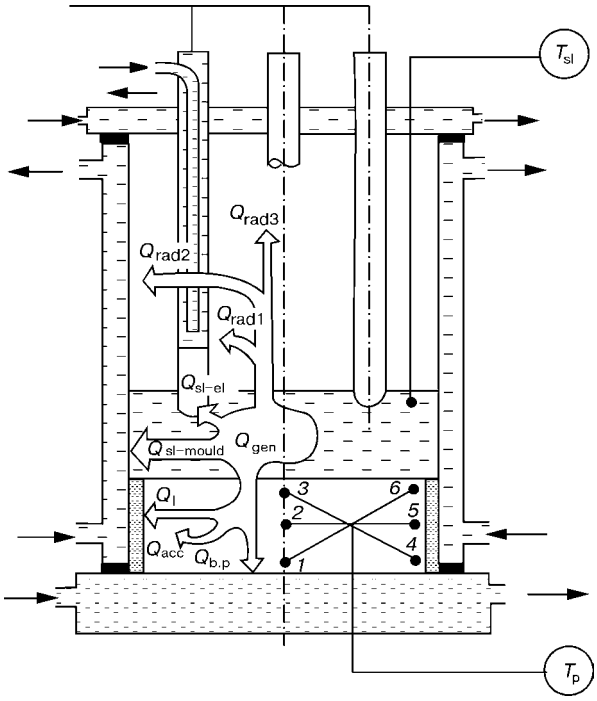

Figure 4. Scheme of measurement of thermophysical parameters and distribution of power supplied to the slag pool (for designations see the text)

As to a three-phase diagram of supply of electroslag installations, then in this case the current circuits can be short-circuited between the electrodes as in the bifilar diagram. Therefore, the nature of heat generation in the slag pool and movement of the slag melt in three-phase diagram is closer to that observed at a bifilar diagram, but not at a single-phase direct diagram.

It should be noted that the heat condition of the slag pool in the electroslag process with non-consumable electrodes is defined by many factors. Major of them are the geometric sizes of the slag pool, diameter of electrodes and distance between them, physical properties of slag, presence of electric resistance at the interface of slag with metal and with a mould, and its parameters. Mathematical model takes into account not only these factors, but also such characteristic as a shape of the lower end of the electrode, i.e. flat, cone-shaped or in the form of a half-sphere. Therefore, in each definite case it is possible to evaluate such characteristics, with allowance for preset conditions, as density of heat source, direction of current passing and its value, voltage drop at separate areas, direction of action of electromagnetic forces. These data are necessary for a proper selection of both design and also technological parameters of the process and ways of their optimization.

General conclusions about the effect of diagram of current supply on heat generation and heat transfer in electroslag heating, made from data of modeling, have found the experimental confirmation, in particular, in study of heat balance of the slag pool in electroslag process with non-consumable electrodes.

Experiments were performed in the following way. A water-cooled mould of 280 mm diameter was mounted on a water-cooled bottom plate (Figure 4). Heat insulating gasket was placed between the mould and bottom plate. A steel billet (primer) with built-in thermocouples *1–6* for temperature measurement was mounted on the bottom plate. Gap between primer and inner wall of the mould was filled with a fine-fraction slag. From the top the mould was closed by a water-cooled cover. Electroslag process was realized using three water-cooled electrodes with graphite tips of 75 mm diameter. Diameter of arrangement of electrodes was 140 mm. Slag ANF-32 was used in experiments. The depth of slag pool was 90 mm. Power source was transformer TShS-3000 / 3, which can be switched by the low-voltage side for the single-phase and three-phase current. At a single-phase diagram of current supply all three electrodes were connected by a direct diagram: electrode–bottom plate, i.e. they were connected to one of the poles of transformer and the another pole was connected to the bottom plate. In the process of experiments the temperature was measured periodically at the slag pool surface and at the 5 mm distance from the metal primer.

Heat energy, generated in the slag pool, is distributed in the melting space as follows (see Figure 4):

$$Q_{gen} = Q_{sl-m} + Q_{sl-mould} + Q_{rad} + Q_{sl-el}, \quad (3)$$

where Q_{gen} is the heat generated in slag; Q_{sl-m}, Q_{sl-el} are, respectively, the heat flow from slag pool to metal (primer) and electrodes; $Q_{sl-mould}$ is the heat flow through the lateral surface of the slag pool to the mould; Q_{rad} are the total losses of heat for radiation from slag pool mirror.

Heat losses for radiation can be evaluated by the known Stefan--Boltzmann expression:

$$Q_{rad} = \varepsilon\sigma_0 F(T_s + 273)^4. \quad (4)$$

Here, ε is the emissivity factor (molten slag); σ_0 is the constant of radiation of absolutely black body; F is the area of emitting surface; T_s is the temperature of slag pool mirror.

Heat losses from slag pool through electrodes are the part of a general flow Q_{el}, removed by water of electrode cooling, i.e.

$$Q_{el} = Q_{sl-el} + Q_{rad1}, \quad (5)$$

where Q_{rad1} is the flow of radiated heat, absorbed by the surface of electrodes.

In the process of experiments, to evaluate the share of heat, emitted into electrodes (Q_{rad1}), one of them was removed from the slag melt for a short time. The occurring change in amount of heat removed by water of electrode cooling, which is determined by the method of calorimetry, allows calculating of value Q_{sl-el}.

Heat flow from slag pool to mould wall is found from expression

$$Q_{sl-mould} = Q_{mould} - Q_{rad2} - Q_l, \quad (6)$$

where Q_{mould} is the heat flow removed by water of mould cooling; Q_{rad2} is the heat flow emitted to the mould wall; Q_l is the heat flow to the mould wall through the primer lateral surface.

Value Q_{mould} is measured by direct calorimetry, Q_l is calculated with allowance for temperature field of primer and heat conductivity of slag mass, Q_{rad2} is found by subtraction of heat emitted to electrodes Q_{rad1} and cover Q_{rad3} from heat losses for radiation from the slag pool surface Q_{rad}.

Heat flow from slag pool to metal (primer) can be determined either from expression (3)

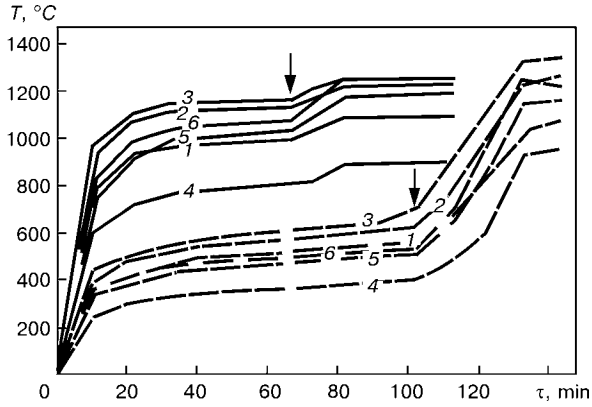

Figure 5. Change in temperature of metal in electroslag heating at single-phase (*solid lines*) and three-phase (*dashed lines*) diagram of current supply: *1–6* — numbers of thermocouples (see Figure 4); moment of change in power is shown by arrows

$$Q_{sl-m1} = Q_{gen} - Q_{sl-mould} - Q_{rad} - Q_{sl-el}, \quad (7)$$

or by summing the items of distribution of heat flow entering the primer:

$$Q_{sl-m2} = Q_{b.p} + Q_{acc} + Q_l + Q_{melt}, \quad (8)$$

where $Q_{b.p}$ is the heat flow, removed by water, cooling the bottom plate, and determined by calometry; Q_{acc}, Q_{melt} is the amount of heat accumulated by the primer (i.e. spent for metal heating) and entered for its pre-melting, respectively.

Heat entered for primer heating is found from expression

$$Q_{acc} = m_p\, c_m\, T_p, \quad (9)$$

where m_p and T_p are the mass and mean temperature of the primer; c_m is the specific heat intensity of metal.

Due to the fact that the mass of pre-melted metal under the conditions of experiments was negligible, the heat consumption for this item of heat balance was not taken into account.

The main data of thermophysical measurements in the process of electroslag processing of metal at different diagrams of current supply are given in Table 1 and in Figure 5, results of calculation of separate items of heat balance are summarized in Table 2.

Analysis of results proves that under the conditions of experiments at 65–70 kW power (mean specific power is 13–14 kW / dm^3), supplied to the slag pool, the share of heat, entered from slag melt to metal, is about 16 % from the total heat generation in slag at

Table 1. Data of thermophysical measurements at different diagrams of current supply

Diagram of current supply	Power supplied, kW	Deepening of electrodes into slag, mm	Consumption of water for cooling (kg / h) / difference of temperatures of supplied and drained water (°C)						Slag temperature, °C	
			Mould	Bottom plate	Cover	Electrodes			At surface	Near primer
						1	2	3		
Single-phase	70	30	2322.4 / 16.5	165.4 / 21.1	324.7 / 8.5	260.1 / 15.8	272.3 / 14.1	244.9 / 15.6	1550	1540
	95	50	2571.2 / 20.8	418.4 / 15.8	372.6 / 10.4	266.3 / 18.7	263.4 / 17.5	234.8 / 20.1	1650	1680
Three-phase	65	30	3003.4 / 11.7	71.9 / 26.0	289.3 / 12.8	421.2 / 11.3	373.5 / 11.7	225.1 / 18.3	1580	1535
	106	55	3668.5 / 16.2	316.7 / 21.5	320.4 / 15.2	488.9 / 12.1	451.7 / 12.0	230.3 / 21.7	1700	1690

Table 2. Calculation of heat balance for electroslag heating at different diagrams of current supply

Diagram of current supply	Constituents of heat balance											
	Q_{gen}	Q_{mould}	Q_{rad1}	Q_{rad2}	Q_{rad3}	Q_{l}	$Q_{sl-mould}$	Q_{sl-el}	$Q_{b.p}$	Q_{acc}	Q_{sl-m1}	Q_{sl-m2}
Single-phase	70 / 100	44.57 / 63.67	7 / 10	14.11 / 20.16	3.21 / 4.59	2.72 / 3.89	27.74 / 39.63	6.69 / 9.56	4.06 / 5.80	4.84 / 6.91	11.27 / 16.10	11.62 / 16.60
	95 / 100	62.20 / 65.47	8.98 / 9.45	16.62 / 17.49	4.51 / 4.75	3.11 / 3.27	41.31 / 43.48	8.07 / 8.49	7.69 / 8.09	5.57 / 5.86	15.29 / 16.09	16.25 / 17.11
Three-phase	65 / 100	40.87 / 62.88	8.19 / 12.60	13.57 / 20.88	4.31 / 6.63	1.22 / 1.88	26.08 / 40.12	7.22 / 11.11	2.17 / 3.34	2.54 / 3.91	5.85 / 9	5.93 / 9.12
	106 / 100	69.12 / 65.21	9.49 / 8.95	18.21 / 17.18	5.67 / 5.35	3.26 / 3.08	47.66 / 44.96	9.55 / 9.01	7.92 / 7.47	5.79 / 5.46	15.45 / 14.58	16.97 / 16.01

Note. Values of constituents are given in kilowatts (numerator) and percents (denominator).

a single-phase diagram of current supply and about 9 % at a three-phase diagram. The above-mentioned difference is explained in this case by the specifics of current distribution revealed in a slag pool at different diagrams of current supply and phenomena, connected with this, of heat generation and heat transfer. Namely, the heat generation and slag flows near the primer are much weaker in experiments at a three-phase diagram of current supply and deepening of electrodes into slag for 30 mm as compared with those observed at a single-phase diagram under similar conditions that predetermines the difference under the conditions of heat dissipation from slag to metal.

When the electrode deepening into slag is changed, as was expected, the values of heat flows from slag to metal at single-phase and three-phase diagrams of current supply occurred to be commensurable (see Table 2 and Figure 5). In addition, the following fact attracts attention that in the first case, when the direction of slag flows is not almost changed in spite of increase in slag temperature, the heat share, entering the metal, is remained at the same level. This is an indirect confirmation of the fact that it is the mode of movement of slag melt near the boundary with metal that influences greatly the intensity of heat exchange.

The following conclusion can be made on the basis of obtained results which were confirmed also by additional experiments, including those with change in position of electrodes in a slag pool at unchanged power supplied to the slag. At a single-phase direct diagram of current supply the share of heat supplied from slag to metal is remained approximately at the same level in changing of electric parameters of the electroslag process. At a three-phase diagram of current supply the electrical condition and the arrangement of electrodes in a slag pool, connected with it, have a great influence on the amount of heat entered the metal. Consequently, when the three-phase power source is used, it is necessary to take into account the above-mentioned peculiarities of heat exchange between the slag and metal for the optimum selection of technological parameters of electroslag heating and melting of metal.

1. (1978) *Thermal processes in electroslag remelting.* Ed. by B.I. Medovar. Kiev: Naukova Dumka.
2. Lyuty, I.Yu., Latash, Yu.V. (1982) *Electroslag melting and refining of metals.* Kiev: Naukova Dumka.
3. Demchenko, V.F., Krikent, I.V. (2002) Mathematical modeling of electromagnetic phenomena in electroslag process. *Matemat. Modelirovanie*, 18(**1**), 16–20.
4. Makhnenko, V.I., Demchenko, V.F., Tarasevich, N.I. et al. (1985) Computational system for investigation of current distribution in slag pool. *Problemy Spets. Elektrometallurgii*, **1**, 14–19.
5. Rouson, J.D., Douson, D.I., Kirhem, N. (1975) Motion of slag and metal in ESR process. In: *Electroslag remelting*. Issue 3.

ELECTRON BEAM SURFACE MELTING OF ZIRCONIUM INGOTS

N.P. TRIGUB, S.V. AKHONIN and **A.N. PIKULIN**
E.O. Paton Electric Welding Institute, NASU, Kiev, Ukraine

This article presents technology of electron beam surface melting of cylindrical zirconium ingots and experimental determination of optimum technological parameters. Metallographic analysis of ingots showed that surface melted layer is characterized by the absence of macropores, discontinuities and other defects of casting origin.

Keywords: *electron beam surface melting, zirconium, ingot*

One of the final stages in production of high-quality cast zirconium billets is the remelting in vacuum-arc or electron beam installation [1]. In this case the surface layer of the ingots produced has different kinds of defects. Usually, the mechanical treatment of surface of ingots and billets is used to remove them, that leads to significant losses of metal (from 5 to 15 % of mass of the ingot treated) in the form of chips or metal-abrasive dust [2].

To reduce the metal losses and to replace the mechanical treatment, the technology of melting of a lateral surface of ingots by electron beam has been developed [3] and the appropriate equipment for its realization has been manufactured at the E.O. Paton Electric Welding Institute of the NAS of Ukraine [4].

This method is based on the principle of heating and melting of a surface layer of the ingot simultaneously in the entire length using electron beams. By electron beam scanning along the ingot generatrix the length of the zone of surface melting by one gun was 0.2–0.3 m, while the width of the molten metal pool did not exceed 0.02 m. During the process of surface melting the ingot is rotated around the longitudinal axis and, thus, the molten metal pool, which is set along the ingot generatrix, is moved along the entire its lateral surface.

Electron beam treatment of the surface layer of ingots and billets has certain advantages, such as the presence of vacuum in a furnace space as a protective and refining medium, high density of supplied power, precision, simplicity in monitoring and control of technological parameters.

To optimize the technological parameters of the process of surface melting of zirconium ingots of 360 mm diameter, a series of experimental melts with in-process measurement of the following parameters was made: power of electron beam heating, size of surface melting zone, linear rate of melting, time of melting, residual pressure and melting chamber inleakage. 60 melts were performed in total, whose technological parameters are given in Table 1.

Vacuum 10^{-4}–10^{-5} mm Hg was maintained in the melting chamber during surface melting, inleakage into melting chamber of the installation did not exceed 10 l / (μm·s). Width of molten metal pool at the zirconium ingot lateral surface was 15 mm.

To compare the quality of zirconium ingot surface before and after surface melting, a fragment of ingot with and without melted lateral surface is given in Figure 1. After treatment of the surface by the electron beam, it acquires a smooth microrelief, the rough-

Table 1. Main conditions of experimental melts of zirconium ingots

Technological operation	Time of operation, min	Specific power of heating, kW / cm^2	Linear speed of ingot rotation, mm / min
Preheating	23	0.66	51.3
Surface melting	34	1.20	33.2
Preheating	22	0.56	51.2
Surface melting	33	1.29	34.2
Preheating	22	0.63	50.9
Surface melting	20	1.44	57.2
Preheating	22	0.64	40.9
Surface melting	22	1.80	51.3

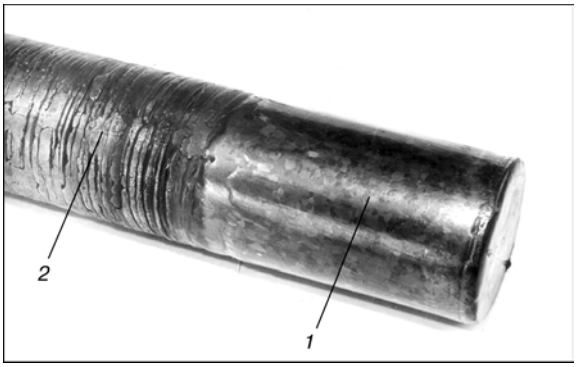

Figure 1. Appearance of zirconium ingot with melted (*1*) and non-melted (*2*) lateral surface

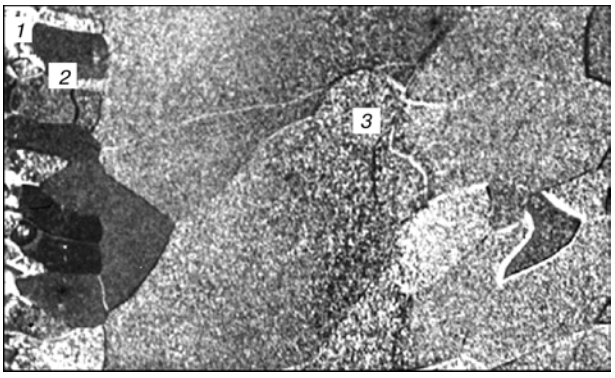

Figure 2. Macrostructure of transverse templet of zirconium ingot with as-melted lateral surface: *1* — as-surface melted layer; *2* — heat-affected zone; *3* — base metal

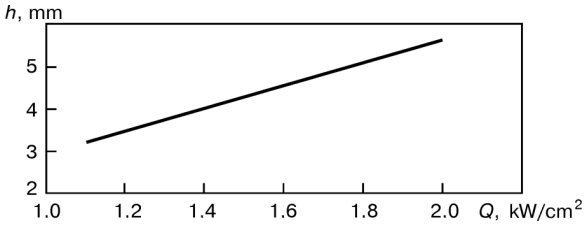

Figure 3. Dependence of melting depth *h* on specific power of electron beam heating *Q*

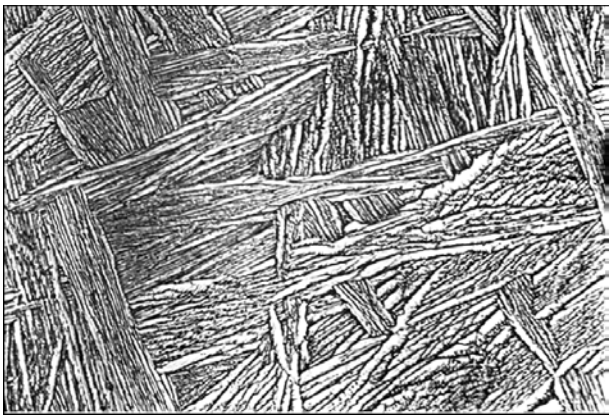

Figure 4. Microstructure of as-surface melted layer of zirconium ingot (×500)

ness being within the ranges of 3–4 class at a surface waviness of 0.2–0.6 mm, respectively.

Metallographic examinations of ingots with a melted lateral surface were carried out on the specimens, cut out from longitudinal and transverse templets. To reveal the macrostructures of zirconium alloy, a reagent of the following composition was used: 10 ml of hydrofluoric acid, 60 ml of hydrogen peroxide and 50 ml of water.

Metal of ingots, subjected to surface melting by electron beam, is characterized by the absence of macropores, discontinuiries and other defects of casting origin. The base metal possesses a polyhedral grained structure of α-solid solution (Figure 2).

The layer melted around the ingot circumference, whose depth was 3–5 mm, is characterized by a fine-crystalline structure. As the investigations showed, the depth of melting of more than 3 mm ensures the removal of all the melting defects from the lateral surface of ingots.

The processing of results of experimental melts, performed at different conditions, showed (Figure 3) that the melting depth depends almost linearly on specific power of the electron beam heating.

Structure of the heat-affected zone of 90–95 mm size, stipulated by temperature effect of electron beam, is presented by grains which are elongated in the direction of the ingot center.

Examination of microstructure was made in optical microscope «Neophot 32» after etching in a reagent of the following composition: 10 ml of nitric acid, 10 ml of hydrofluoric acid and 10 ml of water. It was noted that the nature of structure of zirconium alloys depends of the rate of cooling and content of alloying elements. Surface melting zone is characterized by a laminated structure of a basket type, similar to structure of a cast base metal (Figure 4). This structure is formed as a result of a polymorphous transformation of β-phase in the process of cooling. In the heat-affected zone the acicular microstructure has a finer nature.

Table 2. Distribution of impurities and alloying elements in ingots of zirconium alloy E-125

Region examined	Place of sampling	Element content, %										
		C	N	O	H	Fe	Si	Cu	Al	Ni	Cr	Nb
As-surface melted layer	H = 1	0.02	0.0032	0.05	0.00030	0.009	0.0046	0.0010	0.0046	0.0049	0.0040	2.5
	H = 3	0.02	0.0030	0.04	0.00029	0.010	0.0048	0.0011	0.0046	0.0048	0.0043	2.5
	H = 5	0.02	0.0030	0.04	0.00030	0.0098	0.0050	0.0012	0.0047	0.0049	0.0046	2.5
HAZ	H = 15	0.02	0.0034	0.05	0.00043	0.015	0.0074	0.0014	0.0056	0.0052	0.0058	2.5
	H = 40	0.02	0.0032	0.04	0.00038	0.013	0.0075	0.0010	0.0046	0.0061	0.0054	2.5
	H = 65	0.02	0.0030	0.04	0.00037	0.014	0.0058	0.0012	0.0052	0.0049	0.0043	2.5
Ingot base	Centre	0.02	0.0037	0.05	0.00054	0.014	0.0070	0.0010	0.0055	0.0049	0.0049	2.5
	1 / 3R	0.02	0.0039	0.05	0.00050	0.012	0.0079	0.0012	0.0060	0.0051	0.0052	2.5
	2 / 3R	0.02	0.0036	0.05	0.00053	0.015	0.0061	0.0011	0.0053	0.0051	0.0048	2.5

Note. Each value is a mean value from five measurements; H — depth, mm.

To determine the effect of electron beam surface melting on the composition of metal of an ingot lateral surface at the depth of 1.3 and 5 mm, samples for the chemical analysis were taken. In addition, the samples were taken from the heat-affected zone and ingot base. Results of chemical analysis of alloy E-125 are given in Table 2.

Processing of obtained values of distribution of impurity elements in zirconium ingot section shows that in as-melted layer the content of hydrogen, iron, aluminium, silicon and chromium is reduced, while the rest impurities are at the level of values of the ingot base. Here, the reduction in content of hydrogen is observed not only in as-melted layer, but also in the heat-affected zone, that is stipulated by a high mobility of hydrogen in a solid zirconium. Uniformity of distribution of alloying element of niobium is not violated as a result of surface melting.

Measurement of hardness of transverse templets of as-surface melted ingots showed that the mean hardness of zirconium of electron beam melting is about *HV* 140 (Figure 5). Decrease in hardness on ingot metal in the zone of surface melting is stipulated by a decrease in content of interstitial impurities, and the highest increase in hardness of zirconium in the heat-affected zone is stipulated by the presence of quenching conditions.

Thus, the performed investigations showed that the zirconium ingot with a surface layer, melted by electron beam, is characterized by the absence of macropores, discontinuities and other defects of casting origin, and also by the more pure metal as to the chemical composition, and made it possible to develop the technology of electron beam surface melting, which increases the efficient metal yield by 5–15 %.

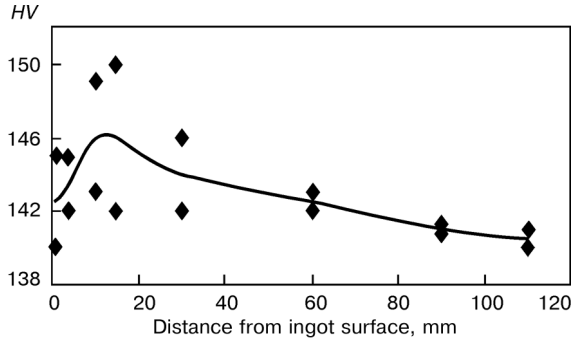

Figure 5. Hardness of zirconium ingots subjected to electron beam surface melting

1. Tikhinsky, G.F., Kovtun, G.P., Azhazha, V.M. (1986) *Production of super-pure rare metals*. Moscow: Metallurgiya.
2. Shuravlyov, M.V. (1953) *Methods of metal surface defect removal*. Moscow: Metallurgizdat.
3. Paton, B.E., Trigub, N.P., Kozlitin, D.A. et al. (1997) *Electron beam melting*. Kiev: Naukova Dumka.
4. Trigub, N.P., Zhuk, G.V., Pikulin, A.N. et al. (2003) Electron beam installation UE-185 for fusion of surface layer of ingots. *Advances in Electrometallurgy*, **3**, 10–12.

MANUFACTURE OF TITANIUM PIPES FROM METAL PRODUCED BY EBCHM METHOD

S.N. ANTONOV[1], **V.P. REVENOK**[1], **A.V. ZHURAVLYOV**[1], **N.V. ANTIPIEVA**[1], **N.E. KOPYLOVA**[1], **V.D. PETROV**[2], **A.N. KALINYUK**[3] and **O.N. KOZLOVETS**[3]

[1]CJSC «SETAB Nikopol Works», Nikopol, Ukraine

[2]Research Institute of Structural Materials «Prometej», St.-Petersburg, Russia

[3]R&P Center «Titan» of the E.O. Paton Electric Welding Institute, NASU, Kiev, Ukraine

At CJSC «SETAB Nikopol Works», the cold-worked pipes, made of ingots, produced from titanium alloy PT-1M using the method of electron beam cold hearth melting at R&P Center «Titan» of the E.O. Paton Electric Welding Institute of the NAS of Ukraine, were manufactured. By its properties the forged billet, produced from these ingots, meets the requirements of TS 1-5-132–78. Cold-worked pipes, manufactured from it, satisfy the requirements of GOST 22897–86 and TS 14-3-820–79. Quality of the surface, content of impurities, mechanical and technological properties of ready pipes are similar to the same characteristics for the pipes manufactured from the VAR metal.

Keywords: *ingot, billet, electron beam melting, cold hearth, vacuum-arc remelting, pipe, properties*

At present the main manufacturer of cold worked pipes, made from titanium alloys, in Ukraine is CJSC «SETAB Nikopol Works». This close joint stock company was established as a result of reconstruction of OJSC «Nikopol South Pipe Works» on the base of a shop specialized in production of these pipes.

Earlier, the production of cold-worked titanium alloy pipes was mastered from a billet of vacuum-arc remelting. Disintegration of the former USSR has led to the break in traditional relations between the enterprises of the CIS countries, resulting in reduction of the delivery of billets for manufacture of titanium alloy pipes in Ukraine, in particular from JSC VSMPO (Verkhnyaya Salda city, Russia). This caused the problem in searching for raw materials to melt the metal and to manufacture pipes from it.

Today, the vacuum electron beam cold hearth melting (EBCHM) [1–4] is the most effective and economic method of producing non-ferrous metals and alloys, in particular titanium, and R&P Center «Titan» of the E.O. Paton Electric Welding Institute is the main supplier of EBCHM ingots in our country.

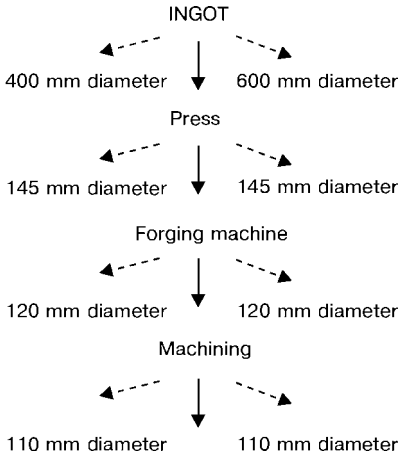

Figure 1. Scheme of producing pipe billet of 110 mm diameter

Cold-worked pipes of (10–19) × (1.5–2.5) and 89 × 4 mm sizes were manufactured from ingots of titanium alloy PT-1M, produced by EBCHM, at «SETAB Nikopol Works» in collaboration with «Prometej». Ingots of 400 and 600 mm diameter and 2000 mm length were used for manufacture of 110 mm diameter tubular billet. Forging was performed at temperatures of β-region in hydraulic press and forging machine using a scheme shown in Figure 1. Pipes were manufactured by hot rolling in the TPA 140 type installation with their subsequent cold processing in mills of cold rolling of pipes [5].

Macro- and microstructure, mechanical and technological properties (flattening, expansion) were examined in ingots, billets for working and in processed hot-rolled and cold-worked pipes, and the hydrogen content was also determined. The quality of pipes was evaluated for conformity to GOST 22897–86 and TS 14-3-820–79.

The obtained results showed that the chemical composition of EBCHM ingots is in a complete compliance with requirements of OST 1.92077–91 and characterized by homogeneity (Table 1).

Macrostructure of the billet is dense, homogeneous, without defects, with a grain value of 2–4 marks (in 8-mark scale). Here, the amount of a structural constituent of 4 mark is prevailing in the billet produced from a head part of the 400 mm diameter ingot. Macrostructure of the billet, manufactured from 600 mm diameter ingot, is characterized by prevailing of a macrograin of 2-mark value.

Microstructure of billets of 110 mm diameter contains, not depending on initial size of the ingot, a mixture of coarse-laminar colonies of α′-phase with a value of a former β-grain of 3–2 mark in scale of GOST 5639–82 and separate regions of a recrystal-

Table 1. Chemical composition of ingots from alloy PT-1M of EBCHM

Ingot diameter, mm	Place of sampling	Element content, %						
		Ti	Àl	Fe	Ñ	Si	N	Î
400	Head part	Base	0.40	0.08	0.01	0.02	0.027	0.08
	Middle part	Same	0.30	0.09	0.02	0.01		
	Bottom part	»	0.50	0.08	0.01	0.01		
600	Head part	»	0.45	0.08	0.01	0.02	0.024	0.09
OST 1.92077–91		»	0.20–0.70	0.20	0.10	0.10	0.040	0.12

Table 2. Mechanical properties of 110 mm diameter billet from alloy PT-1M of EBCHM

Ingot diameter, mm	Ingot part	Mechanical properties							[Í], %
		at 20 °Ñ					at 150 °Ñ		
		σ_t, MPa	$\sigma_{0.2}$, MPa	δ_5, %	ψ, %	*KCU*, J / cm^2	σ_t, MPa	$\sigma_{0.2}$, MPa	
400	Head part	43.5	36.5	31	62	20.5	33	24.5	0.004
	Bottom part	42.5	35	32	64	18.8	33	24.5	0.004
600	Head part	43	35.5	27	61	14.4	32	24.5	0.005
	Bottom part	44	37	29	63	16.3	32	26	0.005
TS 1-5-132–78		35–50	25	22	45	12	22	16	0.007

lized α-phase, that is typical for a hot-worked state of metal.

Mechanical properties of the billet, determined in as-delivered section on longitudinal specimens after annealing, corresponded to rates of TS 1-5-132–78 (Table 2).

The strength properties of a pressed billet, independent of initial diameter of ingot, are almost at the same level: $\sigma_t \sim 43$, $\sigma_{0.2} \sim 36$ MPa. Characteristics of ductility (elongation, impact strength) of the billet, manufactured from ingot of 400 mm diameter, are somewhat higher than those of the billet from 600 mm diameter ingot. This is explained by the higher content of hydrogen in the billet (see Table 2) due to large number of intermediate preheating of 600 mm diameter ingot during forging and, consequently, high gas saturation. However, all the forged billet possessed a sufficient margin of ductility for the next working.

Hot rolling of processed pipes made from above-mentioned billet was performed after heating up to temperatures of β-region and finished in α-region. The process of deformation in all the regions was stable and did not differ from the process of rolling the pipes manufactured by the existing technology. In hot working the β-grain is refined and microstructure with the formation of fine-grain α-phase of a laminar type is equalized. Differences in microstructure depending on initial size and section of ingot (head or bottom part) was not observed, but a negligible scattering in elongation values was preserved. This microstructure of hot-rolled pipes in combination with a sufficiently high margin of ductility (δ_5 = 27 % in pipes from 600 mm diameter ingot and 29 % from 400 mm diameter ingot) provided a satisfactory proceeding of the process of cold working of pipes.

Hot-rolled pipes were manufactured using the accepted technology in mills of cold-rolling of pipes for 5–6 passes with reduction for one pass from 45 to 55 %. Quality of surface of pipes was satisfactory. Microstructure of ready pipes consisted of equiaxial grains of α-phase of 7–9 marks. 30 % of pipes were subjected to check tests.

Table 3. Hydrogen content (%) in pipes manufactured from EBCHM ingot of 400 mm diameter

Pipe size, mm	Spectral method		RH-2		Laser probe ECHO-4		
	External surface	Wall section	External surface	Internal surface	External surface	Wall section	External surface (milled)
53 × 6	0.0051	0.0047	0.0054	0.0052	0.0036	0.0046	0.0036
89 × 4	0.0049	0.0047	0.0046	0.0048	0.0043	0.0052	0.0043
56 × 3	0.0052	0.0049	0.0048	0.0047	0.0047	0.0041	0.0046

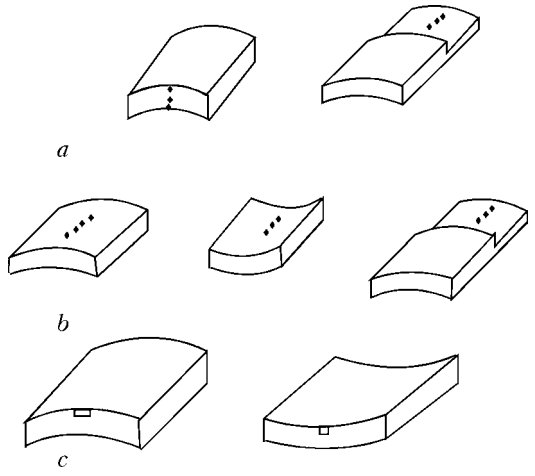

Figure 2. Scheme of determination of hydrogen content on pipe specimens using different methods: *a* — spectral method; *b* — laser probe ECHO-4; *c* — RH-2

Independently of the initial ingot size, the mechanical properties of the ready pipes in length were at the same level and in compliance with the requirements.

Technological tests of pipes (for flattening and expansion) showed the good results. Hydrogen content in ready pipes, manufactured from 400 mm diameter ingot, was determined after mechanical treatment of external surface by machining for 0.2 mm depth and in section of pipe wall using different methods, such as spectral method using procedure RD 5.9184–90, laser probe ECHO-4 and in gas analyzer, RH-2 without mechanical treatment. Independently of site of determination (external surface or pipe wall section, external or inner surface) all the methods gave the almost similar results as to the hydrogen content, i.e. about 0.005 % (Table 3). Sites of determination of hydrogen content are shown in Figure 2.

Acceptance control of hydrogen content in accordance with requirements of the standard documentation was made using a spectral method. Pipes, manufactured from 400 mm diameter ingot, contained 0.005 % hydrogen, pipes from 600 mm ingot — 0.006 %, while the GOST 22897–86 admits not more than 0.008 % and TS 14-3-820–79 — not more than 0.007 %.

In total, 6 batches of pipes of 2000 kg total weight were manufactured. Efficient metal was 99.5 %.

The investigations showed that the cold-worked pipes, made from titanium alloy PT-1M, manufactured from ingots produced by the EBCHM method at the R&P Center «Titan», are in conformity to the requirements of GOST 22897–86 and TS 14-3-820–79 by the quality of surface, mechanical and technological properties, and also by the hydrogen content. Ingot of 400 mm diameter and 2000 mm length is optimum for manufacture of cold-worked pipes.

1. Wood, J.R. (2002) Producing Ti–6Al–4V plate from single-melt EBCHM ingot. *JOM*, February, 56–58.
2. Kalinyuk, A.N. (2002) Development of electron-beam melting of titanium and its alloys. In: *Special electrometallurgy: yesterday, today, tomorrow*. Kiev: Politekhnika.
3. Antonyuk, S.L., Molyar, A.G., Kalinyuk, A.N. et al. (2003) Titanium alloys for aircraft industry of Ukraine. *Advances in Electrometallurgy*, **1**, 9–13.
4. Kalinyuk, A.N., Trigub, N.P., Zamkov, V.N. et al. (2003) Microstructure, texture and mechanical properties of EB melted Ti–6Al–4V alloy. *Materials Sci. and Eng.*, A346, 178–188.
5. Vakhrusheva, V.S., Buryak, T.N., Ladokhin, S.V. et al. (2001) Application of cast billets of new type for producing of titanium tubes. *Metallurgich. i Gornorudnaya Promyshlennost*, **1**, 60–62.

STUDY OF GAS PHASE COMPOSITION IN PLASMA-ARC MELTING OF TITANIUM FROM A PRESSED BILLET

M.L. ZHADKEVICH[1], **V.A. SHAPOVALOV**[1], **V.V. TELIN**[2], **S.M. TESLEVICH**[2], **V.S. KONSTANTINOV**[1], **G.F. TORKHOV**[1] and **V.R. BURNASHEV**[1]
[1]E.O. Paton Electric Welding Institute, NASU, Kiev, Ukraine
[2]«Zaporozhie Titanium-Magnesium Works», Zaporozhie, Ukraine

Composition of gas atmosphere was studied in melting of a pressed spongy titanium billet. It was established that content of hydrogen and moisture in the zone of melting is changed depending on the rate of billet melting, grade of spongy titanium, consumption of plasma-forming gas, terms of storage of a pressed billet.

Keywords: *spongy titanium, pressed billet, plasma, hydrogen, gas phase, moisture, melting*

As was outlined many times, the main problem in titanium production consists in reduction of its cost and guarantee of high quality of metal in the entire technological cycle. One of the most important places in this cycle belongs to the ingot melting. In many countries, dealing with titanium production, a vacuum-arc remelting of a pressed electrode is still remained to be the leading technological process of the ingot producing, in which the manufacture of a pressed electrode is an expensive operation, but guaranteeing the melting of the high-quality ingot [1].

At all the stages of progress and upgrading of the technology of melting the attempts were made in producing ingots from a lumpy charge, eliminating the stage of pressing. With an appearance of independent heat sources, such as plasmatrons, electron guns, high-frequency electromagnetic field and so on, the interest to the remelting of a non-compact charge was greatly increased [2–4].

In particular, during several years a series of experimental, experimental-industrial installations has been created, in which a low-temperature plasma was used for remelting of a non-compact charge as a heat source. Plasmatron with a tungsten or graphite electrode serves as a generator of plasma. Ingots of different shapes were produced in furnaces, which then were used for next processing for a sheet or a shaped casting [5]. However, during melting of a gas-saturated charge, an intensive gas evolution from a molten metal was observed accompanied with spattering of particles from the melt which solidified on plasmatron nozzles and became getters for oxygen and nitrogen.

In the process of melting the solidified spatters are saturated with gases, added with new portions of molten metal particles, saturated with gases, coming from the pool. Metal is gradually melted under the action of high temperature of plasma jets, and the drops of molten metal enter the melt. Moreover, the solidified piece of metal can also enter the molten pool under the action of some disturbances. The temperature of melting of gas-saturated metal is higher by several hundreds of degrees than the temperature of melting the parent metal, therefore, the entered drops or pieces are not dissolved completely in the melt and can serve a cause of formation of inclusions in the ingot.

It should be noted in addition that the plasma furnaces for remelting of bulk charge have a complex design, a large internal volume for charge, require application of powerful pumping systems for charge degassing, are difficult in control and so on.

Taking into account the above-mentioned problems and demand for producing the high-quality metal for critical products, which do not admit the presence of inclusions, it seems rational to use a compact billet as a remelting material. It can be produced by different methods, including also pressing.

We have performed experimental melting of a spongy titanium, pressed into a consumable billet of 40 mm diameter and up to 300 mm length. The main attention was paid here to the behavior of gas impurities, in particular hydrogen and moisture, which are contained in a pressed billet and influence greatly the quality of the melted metal.

Samples of a spongy titanium to produce a consumable billet were taken from different places of containers designed for its storage. The total weight of a sample from pieces of 12–25 mm size is 10 kg. Then, they were crushed in a conical crusher to the size of not more than 5–10 mm and refined in a slotted screen to obtain a certified sample of mass of up to 5 kg with its subsequent division into 4 parts of up to 1.2 kg mass each. One of samples was intended for manufacture of a consumable billet using a method

*Nazarenko S.P. participated also in this work.

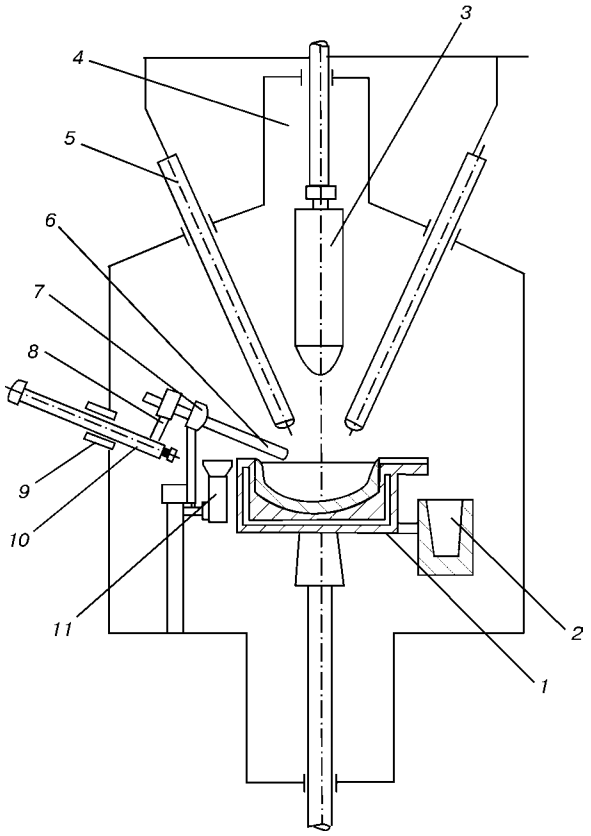

Figure 1. Scheme of a modified 4-plasmatron laboratory installation UPP-3: *1* ---- skull crucible; *2* ---- mould; *3* ---- pressed billet; *4* — chamber; *5* — plasmatron; *6* — water-cooled tip; *7* — plasma cut-off; *8* — holder; *9* ---- packing; *10* — rod; *11* — accumulator

of pressing through a feed-through matrix in a hydraulic press of 1600 kN force. The as-pressed billets were packed into a double-layer polyethylene packs, where they were stored before melting.

The melts were performed in the experimental modified 4-plasmatron plasma-arc furnace UPP-3, the diagram and general view of which are shown in Figures 1 and 2. It includes a melting chamber, 4 plasmatrons with mechanisms of their adjustment, a mechanism of billet feeding, a copper water-cooled crucible, a metal chill mould, a vacuum system, cooling system and power sources.

Hydrogen content was measured by a gas analyzer TG1120 in a set with a potentiometer KSM2. To determine the moisture content a coulometer of humidity of «Bajkal-1» type was used. Gas sampling was made through the chamber upper part having an outlet into atmosphere. To prevent the enter of dust particles into a measuring gauge a fine filter was mounted at a gas exhaustion branch pipe.

Before melting starting the walls of the melting chamber, copper crucible and casing of plasmatrons were cleaned carefully from sublimates formed in the previous melting. The walls were cleaned by a metallic brush, and then by a cloth wetted with a technical alcohol. Then, a consumable electrode was connected to a mechanism of billet feeding and lifted beyond the nozzle section of plasmatrons to prevent its premature melting at the moment of plasmatrons switching-on and pool setting in a crucible. To prevent the crucible burn-out at the moment of switching-on of plasmatrons, a templet of a commercial titanium was placed on its bottom. A metal mould for metal pouring was preheated for 2 h up to 300–400 °C before installing into a furnace chamber. The furnace, prepared for melting, was subjected to degassing for 45–60 min until residual vacuum of 26–33 Pa, then to in-leak testing and then to filling of the furnace internal volume with argon up to excessive pressure 0.02 MPa.

Melting was started by ignition of two plasmatrons at minimum conditions (300 A current and 40 V voltage). After melting the priming templet and partial heating of the consumable billet, the latter was fed into the zone of melting. The time of the primer melting and billet heating was 2–3 min. The billet was fed at different speed and, depending on the power of plasmatrons, it varied from 2 to 7 mm / min. The current load at plasmatrons was maintained in the ranges of 300–400 A. Gas consumption at plasmatrons was 4–10 l / min. Melting was performed in a continuous argon atmosphere.

Duration of melting of 40 mm diameter and up to 300 mm long billet was 25–30 min. After complete melting of the billet into a crucible, it was inclined

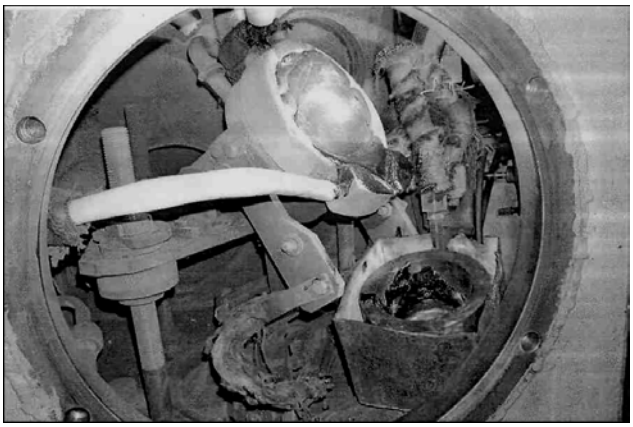

Figure 2. Melting chamber with a crucible and mould for a pressed billet remelting

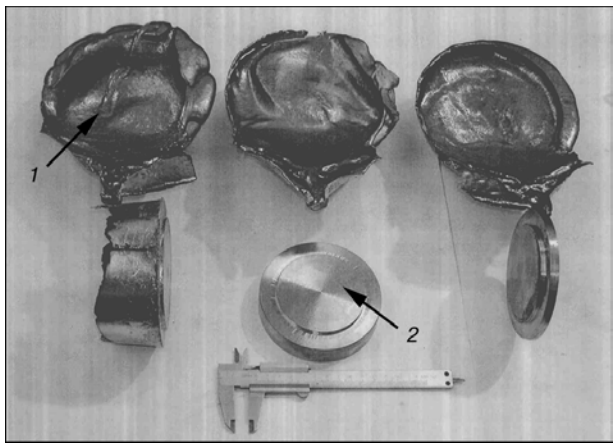

Figure 3. Cast (*1*) and machined (*2*) samples from commercial titanium of 120 mm diameter and 7 mm height

and molten metal was poured out into a mould for solidification.

After cooling, the templet of 120 mm diameter and 5–7 mm height (Figure 3) was withdrawn from the mould, the surface was machined and samples were taken for determination of hydrogen concentration in the metal. Sampling of exhausting gas from the furnace for determination of hydrogen and moisture content was made after switching-on of the plasmatrons for melting. Amount of hydrogen was measured by a meter at the moment of plasmatrons switching-on.

The hydrogen presence in the melting chamber, as was already shown in other works [6], was caused by the heat effect of plasma jets on melting chamber walls, nozzle and casing of plasmatrons, crucible wall and billet being remelted. As a result of an intensive heating the moisture from the chamber walls is removed and spread by the plasma jet flows over the entire internal volume of the installation. A part of it enters the heated titanium primer, thus leading to the moisture decomposition into oxygen and hydrogen which is transferred into the furnace atmosphere.

At the moment of the primer melting a short-time increase in hydrogen content and then its reduction are observed. At the next feeding of a pressed billet, manufactured from high-quality spongy titanium, into the zone of melting, a gradual increment in hydrogen amount during 5–10 min and then its reduction, firstly intensive and then delayed, was noted.

With increase in consumption of a plasma-forming gas, the maximum evolution of hydrogen is decreased depending on the amount of supplied inert gas, as, here, the speed of the billet feeding and supplied power remain constant.

Figure 4 presents the curves characterizing the hydrogen behavior in the process of melting of a pressed billet with change in consumption of the plasma-forming gas. The billet feed speed in this case was 2 mm / min, current at each of two plasmatrons was 300 A. It is seen from Figure that with increase in plasma-forming gas consumption from 10 to 40 l / min the hydrogen content in the gas phase is decreased from 1.0 down to 0.5 vol.%.

The hydrogen behavior at different speeds of the pressed billet feeding into the zone of melting was studied during experimental melts. Figure 5 presents curves, illustrating the hydrogen behavior at a linear rate of the billet movement of 2–7 mm / min at a constant consumption of the plasma-forming gas. It is seen from the Figure that with increase in melting rate the maximum content of hydrogen in the furnace atmosphere is increased from 0.48 up to 1.60 vol.%. Moreover, the rates of hydrogen content decrease in gas atmosphere after reaching the maximum are delayed with increase in speed of the billet feeding.

The similar mode of hydrogen behavior was observed in melting of the pressed billet at the 2 mm / min speed of its feeding with 5 l / min gas consumption at the plasmatron and current change

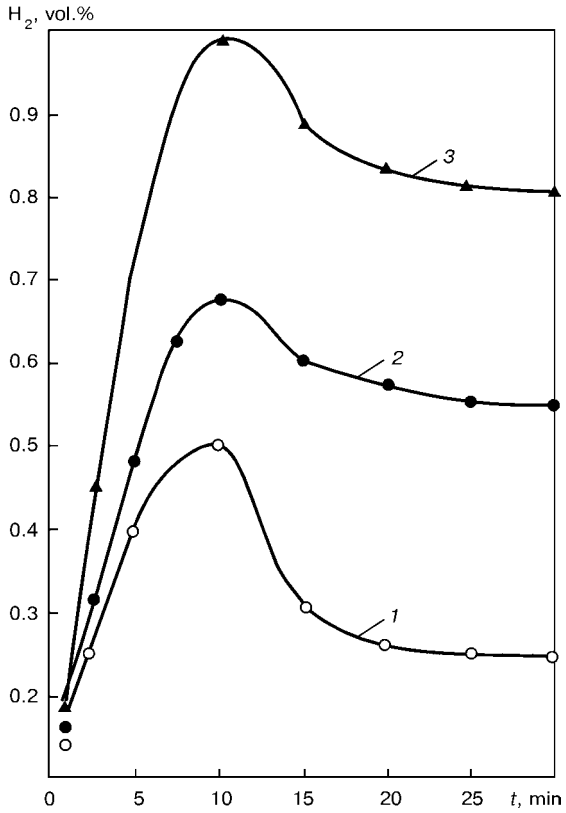

Figure 4. Dependence of hydrogen content in the furnace melting volume on change in consumption of plasma-forming gas (argon): 10 (*1*), 30 (*2*) and 40 (*3*) l / min

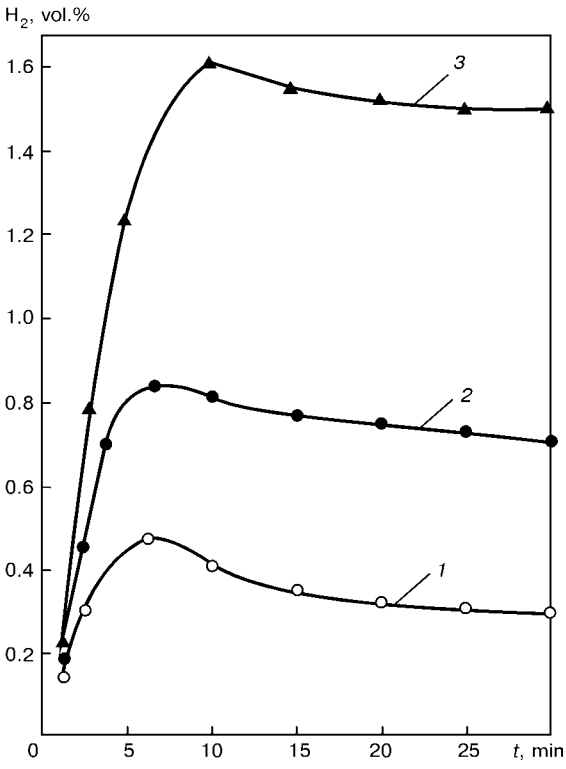

Figure 5. Variation in hydrogen content in melting space of the plasma installation in melting at different speeds of billet feeding: 2 (*1*), 4 (*2*) and 7 (*3*) mm / min

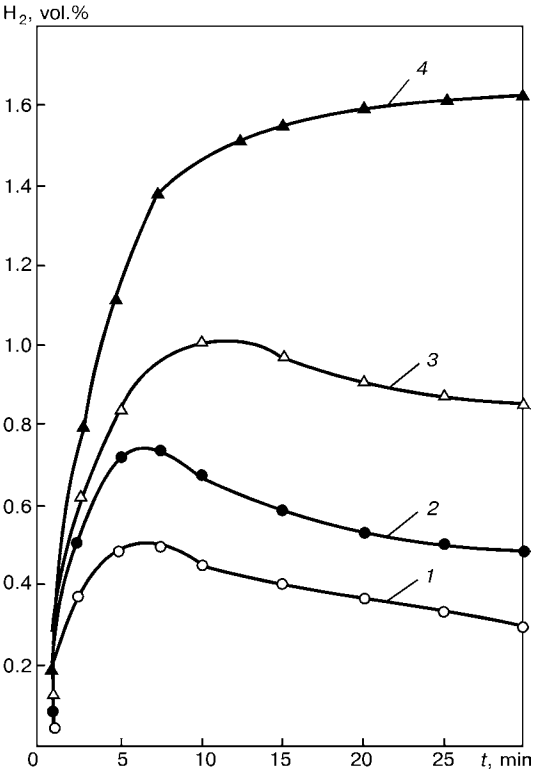

Figure 6. Dependence of hydrogen content in gas phase in a pressed billet melting on change in current load at plasmatrons: 600 (*1*), 800 (*2*), 1200 (*3*) and 1600 (*4*) A

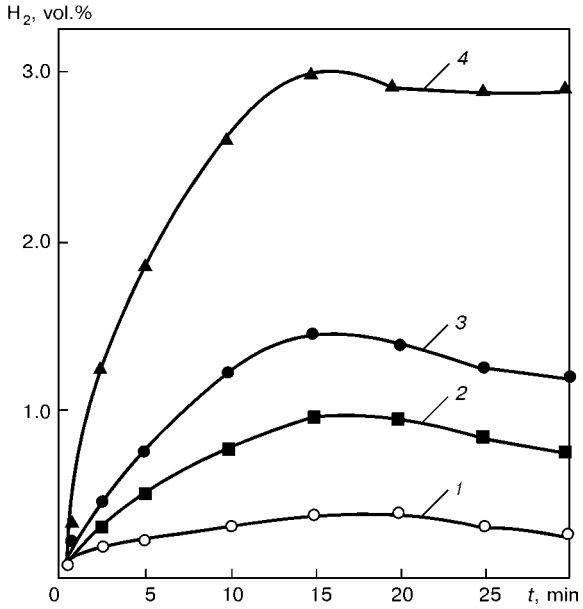

Figure 7. Variation of hydrogen content in the furnace gas atmosphere in remelting of billet taken from packing in a day of melting (*1*) and after storage during 1 (*2*), 2 (*3*) and 4 (*4*) days

from 300 to 400 A at each of four plasmatrons. The obtained data are presented in Figure 6. It is seen from the Figure that with increase in supplied power the maximum content of hydrogen is increased from 0.35 up to 0.80 vol.% and then it is decreased gradually. The increase in hydrogen content in this case can be explained by the intensified effect of more powerful arcs on the chamber walls and billet being remelted, that intensifies the processes of moisture evaporation and its interaction with a molten titanium.

Then, we have studied the hydrogen behavior in melting of the consumable electrode having different terms of storage in the open air. Melts were performed at a speed of the billet feeding of 2 mm / min, 300 A current at each of four plasmatrons and 4.5 l / min argon consumption.

As the curves of hydrogen behavior in remelting of billets, stored in the open air from one to four days, showed (Figure 7), the maximum amount of hydrogen is increased from 0.2 vol.% in melting conductance in the day of electrode removal from a sealed pack up to 3.0 vol.% at its storage up to four days.

It was stated in determination of hydrogen content in cast samples that its concentration in metal is varied from 0.01 to 0.0198 wt.% and, in accordance with the Sieverts law, depends on a partial pressure of hydrogen in the zone of melting, but exceeds the equilibrium. This confirms the results obtained earlier [6].

Analysis of results of experimental melts confirms also that the amount of a supplied pure argon into melting chamber is the only and effective technological procedure which leads to the reduction of hydrogen content in the cast metal.

The measurements of moisture amount in the composition of the used plasma-forming gas showed that its maximum content in the furnace atmosphere in remelting of the pressed billet from the spongy titanium TG100 is increased from 30 up to 60 ppm with increase in plasmatrons current from 600 up to 1600 A. Similar relationships were obtained in remelting of pressed billets at terms of storage from 1 to 4 days. With change in a rate of the pressed billet movement into the zone of melting from 2 up to 7 mm / min the maximum content of moisture is increased in the ranges of 32–53 ppm.

Analysis of behavior of the moisture microimpurities in plasma melting showed that the most effective method of reduction in moisture content, as well as in hydrogen, is the feeding of a large amount of a pure plasma-forming gas.

1. Andreev, A.L., Anoshkin, N.F., Borzetsovskaya, K.M. et al. (1978) *Melting and casting of titanium alloys*. Moscow: Metallurgiya.
2. Lakomsky, V.I. (1974) *Plasma-arc remelting*. Kiev: Tekhnika.
3. Movchan, B.A., Tikhonovsky, A.L., Kurapov, Yu.A. (1973) *Electron beam melting and refining of metals and alloys*. Kiev: Naukova Dumka.
4. Kleites, P.J. (1973) Induction-vacuum remelting. In: *Vacuum metallurgy*. Moscow: Metallurgiya.
5. Latash, Yu.V., Konstantinov, V.S., Galkin, P.N. et al. (1985) Application of plasma-arc technology in melting of titanium ingots from titanium manufacturing waste. *Problemy Spets. Elektrometallurgii*, **3**, 65–70.
6. Grigorenko, G.M., Konstantinov, V.S. (1979) Interaction between hydrogen and molten titanium in plasma melting. *Ibid*., **8**, 97–101.

APPLICATION OF BOTTOM POURING IN PLASMA-ARC SKULL MELTING

V.A. SHAPOVALOV, Yu.A. NIKITENKO and **V.R. BURNASHEV**
E.O. Paton Electric Welding Institute, NASU, Kiev, Ukraine

The article describes feasibility of application of a bottom pouring out of metal in use of refractory ceramic materials and plasma-arc melting in a copper water-cooled crucible, and also protection of the copper crucible from the action of a direct plasma flow.

Keywords: *refractory materials, plasma-arc melting, skull, copper water-cooled crucible, amorphous and microcrystalline metals*

There are many methods of casting of steels and special alloys in the modern metallurgy, a bottom pouring out is among them. The main drawbacks of this method are the use of a gate, thus complicating greatly the design and service of the furnace. The advantage of a bottom pouring out, as compared, for example, with pouring out at a unit inclination or with an intermediate crucible, consists in metal pouring from a molten pool center, that contributes to reduction in content of non-metallic inclusions in the casting, because entrapping of some amount of slag and oxide films in molten metal is possible at the overflow of metal beyond the edge of the melting unit that leads to inhomogeneity of ingots and different types of defects.

In the present work the bottom casting of metal to a drum-cooler was used for producing thin strips with an amorphous and microcrystalline structure (method of spinning) to reduce the distance from the melt to the drum-cooler to minimum. This technological diagram eliminates the formation of crystalline nuclei in melt and improves the conditions of amorphization. Arrangement of a pouring nozzle in the lower part of the molten pool provides a continuous feeding of metal under the excessive pressure of gas and natural gravity force and, consequently, a flow continuity. Thickness of strip, as well as properties of products, depend greatly on the rigidity of structure and value of a gap between the pouring nozzle and drum-cooler [1]. The process of spinning itself consists in metal melting, its «extrusion» under excessive pressure of inert gas through a forming slot to the drum-cooler and rapid quenching. In the world practice [2, 3] a thick-walled ampoule of refractory ceramics, quartz more often, placed into electromagnetic field of the inductor, is used to produce this type of the products.

Materials, which have a contact with molten metals in the melting unit, can be divided into oxide, carbide and metallic materials.

Interaction with oxide materials. These materials (Table 1) can consist of pure refractory oxides or mixture of oxides. The main criterion of selection of one or another refractory is its temperature of melting and softening, moreover, these temperatures are lower in refractories, consisting of several components, than in pure oxides. A complete loss in the material strength is associated with the temperature of melting, while the occurrence of mould deformation at 0.2 MPa stress is due to the temperature of softening. As the practice shows, the temperature of softening the refractory ceramics is one of the main criteria in selection of alloys to be subjected to working. In operation of refractories at limiting temperatures the rigidity of structure is violated, and at the final stage of spinning it can lead to its failure when the excessive pressure of gas is abruptly supplied into the heated ampoule. At high temperatures the dimensions of the ampoule are also increased due to a total coefficient of linear temperature expansion (CLTE) that disturbs the fine settings of the process and makes pouring out poorly controllable. It is possible to increase the structure rigidity by increase in thickness of ampoule walls, but this increases the power consumption depending on the magnetic permeability of the material. Oxide materials possess a rather low heat conductivity, and the rapid metal heating in electromagnetic field of

Table 1. Properties of some oxide materials used in melting units

Parameter	SiO_2	MgO	Al_2O_3	CaO	Cr_2O_3	ZrO_2	$3Al_2O_3 + 2SiO_2$
T_{melt}, °C	1730	2800	2050	2980	2440	2700	1830
T_{soft}, °C	1400	2000	1950	2400	2000	2500	1750
ρ, kg / m^3	2.30	3.60	3.90	3.32	5.21	5.60	3.16
$\lambda_{100\ °C}$, W / (m·K)	0.0038	0.0860	0.0540	0.3640	–	0.0046	0.0129
$CLTE_{25–1000\ °C} \cdot 10^{-6}$, °C^{-1}	13.9	11.4	8.0	13.9	–	7.2–8.1	5.5

Table 2. Properties of some carbide materials used for lining

Parameter	TiC	ZrC	SiC	NbC	$Â_4Ñ$
T_{melt}, °Ñ	3257	3530	2205	3613	2450
ρ, kg / m^3	4.93	6.72	3.20	7.56	2.50
$\lambda_{100\ °Ñ}$, W / (m·K)	0.041	0.049	0.019	0.034	0.07–0.20
$CLTE_{25–1000\ °Ñ} \cdot 10^{-6}$, °C^{-1}	7.95	7.01	4.74	7.21	4.50

the inductor leads to the expansion of the internal surface without change in external dimensions and, as a consequence, to cracking and failure of the ampoule.

Insufficient refractoriness of the material is one of causes of a mechanical fracture of lining and melt contamination with large foreign particles of non-metallic inclusions which in this case are called exogenous, emphasizing their external origin as regards to the melt.

When the refractory materials are applied, the following important problems are faced, such as their reactivity and formation of non-metallic inclusions in the melt. Interaction of metal melts with oxide refractory materials by Me + RO = MeO + R reaction is most hazardous. The reduced element is dissolved in metal melt and contaminates it. The forming oxide of metal can dissolve in the melt, remain in a free state or form an alloy with a refractory oxide. Similar interaction is observed in attempts to melt the magnesium alloys on oxide lining containing silicon oxide SiO_2. This results, as is known, in failure of lining and contamination of the melt.

A large role in interaction of melts with refractory materials is played by the phenomenon of wetting, which precedes usually the chemical interaction. Pure metals have a poor wetting at the absence of chemical interaction with refractory oxides. Chemical interaction of melt with lining and its wetting with melt causes so-called metallizing of the lining. This phenomenon consists in the fact, that, if the melt does not react chemically with the lining, the metallizing occurs only by impregnation of a porous lining with the melt. This is expressed outwardly in the change of color of a lining layer adjacent to the melt and in significant increase in its physical density. If the chemical reaction is possible between the melt and oxide lining, the interphase energy is reduced to zero, the surface tension is decreased respectively, and the spontaneous suction of melt into pores is occurred.

Interaction of metal melt with oxide lining can be accompanied also by such phenomenon as lining corrosion which is explained by the appearance of a molten alloy of metal oxide MeO with lining oxide RO. The appearance of this molten alloy is possible, if there is a region of fusible compositions in the MeO–RO system and melting is performed at the temperature exceeding their melting point. To avoid the lining corrosion, it is necessary to select such material for the melting unit that the temperature of melting was much lower not only of melting points of refractory material oxides, but also of possible eutectic temperatures in MeO–RO systems.

Interaction with graphite, carbide and metal materials. Graphite itself is able to work at temperature up to 2500 °C, however, in air, starting from 600–700 °C, it burns out very quickly and is evaporated in vacuum at the temperature above 2200 °C. The main feature of graphite materials consists in a capable dissolution of carbon in metal melts. The graphite refractories are quite suitable for melting the fusible metals, including copper and its alloys, however, it is necessary to protect them from oxidation starting from 600 °C for a long-term operation.

Carbides of transition materials (Table 2) refer to the class of metal-like refractory compounds, being classical representatives of a group of interstitial phases, in which the atoms of carbon are located in voids between the atoms of metals, densely packed into lattices with a cubic or hexagonal symmetry. They possess high temperatures of melting, metal conductivity, low rate of evaporation at high temperatures, but in air or other oxidizing gas media they are easily fractured at temperature above 500–600 °C. Carborundum materials consist of more than 80 % of carborundum –– silicon carbide SiC, and the rest is a binder of refractory oxides. These materials are sufficiently refractory (above 1800 °C), chemically resistant (in air up to 2000 °C, inclusive), they are poorly wetted and difficult in interaction with molten metal.

Among metallic materials, used for manufacture of melting units, only steel and cast iron are widely used. It is clear that the melting crucibles made from these materials can be used only for casting of metals and alloys at a melting temperature commensurable with a temperature of iron melting. Simultaneously, it is necessary to take into account the feasibility of iron dissolution in melt, and the information about this can be obtained from the state diagrams of iron–molten metal systems.

Melting in a skull crucible. Problem of a direct oxidation-reduction (redox) reaction between the molten metal and refractory lining becomes almost unsolved in case of application of refractory metals, starting from titanium. All the refractory metals of the IV–VI groups of the periodic system are so active as regards to oxygen, that no refractory oxides withstand the action of their melts.

The high activity in combination with a high refractoriness of these metals made to use a special method of melting using a water-cooled melting crucibles, playing simultaneously the role of moulds, and also such powerful heat sources as plasma-arc and electron beam sources. There are no refractory materials in these melting installations. The melt contacts the solid crust, growing from a metal surface and cooled with water from the opposite side. Working walls of the mould are made usually of copper. Owing to the water cooling the copper wall at the working surface is heated up to 300–400 °C, therefore, the metal melt, contacting such a «cold» wall, is solidified at once, forming the so-called skull. Melting is performed without a direct contact of melt with a copper jacket [4].

In our case it was impossible to avoid the interaction of melt with refractories in melting in a copper water-cooled crucible, because the pouring out was realized through a changeable ceramic nozzle. However, the application of the refractory ceramics in this

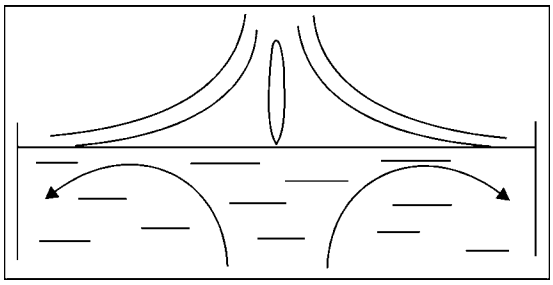

Figure 1. Stirring of molten metal pool in plasma-arc melting

variant allowed us to reduce greatly the area of contact of melt with refractory materials, preserving here the rigidity of the structure. Minimum size of the nozzle (5 mm) gave an opportunity to reduce also the total linear expansion in heating. The application of plasma-arc heat source allowed us to perform melting in a protective atmosphere of inert gas and to refine simultaneously the melt from non-metallic inclusions.

The refractory material for manufacture of an insert-nozzle is selected from the conditions of its heat resistance and degree of reactive interaction with the melt. In a perfect case the molten metal should not wet the ceramics and form a chemical compound with it, but this is almost impossible in practice as the alloys, subjected to working, have complex compositions and ceramics consist of several refractory compounds.

Different types of interaction between the melt and nozzle lead to the slot washing out. Due to this, the shape and amount of flowing molten metal are changed, and, consequently, the defects in strip shape are appeared in the form of roughness of surface and edges, freezing of drops, difference of thickness both in width and length.

The metal heating from the top by the powerful source causes the natural convective flows in a pool, dissipating the heated masses from its surface and supplying the colder masses from the depth of layers. The water-cooled crucible and dynamic pressure of gas contribute greatly to the formation of macroflows in the melt which predetermine the pool shape (Figure 1), therefore, the crucible is tried to be made of a larger diameter to increase the area of a possible contact of a plasma flame with a molten metal pool.

The effect of crucible volume on the coefficient of molten metal pouring out (ratio of mass of poured out metal to mass of total molten metal) at optimum specific heat power was described in detail in work [5]. To maintain the optimum volume of the molten metal and to provide the required its overheating the coefficient of a crucible shape, which is determined as a ratio of crucible depth to its diameter, was selected equal to 0.2–0.4. This technique gave an opportunity to produce the pure metal, to maintain a stable gap between the nozzle section and drum-cooler surface in accumulation of large volumes of molten metal, and also a constant rate of metal flowing out. Excessive increase in transverse sizes of the crucible will lead to the metal freezing near the crucible walls and, in general, to the impossibility of melting metal having the contact with cold walls.

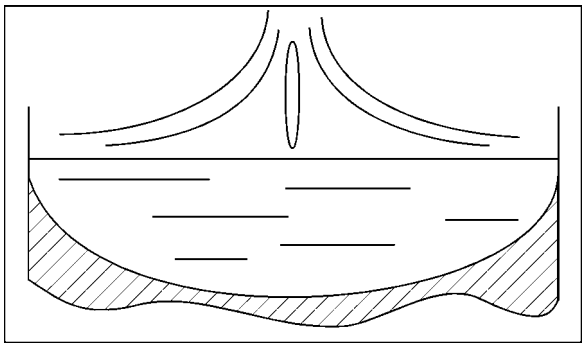

Figure 2. Partial metal melting in a vertical axis

Taking into attention, that transfer of heat energy in the molten metal is realized downward from a large area, the molten metal pool is made shallow as to the width. Consequently, it is rational to make the crucible deeper, otherwise a solid crust of metal on the pool bottom is formed and metal pouring out through the bottom will become impossible (Figure 2). To increase the coefficient of pouring out, the crucible is made also in the form of an assumed pool with a rounded bottom (Figure 3), that provides a more uniform distribution of temperature and complete melting of the metal.

From the other side, such powerful source of heating as plasma-arc source, can become a cause of fusion of the copper crucible itself at a complete pouring out of the melt. Later on, this will lead to the contamination of molten metal with copper and to the crucible replacement. Otherwise, at next use of this crucible and multiple fusion of the working surface the burn-through of water-cooling channels and accident can occur.

There is one and very simple method of the crucible protection, namely a partial pouring out the metal at which the arc is burning towards the molten metal, not damaging the crucible. However, for melting and casting of small volumes of metal, when the pouring out takes several seconds, it is very difficult to find a moment for interruption of casting or switching on of the plasmatron. The automatic switching off at the moment when some metal is still remained on the

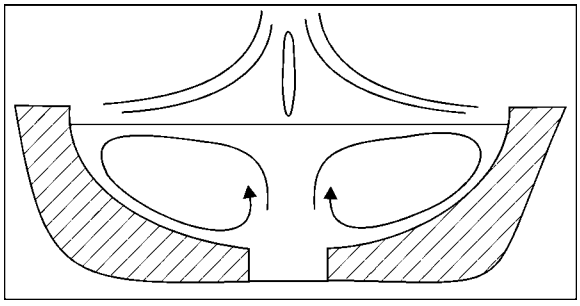

Figure 3. Rounded shape of a skull crucible

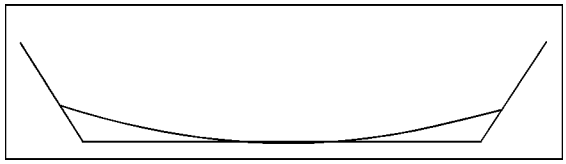

Figure 4. Optimum section of a water-cooled crucible in plasma-arc skull melting with a bottom pouring out

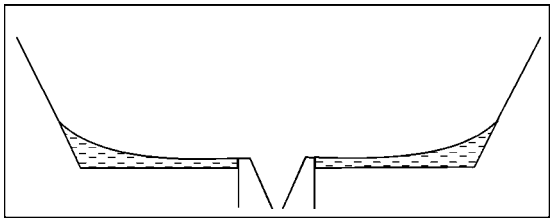

Figure 5. Method of crucible bottom protection from fusion by a uniform distribution of a non-poured metal

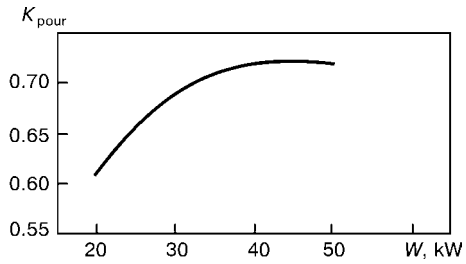

Figure 6. Dependence of coefficient of pouring out K_{pour} on the plasmatron capacity W for alloy 10NSR

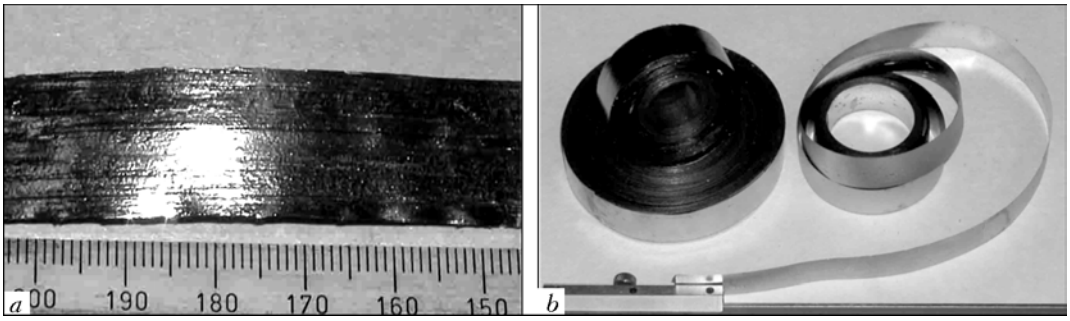

Figure 7. Appearance of strips produced from alloys 10NSR (*a*) and PN-88 (*b*)

crucible bottom is rather difficult due to a negligible change in power parameters and rapid proceeding of the pouring out process, therefore, the switching off has to be made manually, that can lead to an accident.

We have selected another solution of this problem, namely to make the crucible bottom flat (Figure 4). This has led to a partial freezing of metal in the crucible corners and decrease in coefficient of pouring off (Figure 5), but allowed us to remain a guaranteed part of non-poured metal and to protect the crucible bottom. For fluid alloys the pouring nozzles are made longer, this resulting in automatic interruption of pouring out, when the level of melt is lowered to the nozzle (Figure 6) and, thus, protecting completely the crucible bottom.

Thus, the use of ceramic materials as melting units is connected with a number of difficulties which can be avoided in plasma-arc melting. The application of the plasma-arc heating and cold crucible provides a complete heating of the metal and stable pouring out and allows also metal refining from non-metallic inclusions in a controllable atmosphere. Problems, connected with a plasma-arc melting and protection of the melting crucible, are solved quiet simply by the selection of optimum geometric sizes of the crucible, which makes the bottom pouring controllable and safe.

Producing of quality strips, wires, flakes is based on a clear representation and understanding of the process of melting, knowledge of physical-chemical properties of metal and nozzle material. Determining factors, as a rule, are the casting properties of the alloy, subjected to working, such as melting temperature, fluidity and susceptibility to film formation. Important parameters are also wetting of ceramics with a melt and physical and chemical processes proceeding in this case. All the rest technological parameters of melting and pouring out depend on such characteristics of metal as width of slot, gap height, number of drum revolutions, excessive pressure in chamber in pouring out and others.

The main branch of application of amorphous and microcrystalline strips is the manufacture of hard-to-deform brittle brazing alloys, which are difficult to manufacture in the form of rolled products by the conventional methods of plastic working, therefore, they are used in brazing in the form of powders or rather large castings. Methods of super-rapid quenching allow solution of four important problems simultaneously: manufacture of strips and wires, convenient for application in the process of brazing; fixation of different proportions of components and preserving of a non-equilibrium composition in a solid state; uniform distribution of alloying components over the entire section of strip; producing of amorphous structure necessary for the improvement of the quality of brazed joints.

Technology of the plasma-arc skull melting with a bottom pouring out allows producing of amorphous and microcrystalline strips with a sufficiently wide range of compositions. As an example, Figure 7 presents the strips produced from alloy 10NSR and brittle brazing alloy on nickel base PN-88 of 50–60 μm thickness and 15 mm width.

1. Torkhov, G.F., Granovsky, V.K., Rejda, N.V. et al. (1990) Plasma-arc installation for producing of strip of amorphous materials. *Problemy Spets. Elektrometallurgii*, **2**, 78–80.
2. Qchin, P., Dezellus, A., Plaindoux, Ph. et al. (2001) Rapid solidification techniques applied to the preparation of shape memory alloys. In: *Metal physics and advanced technologies.* Special issue, Vol. 23, 83–92.
3. Zhadkevich, M.L., Shapovalov, V.A., Torkhov, G.F. et al. (2003) Producing of amorphous and nanocrystal materials using plasma-arc heating (Review). *Advances in Electrometallurgy*, **4**, 28–33.
4. Kurdyumov, A.V., Pikunov, M.V., Chursin, V.M. et al. (1986) *Manufacturing of non-ferrous castings*. Moscow: Metallurgiya.
5. Demchenko, V.F., Granovsky, V.K., Tarasevich, N.I. (1980) Study of process of molten metal pool formation in plasma-arc skull melting using computer. *Problemy Spets. Elektrometallurgii*, **12**, 96–100.

DEFINING OF PERSPECTIVE TRENDS IN DESIGNING OF LARGE-CAPACITY FURNACES FOR PRODUCTION OF LARGE-SIZED TITANIUM CASTIGS

A.N. PANOV
Research Institute of Structural Materials «Prometej», St.-Petersburg, Russia

From results of investigations the most rational variant of design of a skull 7 t capacity furnace was defined. Possible variants of large-capacity furnaces and rationality of their design from the point of view of nature of melting the different-diameter consumable electrodes and thermal and hydrodynamic processes proceeding in molten pool of crucible of different capacity were considered.

Keywords: *vacuum-arc and melting-casting unit, consumable electrode, crucible, melt, skull, molten pool, furnace*

Over 40 years the Research Institute of Structural Materials «Prometej» is dealing with designing of vacuum-arc melting-casting units for production of shaped castings from titanium-base alloys for products of ship-building and power engineering, operating under conditions of a long-term effect of aggressive media.

Routine of production of unique large castings from titanium alloys showed that capacities of melting-casting units, put into service, were behind the continuous demands of industry for a single mass of the metal being melted. Over the recent year the works are carried out at «Prometej» for designing the melting-casting units of the new generation with wide technological capabilities, more sophisticated characteristics of proceeding heat processes, and also works on defining the ways of creation of large-capacity furnaces on the basis of the available industrial experience gained in service of operating furnaces.

The present work is a constituent part of these perspective investigations. It was fulfilled to analyze the possible variants of large-capacity furnace, to define the optimum capacity and most rational design solution.

Variants of furnaces designing. At present two types of melting-casting units, in which the consumable electrodes are used as charge materials, are applied in the national melting practice for manufacture of shaped castings from titanium and other refractory metals. By the principle of metal casting, they are divided into furnaces with casting after interruption of arc discharge burning and furnaces at arc burning to the melt. These technical and technological advantages of furnaces with casting «without arc break», as a feasibility of active effect on overheating of melt to be subjected to casting, relatively small height, low metal consumption, reliability and safety in operation and simplicity in maintenance, give grounds to consider that the method of melt casting at burning arc will be basic in the creation of new designs of skull melting-casting units.

The traditional single-crucible diagram has found the most wide spreading in industry, on the basis of which a variety of melting-casting units, different both in capacity, and also in the method of metal casting, was created. Two-crucible diagram was realized in the design of furnace «Neva-5», the largest furnace at the present time. Possibilities of design of furnaces by multi-crucible (more than two) diagrams did not find a worthy attention until now, though the producing of a preset mass of metal can be provided using both one and also several crucible units, producing in total the required amount of metal required for casting into moulds.

Therefore, 1-, 2-, 3 - and 4-crucible variants as a possible designing of a large-capacity furnace were taken by us for consideration. The feasibility to increase the number of crucibles above four was not considered because of design difficulties in installing the units of a crucible rotation mechanism.

To define the furnace capacity, the calculation of melt mass at different depth of the molten pool was made with allowance for existing capacities of preparatory casting: consumable electrodes of 100–160 mm diameter and 600–1200 mm diameter ingots of the first remelting, which can also be used as electrodes (Figure 1).

The routine of service of «Neva-4» furnace showed that the real depth of the molten pool can exceed significantly the recommended depth ($h_{m.p} = 0.5d_{m.p}$) [1] and reach 0.8 of its diameter, therefore, coming from the results obtained, it can be stated that at $h_{m.p} = 0.8d_{m.p}$ the mass of molten pool will be 7476 kg in use of one consumable electrode of 1000 mm diameter, 7652 kg in use of two electrodes of 800 mm diameter, 7368 kg in use of three 690 mm diameter electrodes and 8216 kg in melting of four electrodes of 650 mm diameter. Thus, it seems to be theoretically feasible to design a skull furnace that will produce the molten pool of a total capacity of about 7 t.

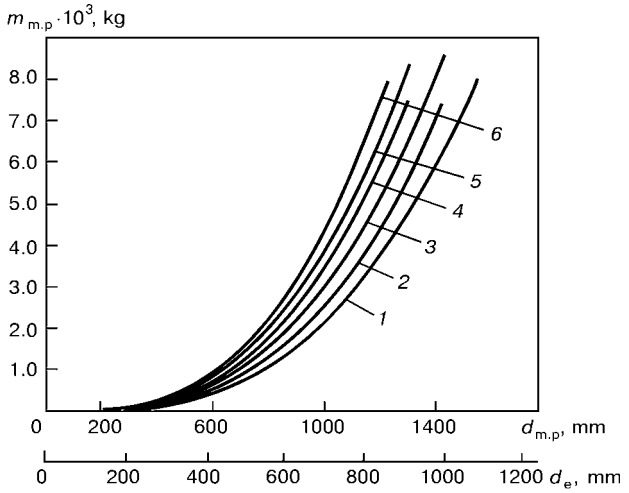

Figure 1. Dependence of molten pool mass on its diameter at ratio $d_e / d_{m.p}$ = 0.7 and depth of molten pool $h = 0.5d_{m.p}$ (*1*), $0.6d_{m.p}$ (*2*), $0.7d_{m.p}$ (*3*), $0.8d_{m.p}$ (*4*), $0.9d_{m.p}$ (5), $1.0d_{m.p}$ (*6*)

To select the optimum variant of design, it is necessary to study the technical, heat-engineering and economic factors of each of the above-described variants.

Study of nature of melting consumable electrodes of different diameter. The nature of heat processes was studied for 600–1200 mm diameter electrodes, which were seldom used earlier or not used at all in the routine of casting manufacturing. The investigations were carried out using analytic methods of analysis of heat processes allowing prediction of their proceeding in electrodes and pools with increase in a scale factor on the basis of results obtained in conductance of melting in furnaces of a lower capacity. The ratio of diameter of electrode and pool was taken standard for a skull melting, i.e. 0.7.

Calculations were performed for a final stage of melting, when the processes of heat transfer are transformed into a quasi-stationary state, that makes it possible to use formulae used for the stationary state. The determination of axial temperature field of the consumable electrode in a steady condition was made by formula of Prof. Rykalin [1, 2]:

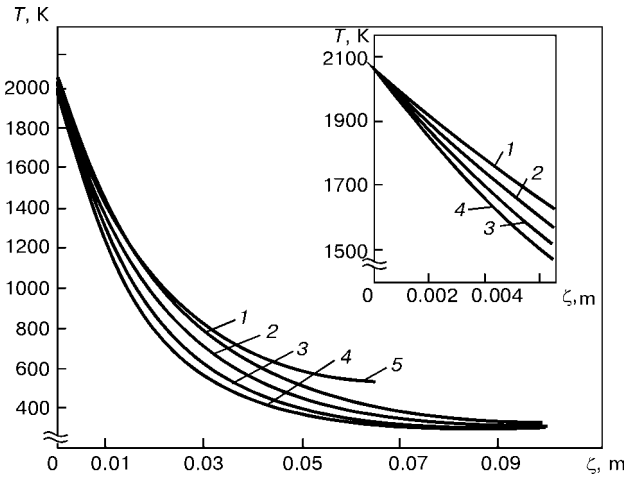

Figure 2. Temperature field of electrode at different linear rates of melting: 1.2 (*1*), 1.4 (*2*), 1.6 (*3*), 1.8 (*4*) m / h; *5* — data of [1]

$$\dot{O} - \dot{O}_0 = (\dot{O}_{end} - \dot{O}_0)\, e^{\frac{-v\,\zeta}{a_m}},$$

where T_0 is the initial temperature; T_{end} is the temperature of surface of melting end; v is the linear rate of melting; ζ is the coordinate of section, calculated from the melting end; a_m is the coefficient of thermal diffusivity.

Heat fields of large-diameter consumable electrodes at 1.2–1.8 m / h linear rates of melting, used in a skull melting, were calculated. It was established that mode of patterns of temperature fields of electrodes of different geometric parameters is identical and does not depend on time (Figure 2). There is a 1.0–1.5 mm thick layer of the molten metal at the end of the consumable electrode, from which the drops are formed, overheated somewhat higher than liquidus in the process of formation. When the drop mass exceeds the surface tension force, it is detached, and, passing the zone of arc discharge, falls onto the molten pool mirror. The main temperature drop is observed at the area of 60 mm length, it reaches approximately 400 K at the depth of about 100 mm. Moreover, with increase in a linear rate of melting the more abrupt reduction in temperature along the length of the examined area of electrode and decrease in thickness of melt layer at the heated end are occurred. Thus, an approximate thickness of melt layer at the fused end was determined and a stub length, required for prevention of holder heating, and, consequently, the efficient length of the consumable electrode for melting conductance were established.

Investigation of heat and hydrodynamic processes in molten pool of skull crucibles of different capacity. Study of hydrodynamic processes are carried out on different models because of impossibility of visual observation of their proceeding, and also by use of thermocouples for measurement of temperatures.

It was considered for a long time that the heat transfer in the pool volume is occurred, due to drop of temperatures, by a convective transfer from the mirror surface along the lateral skull downward to the bottom skull. Here, the intensity of hydrodynamic processes and heat transfer can be increased by setting the solenoid magnetic field to the pool, resulting in stirring of the pool under the action of centrifugal forces and intensive supply of a hot melt from a central (under-electrode) zone of the mirror to the lateral skull. It was also considered on this basis that metal on mirror has the highest temperature, and metal on the molten pool bottom has the lowest temperature, close to the melting temperature [3].

Later on, the information has appeared in literature about the presence of a thermal nucleus in the volume of pool, surrounded by a thermal boundary layer [1]. Movement of metal in them in the pool of the skull crucible is characterized as turbulent, accompanied by the intensive stirring of melt in the horizontal and vertical planes, however, the factors

are not defined which predetermine the processes proceeding by this scheme.

To create an objective pattern of a hydrodynamic molten pool and proceeding of heat transfer processes in it, the results of study of effect of current, passing through the melt pool, and disturbing factor of magnetic masses on the mode of liquid motion, made at the E.O. Paton Electric Welding Institute on models, where mercury was used as an operating liquid, were analyzed [4]. At «Prometej» the investigations of nature of proceeding of the hydrodynamic processes in the molten pool volume at falling the jet of the molten metal on its surface, and also the direct observation of the processes on the pool surface were performed using the method of hydromodeling, and the indirect data from results of melting and skull condition were studied.

The carried out analysis gives an opportunity to offer the following scheme of proceeding of hydrodynamic processes stipulating the heat processes in the melt pool and processes of heat transfer to the skull (Figure 3).

The determinant factor of hydrodynamics of the pool is the flow of melt, falling in the form of a drop rain from the end of the consumable electrode onto the mirror. This forms a column of the hottest metal (thermal nucleus) in the pool volume, which is equal to the diameter of the consumable electrode and surrounded by a thermal boundary layer of melt, in which the melt movement occurs with the much lower intensity. The depth of pool piercing is defined by the force of pressure of melt jet against the mirror and depends on the linear rate of electrode melting. In melting at an increased rate the head part of the thermal nucleus can reach the pool bottom at the initial period and cause the pre-melting of the skull. This can be also caused by increase in a linear rate of melting above the optimum values during the melting. At normal conditions, the head part of the thermal nucleus does not contact a bottom skull, but it is removed from it by a transition layer.

The second factor, intensifying the pressure on melt and contributing to the formation of a thermal nucleus is the current passing through the pool from the mirror to the bottom. At the region of the head part of the thermal nucleus the melt is lifted by a counterflow along the nucleus surface to the mirror, then it is forced out to a lateral skull by convection and, by gradual cooling, it is lowered to the crucible bottom, where it is trapped by a flow of metal lifting by a counterflow over the nucleus surface. Thus, the thermal nucleus preserves its shape during melting, changing only its position in height and slightly mixed with a rest part of the melt, concentrated in the transition zone that promotes the overheating preserving. Determinant factor of heat removal to the skull is the thermal boundary layer located between the upward flow and skull.

The superposition of solenoid magnetic field on the pool leads to the melt rotation under the action of centrifugal forces. The mirror surface of the molten

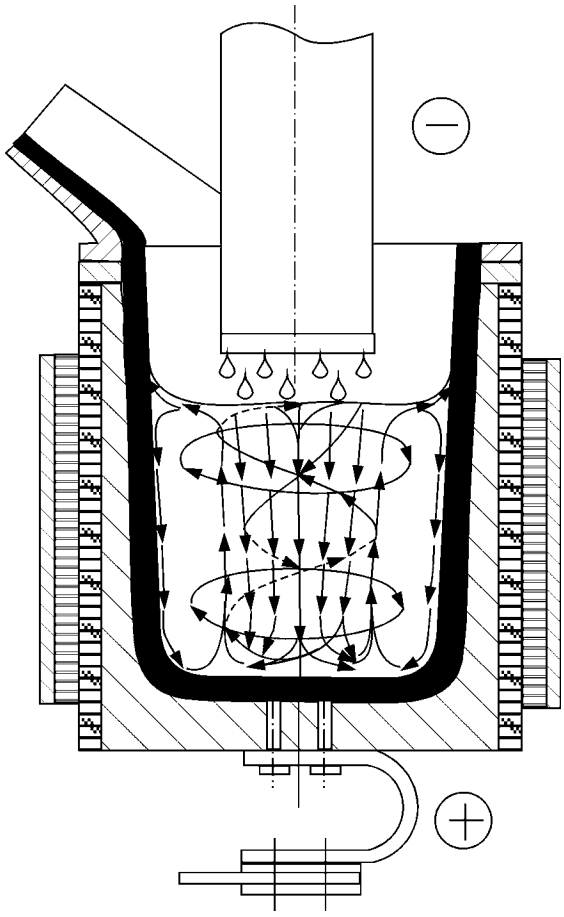

Figure 3. The offered scheme of proceeding of hydrodynamic processes in a skull crucible with solenoid

pool acquires concavity due to increase in the level of melt in the zone of the lateral skull and its decrease in the crucible axial zone, and the area of a decreased pressure is formed. This contributes to the deeper penetration of the overheated metal into the molten pool layers, and the upper part of the thermal nucleus acquires the shape of a truncated cone. The assumption was made during investigations that under the action of the solenoid magnetic field, the direction of melt movement in a thermal nucleus, in counterflow, and also the circulation on a circular contour form the helical lines.

Thus, the magnetic field of the solenoid intensifies the hydrodynamic processes, but its contribution to their development is not decisive due to a short-time rotation of melt in one direction. The most important factors, stipulating the proceeding of hydrodynamic and heat processes are the pressure of melt flow, falling from the consumable electrode end onto the mirror, and direct current passing through the pool.

The presence of a thermal nucleus in the entire height of the pool, where a main overheating is concentrated, and of a thermal boundary layer with a lower temperature explains why the heat removal from pool to skull is uniform in height and will be defined by heat removal from the boundary layer. This allows us to assume that in melting at similar linear rates the specific thermal loads to the skull in

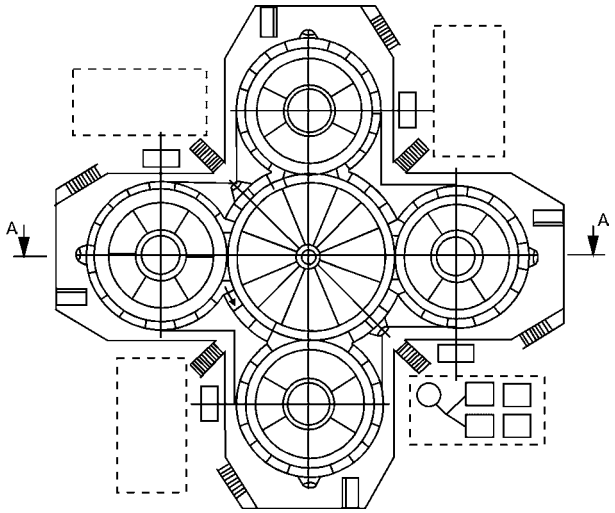

Figure 4. Schematic diagram of 4-crucible large-capacity furnace

large-capacity pools will not almost differ from loads in melting in small furnaces.

The offered scheme of proceeding of hydrodynamic and heat processes shows the basic similarity of the processes occurring in molten pools of large and small skull furnaces, proves the feasibility of producing molten pools commensurable in depth with diameter and explains the differences in design of industrial melting furnaces.

Defining of the most rational variant of furnace design. Analysis of the variants of designs under consideration, shows that, firstly, design of furnace using 1- and 2-crucible scheme will require the use of scarce superpowerful current sources, providing the melting of consumable electrodes of 1000 and 800 mm diameter and maintaining of a molten pool of appropriate sizes.

Secondly, the accumulation of the necessary mass of molten titanium should be made in water-cooled crucibles of 7 or 3.5 t capacity (2-crucible variant), not used earlier in the routine of a skull melting, therefore, to realize these variants the development and mastering of the technology of production of crucibles of a large capacity, which are not manufactured in industry, and also the conductance of research works for the development of optimum power-time conditions will be required.

Thirdly, designing of the crucible of a larger capacity will also be required for the 3-crucible scheme furnace, that is less preferable from the point of view of symmetry of arrangement of crucible units.

So, the variant of furnace using 4-crucible scheme with arrangement of crucibles at 90° angle relative each other around the casting chamber, mounted in the center, seems to be most rational (Figure 4). This will make it possible to use the main composition of completing equipment in the design, which was tested in service of the skull furnace «Neva-5» and manufactured by industry: graphite crucibles, arc current sources, components of vacuum system and consumable electrodes of 600–650 mm diameter.

The application of used units and also a unique experience of multi-scheme and extrascheduled melts in «Neva-5» will reduce the time of manufacture, erection and testing the furnace. Simultaneous accumulation of melt in four crucibles will promote the widening of technological capabilities of producing castings. Thus, the material and finance expenses in furnace construction will be greatly decreased and the period of additional checking of technologically flexible skull furnace for the designed capacity will be reduced.

1. Volokhonsky, L.A. (1985) *Vacuum arc furnaces*. Moscow: Energoatomizdat.
2. Volokhonsky, L.A., Polin, I.V., Novitsky, G.S. (1965) Thermal processes and energy balance of consumable electrode during vacuum arc melting in skull. In: *Vacuum arc melting of metals and alloys*. Issue 5. Moscow: VILS.
3. Bibikov, E.L., Glazunov, S.G. et al. (1983) *Titanium alloys. Manufacturing of titanium alloy shaped castings*. Moscow: Metallurgiya.
4. Paton, B.E., Medovar, B.I., Emelianenko, Yu.G. et al. (1982) Investigation of magnetohydrodynamic phenomena in slag pool during ESR. In: *Problems of special electrometallurgy*. Issue 17.

ABOUT EFFECT OF ATOMIC INTERACTION IN MELTS ON SOLUBILITY OF GASES AND CARBON IN THEM
Part 2. Solubility of hydrogen and oxygen. General conclusions

E.V. PRIKHODKO and **V.F. MOROZ**
Z.I. Nekrasov Institute of Ferrous Metallurgy, NASU, Dnepropetrovsk, Ukraine

Using models of metal melts with BCC-like structure, the solubility of carbon, hydrogen, nitrogen, oxygen and other gases in metal and salt solutions was studied. Close correlations between the solubility a nd integral parameters of atomic interaction were established which allow numerical prediction of solubility of gases and carbon in metal and salt melts of different composition.

Keywords: *solvation, solubility, chemical equivalent of composition, effective charges, physical-chemical modeling*

Results of investigation of atomic interaction with hydrogen participation occupy a special place in the work done by us. From the analysis of comprehensive literature information, having direct or indirect relation to this problem, a conclusion was made (and it was made long ago in works [1–4]), that the description of processes of atomic interaction in hydrogen-containing phases is referred to a number of the most difficult physical-chemical problems, whose solution has a scientific and practical importance for many fields of science and technology. At the same time, the thesis should be recognized justified that the explanation of regularities and results of interaction of hydrogen with other elements in formation of simple compounds at a numerical level is the first necessary stage in study of all the complex of problems connected with atomic interaction of elements with each other. This part of the problem comes far beyond the scope of a private problem about the interaction of some gases with metal and slag melts.

Taking into account the above-described and our positive gained experience of description of effect of electron constitution on structure and properties of molecular and crystalline compounds [5], multi-component metal [6, 7] and salt [8, 9] systems in solid and molten states, we considered that the main aim of investigations carried out was to develop the procedure of numerical calculations of different characteristics of atomic interaction with participation of hydrogen and adaptation of this procedure on the example of analysis of various properties of different materials.

As a working hypothesis, we have taken the hypothesis that all the types of hydrogen interaction with elements of a periodic system, as well as their compounds and alloys should be governed by a single law, common for interaction of any combinations of components both in the presence or absence of hydrogen.

Calculation of parameters of atomic interaction of hydrogen with other elements is possible in the presence of adjusting parameters R_i^0 and tg α in equation

$$\lg R_{i_H}^z = \lg R_{i_H}^0 + Z \text{ tg } \alpha_H, \qquad (1)$$

binding the effective radius with an effective charge of hydrogen.

Selection of numerical values of these parameters was realized using the method of successive approximations and consisted in calculations of their numerical values of integral model parameters Z^Y, d and tg α at different combinations, and also charges of reagents for molecular hydrides of different stoichiometry with a next analysis of effect of these parameters (both separate and also in a set) on main properties of the joints.

On the basis of analysis of data of changing the parameters of atomic interaction of hydrogen with other elements in hydrides of type EH, EH_2 and EH_3 with change in $R_{i_H}^0$ from 0.06 to 0.16 nm and tg α_H from 0.06 to 0.5 the following combination of adjusting parameters was selected: $R_{i_H}^0$ = 0.08 nm and tg α_H = 0.4. Using this parameters, the values $R_{i_H}^{0^+}$ = = 0.0318 nm, $R_{i_H}^{0^-}$ = 0.201 nm were obtained from equation (1).

The most probable values, given in work [10], for covalent, atomic and ion radii of hydrogen, determined by other methods, are 0.032, 0.0779 and 0.208 nm, respectively, i.e. values $R_{i_H}^{0^+}$ and $R_{i_H}^{0^-}$, obtained by equation (1), are in the range of generally accepted values.

Table 1 gives, as an example, the results of calculations of model parameters of structure of molecular hydrogen compounds of different stoichiometry. The subsequent analysis showed that the main properties

Table 1. Model parameters of electron structure of some hydrides

Compound	$d \cdot 10^{-1}$, nm	Z^Y, e	tg α	Compound	$d \cdot 10^{-1}$, nm	Z^Y, e	tg α
BH	1.8826	0.5630	0.299	OH_2	1.5502	0.6179	0.3120
AlH	2.6006	0.6600	0.278	CH_3	1.2280	0.5771	0.3295
InH	2.8388	0.8641	0.253	NH_3	1.3987	0.5533	0.3325
SiH_2	1.7210	0.7977	0.297	PH_3	1.8520	0.6754	0.3238
AsH_2	2.0827	0.8523	0.2945	SbH_3	2.2770	0.8051	0.3185

of molecules of each of isostructural groups are associated functionally ($r > 0.9$) with combination of model parameters. Thus, for example, for hydrides of EH_2 type these relations are realized in the form of equations:

$$d_{ex} = 7.26 - 0.024d + Z^Y - 22.1 \text{ tg } \alpha; \quad (2)$$

$$\omega_e = 450.3d + 554.6Z^Y + 110000 \text{ tg } \alpha - 31745; \quad (3)$$

$$\Delta H = 747.3 - 209d + 670.8Z^Y - 2802 \text{ tg } \alpha, \quad (4)$$

where d_{ex} is the interatomic distance E–H in molecules, 10^{-1} nm; ω_e is the frequency of oscillations, cm^{-1}; ΔH is the enthalpy of formation, kcal / mol. Descriptive models, similar in shape and level of accuracy, were obtained in analysis of molecules of EH and EH_3 types [11].

At the same time, the thesis should be recognized justified [8, 9, 12, 13] that the explanation of regularities and results of interaction of hydrogen with other elements in formation of simple compounds (of types of above-given hydrides) at the numerical level is only the first necessary stage in study of all the complex of problems related to the atomic interaction of elements with each other.

As follows from analysis of Table 2, the effective charges of both hydrogen and also elements interacting with it at the given method of their determination are in the range of acceptable numerical values (from the point of view of classical conceptions of the theory of chemical bonds).

Table 2. Calculated values of effective charges of hydrogen ions in molecules

Molecule	Z_E, å	$Z_ƒ$, å	Molecule	Z_E, å	$Z_ƒ$, å
LiH	0.220	– 0.483	NaH	0.286	– 0.580
BeH	– 0.075	– 0.229	MgH	0.051	– 0.396
BH	– 0.355	0.010	AlH	– 0.103	– 0.274
CH	– 1.100	0.690	SiH	– 0.720	0.276
NH	– 0.895	0.495	PH	– 0.603	0.164
OH	– 0.726	0.330	SH	– 0.486	0.052
FH	– 0.482	0.092	ClH	– 0.296	– 0.130
NH_3	– 1.300	0.285	SH_2	– 0.644	– 0.003
H_2O	– 0.923	0.225	PH_3	– 0.922	0.045
AlH_2	– 0.108	– 0.270	SeH_2	– 0.552	– 0.080
GeH_2	– 0.865	– 0.104	NH_2	– 1.150	0.364
SiH_3	– 0.720	– 0.276	BH_3	– 0.458	– 0.060
AsH_3	– 0.816	– 0.030	SbH_3	– 0.672	– 0.130

Analysis of data, systemized in work [14], about the enthalpies of formation of numerous groups of hydrides of intermetallics produced in interaction of lanthanum and zirconium with elements of iron group (Mn, Fe, Co, Ni) and their analogues (Ru, Rh, Pd), confirmed the validity of procedure, developed in work [15], for expression of thermodynamic properties of melts as the function of model parameters of their electron structure:

$$\Delta H \text{ (kcal / mol)} = 1253.8 - 316.6d - 276.3Z^Y - 73.1\Delta d + 325.8\Delta Z^Y \quad (r = 0.97). \quad (5)$$

Here, the sorption capacity of these materials with respect to hydrogen is described [16] by the equation

$$H / AB = 26.52d - 0.553Z^Y + 42.35 \text{ tg } \alpha - 81.98, \quad (6)$$

where H / AB is the number of atoms of hydrogen per formula unit of the intermetallic.

Let us consider from the similar positions the other experimental data about hydrogen solubility at different pressures P in zirconium alloys. This solubility, designated as X, is associated with a composition of alloys, coded in terms of model parameters (Table 3), by equation

$$X = 8.595 - 0.206P + 9.858d - 8.44Z^Y - 258.5 \text{ tg } \alpha \quad (r = 0.94). \quad (7)$$

Using definite $R^0_{i_H}$ and tg α and physical-chemical model of metal melt, the effect of model parameters of atomic interaction on solubility of hydrogen in different metal melts was investigated.

Thus, representative data given in work [17] about the hydrogen solubility in melts Fe–Al, Fe–B, Fe–Ge, Fe–Ta, Fe–Sn and Fe–Zr at different concentrations of the second component and temperatures are associated with integral parameters of atomic interaction d, Z^Y and tg α and the temperature of dissolution (selected from 228 melts) by the equation

$$[H] \cdot 10^4 \text{ (wt.\%)} = 61.81 + 32.54d - 24.99Z^Y - 165.27 \text{ tg } \alpha + 0.0247T \quad (r = 0.967). \quad (8)$$

Integral parameters of the structure, used in this equation, were calculated with allowance for the hydrogen content. It should be noted that the correlation of hydrogen solubility with parameters of atomic interaction is higher, $r > 0.98$, for each of system separately. Results of comparison of values, calculated by equation (8), experimental values of hydrogen solu-

Table 3. Hydrogen solubility in some zirconium alloys

Compound $Zr_mB_nH_x$	Hydrogen content	$Đ$, MPa	Model parameters of structure of phases (without of hydrogen)			Calculated values X in $Zr_mB_nH_x$
			$d \cdot 10^{-1}$, nm	Z^Y, e	tg α	
ZrV_2	5.40	0.1	3.233	1.935	0.0747	4.80
$ZrMn_2$	3.60	0.8	3.188	1.834	0.0793	3.87
$ZrMn_2$	3.90	1.0	3.188	1.834	0.0793	3.83
$ZrMn_{2.4}$	3.60	2.0	3.168	1.791	0.0796	3.72
$ZrMn_{3.2}$	4.00	3.0	3.138	1.717	0.0801	3.71
$ZrFe_2$	0.16	6.1	3.123	1.760	0.0883	0.44
Zr_3Fe_2	6.40	6.0	3.350	1.763	0.0775	5.47
ZrCo	3.00	0.1	3.240	1.785	0.0855	3.35
Zr_3Co	6.80	0.1	3.370	1.716	0.0798	6.68
$ZrNi_{2.5}$	1.90	2.5	3.126	1.511	0.0983	0.73
ZrNi	2.80	0.1	3.236	1.705	0.0910	2.55
$Zr_{0.36}Ni_{0.64}$	0.58	2.5	3.167	1.602	0.0958	1.01

bility in the above-mentioned melts of iron are presented in Figure 1.

The relation between the hydrogen solubility in melts of iron with carbon [18], vanadium [19], titanium [20], cobalt [21], chromium, molybdenum and nickel [22] at different content of the second component and integral parameters of atomic interaction without allowance for content of a dissolved hydrogen was studied. Correlation of solubility with integral parameters in selection from 79 melts was obtained in the form of equation

$$[H]\ (cm^3 / 100\ g\ Me) = 215.028 + 10.814d + \\ + 2.427Z^Y - 2678.68\ tg\alpha + 0.0122T \quad (r = 0.92). \quad (9)$$

In a graphical form this relationship is presented in Figure 2.

For each from the Fe–Me systems, considered separately, the coefficient of correlation in the regression equation, similar to (9), is at the > 0.96 level. Thus, the melt composition (matrix), presented by convolution in the form of combination of integral parameters of a physical-chemical model (Table 4), defines its absorbing capacity with respect to hydrogen. This gives an opportunity to describe the hydrogen solubility in above-considered systems on iron base [18–22] using one equation (9).

Solubility of hydrogen in each of groups of melts of 3*d*-metals with silicon in Fe–Si–H, Mn–Si–H, Co–Si–H, Ni–Si–H and Cr–Si–H systems, as well as in Ni–Al–H, Ni–Co–H, Ni–Au–H, Ni–Fe–H, Ni–Cr–H systems [23, 24] (Table 5) is associated with the composition of melts by the equation of the type

$$[H] \cdot 10^2\ (at.\%) = a_0 + a_1T + a_2d + a_3Z^Y + a_4\ tg\alpha \quad (10)$$

with a coefficient of correlation > 0.96.

General relationship of hydrogen solubility in the above-mentioned melts of 3*d*-metals with silicon is described by the equation

$$[H] \cdot 10^2\ (at.\%) = -2.174 + 0.024T - 9.915d - \\ - 17.252Z^Y - 293.185\ tg\alpha \quad (r = 0.88) \quad (11)$$

and in melts on nickel base it is described by equation

$$[H] \cdot 10^2\ (at.\%) = 79.647 + 0.025T - 32.674d - \\ - 5.846Z^Y + 3.647\ tg\alpha \quad (r = 0.85). \quad (12)$$

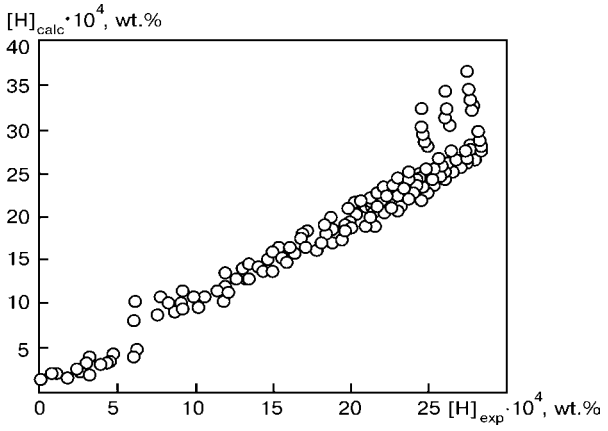

Figure 1. Ratio of experimental and calculated (by equation (8)) values of hydrogen solubility in iron melts with aluminium, boron, germanium, tantalum, tin and zirconium

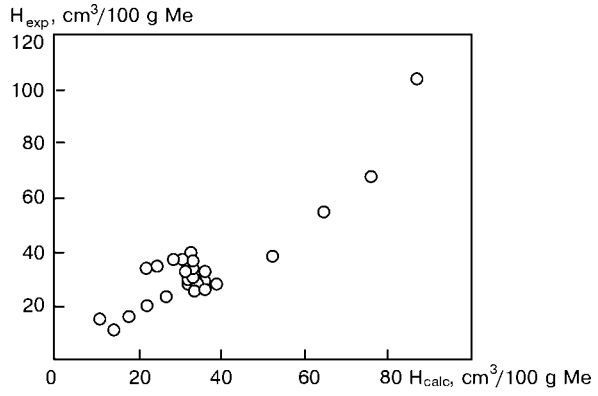

Figure 2. Ratio of experimental and calculated (by equation (9)) values of hydrogen solubility in iron melts

Table 4. Hydrogen solubility in some Fe-base melts and their integral parameters

System	Ì å, wt.%	$d \cdot 10^{-1}$, nm	Z^Y, e	tg α	Ò, °C	H, cm^3 / 100 g Ì å	H_{calc}, cm^3 / 100 g Ì å
Fe–C	1.0	2.6709	1.2066	0.0893	1550	23.38	26.55
	2.0	2.5517	1.2657	0.0906	1550	20.0	21.92
	3.0	2.4573	1.3149	0.0918	1550	16.0	17.80
	4.0	2.3802	1.3557	0.0929	1550	11.08	14.12
	5.0	2.3156	1.3892	0.0939	1550	15.08	10.83
Fe–V	1.4	2.8334	1.1763	0.0878	1560	28.2	32.37
	3.15	2.8403	1.2249	0.0876	1560	29.1	33.10
	4.3	2.8444	1.2557	0.0874	1560	29.5	33.76
	8.0	2.8563	1.3493	0.0869	1560	31.2	35.45
	9.3	2.8600	1.3801	0.0867	1560	32.1	36.10
Fe–Ti	0.42	2.8314	1.1475	0.0880	1605	30.0	32.29
	1.14	2.8379	1.1668	0.0880	1605	32.9	32.41
	1.47	2.8409	1.1756	0.0879	1605	34.2	32.73
	1.79	2.8437	1.1840	0.0879	1605	37.2	32.78
	2.1	2.8463	1.1920	0.0879	1605	39.9	32.83
Fe–Cr	10.0	2.8267	1.4284	0.0857	1600	28.0	39.02
	30.0	2.8289	1.8265	0.0811	1600	38.0	52.34
	50.0	2.8342	1.9927	0.0766	1600	55.0	64.85
	70.0	2.8432	1.9460	0.0723	1600	68.0	76.35
	90.0	2.8592	1.7039	0.0681	1600	104.0	87.19
Fe–Mo	1.0	2.8304	1.1572	0.0878	1590	29.0	32.66
	3.0	2.8362	1.1994	0.0874	1590	28.0	33.90
	5.0	2.8417	1.2414	0.0870	1590	27.0	35.13
	6.0	2.8444	1.2624	0.0868	1590	26.5	35.74
Fe–Ni	1.0	2.8274	1.1534	0.0882	1590	33.0	31.55
	3.0	2.8274	1.1872	0.0886	1590	37.0	30.56
	8.0	2.8276	1.2653	0.0895	1590	37.0	28.34
	16.0	2.8281	1.3713	0.0911	1590	35.0	24.31
	21.5	2.8285	1.4303	0.0921	1590	34.0	21.78

Table 5. Parameters of atomic interaction in some melts of 3*d*-metals and hydrogen solubility in them

System	Me, at.%	$[H] \cdot 10^2$, at.%	*T*, °C	$d \cdot 10^{-1}$, nm	Z^Y, e	tg α
Mn–Si–H	10.0	11.70	1445	2.7918	1.4151	0.0833
	25.0	7.30	1445	2.6532	1.6228	0.0845
	36.9	4.30	1445	2.5730	1.7137	0.0855
	50.0	2.60	1445	2.4964	1.7378	0.0866
	60.0	2.40	1445	2.4391	1.7026	0.0875
	80.0	3.30	1445	2.3053	1.4929	0.0893
	90.0	4.80	1445	2.2143	1.3183	0.0903
Fe–Ni–H	10.3	14.13	1600	2.8255	1.3043	0.0905
	20.6	14.06	1600	2.8265	1.4289	0.0926
	34.8	14.26	1600	2.8232	1.5201	0.0954
	45.8	15.55	1600	2.8299	1.5494	0.0976
	59.4	17.16	1600	2.8328	1.5056	0.1004
	69.7	18.52	1600	2.8359	1.4216	0.1025
	83.9	20.84	1600	2.8423	1.2340	0.1054
	92.3	23.03	1600	2.8483	1.0837	0.1072
	96.8	23.42	1600	2.8520	0.9914	0.1081

Table 6. Thermodynamic and metal-chemical characteristics of oxygen solutions in metal melts

Solvent	$-\Delta H_{[O]}$, kcal / mol	$-\Delta G^{o}_{1873}$, kcal / mol	Characteristics of Me–O bond				
	From data of work [29]		$-\Delta G_{calc}$, kcal / mol	Z_{Me}, e	Z_O, e	Δe, e	ρl_{Me}
Ca	123.9	114.3	102.7	1.832	–1.565	0.367	2.690
Ba	130.0	95.3	109.1	1.866	–1.433	0.433	2.762
Y	131.8	110.7	113.1	1.741	–0.162	1.578	3.821
Ti	128.9	100.0	89.9	1.619	0.770	2.388	4.834
Zr	136.6	103.3	97.1	1.532	0.803	2.336	4.760
Hf	135.7	90.1	94.5	1.498	1.016	2.514	4.964
V	104.5	60.27	70.8	1.492	1.418	2.910	5.550
Nb	95.7	70.08	70.2	1.341	1.660	3.0	5.713
Ta	94.7	66.5	63.7	1.265	1.792	3.057	5.864
Cr	71.2	48.4	44.3	1.340	2.035	2.275	6.298
Mo	60.0	40.0	37.4	1.145	2.317	3.462	6.540
W	47.3	28.6	34.9	1.096	2.368	3.464	6.590

The results obtained can be considered as one more confirmation of validity of the used physical-chemical model of structure of melts and products of their solidification. It is evident, that this circumstance itself, but not only selection of parameters R_i^0 and tg α_i of interstitial atoms, provides the high accuracy of approximation of experimental data. From the other side, calculations for metal–impurity systems as for quasi-homogeneous phases are a rather rough approximation. Selection of scheme of mutual arrangement of atoms of impurity, alloying and matrix subsystems will, undoubtedly, influence greatly the results of these calculations in future. However, there are no yet hopes for receiving such valid information, the values Z_i of impurities are actually virtual states of their electron cloud in perfect interstitial solutions. Nevertheless, this approach is rather effective (especially on the background of usual postulation of charges of components in accordance with conceptions of theory of valency and ion model of chemical bond). Calculated integral and partial characteristics of atomic interaction can be used effectively as parameters of convolution of information about the composition of multi-component systems [25], that is not realizable in the scopes of other numerical methodological approaches to the solution of similar problems.

In particular, as was shown in work [26], the offered methodology was used for analysis and semi-empirical generalization of information about thermodynamic characteristics of the process of deoxidation of metals. Without doubling the fragments of this article, we shall note additionally the following.

It is assumed usually that oxygen forms interstitial solutions with most metals. Therefore, when conducting the calculations, whose results are given in Table 6, it was assumed that oxygen ions are arranged in the interstitial positions at distances a / 2 from ions of metals in structures of appropriate melts.

As a result of analysis several variants of equations can be offered for the given solvents to estimate the Gibbs energy at 1873 °C:

$$-\Delta G^{o}_{1873} = 456.39 + 42.18 Z_{Me} + 94.80 Z_O - 106.04 \rho l_{Me}, \quad (13)$$

where Z_{Me} and Z_O are the charges of ions of metals and oxygen; ρl_{Me} is the charge density at the surface of Me ion (calculated by the procedure of [5, 27]).

Difficulty in the solution of the above-mentioned problem is predetermined, first of all, by significant discrepancies in quantitative estimations of the same parameters in works of different authors. Thus, for example, the estimation of heat of oxygen dissolution in metals by the data of different works are more or less coincided only for the solutions of chromium, molybdenum and tungsten. In other cases the discrepancies are so high that it is impossible to say about the presence of premises for determination of valid numerical values ΔH. Nevertheless, analysis of data, systematized by Kulikov I.S. [28], represents a certain interest from the point of view of checking different

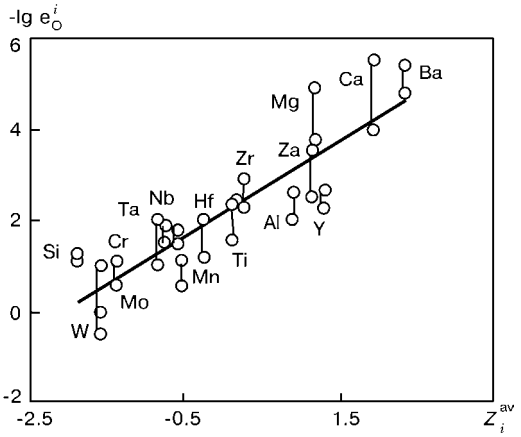

Figure 3. Dependence of parameters of interaction of deoxidizers with oxygen on their charge state in iron melts

hypotheses about most probable positions of oxygen ions in the structure of metal melts.

Surely, the processing of discussion information does not solve completely the problem of estimation of its validity, nevertheless, the comparison of the left and right part (Table 6) in the form of equation (13) will create the base for its future solution.

It is important to consider here the similar relationships not as some individual, isolated, but, in general, as problems of use of integral and partial parameters of interaction for the solution of various problems of physical materials science. As the theory of metallurgical processes has in its disposal these parameters for a long time for calculation of coefficients of activity, the comparison of appropriate thermodynamic information with independent calculation data represents an undoubted interest.

Comparison of these data with those given in literature [29–31] lg e_j^i allowed us to establish [26] that there are clear correlations between them (Figure 3). These correlations, having allowance for the range of scattering the data e_O^i from different data, give an opportunity to consider the problem of estimation of validity of similar information on a radically new basis. Equation was obtained on the base of similar correlations using the method of iterations

$$\lg e_O^i = 2.1Z_i^{av} - 115.7Z_O^{av} - 3.14\Delta e_{i-O} - 192.3, \quad (14)$$

expressing the parameters of interaction of deoxidizers with oxygen as a function of an average charge of each of reagents (deoxidizer Z_i^{av}, oxygen Z_O^{av}) and integral characteristic of hypothetical paired bond between them (Δe_{i-O}) in diluted solution on iron base. Coefficient of correlation is 0.97 between numerical values lg e_O^i, calculated by the equation (14) and most probable (in our opinion). These results confirm the prospects in use of parameters of physical-chemical model of metal melts for the description of processes of atomic interaction with oxygen, proceeding in them.

Let us formulate the main conclusions from the results of the work done, which, in our opinion, will define the place of these results in the existing system of opinions as regards the problem of interaction of gases with melts.

1. At theoretical study of the process of gas dissolution in liquid, the successive stages are usually distinguished (with rather conditional boundaries between them [32–35]), the role of which is analyzed, as a rule, by the information about the structural and chemical composition of the melt.

We share the point of view of researchers who represent the processes with gas participation, such as dissolution, adsorption, diffusion and chemical interaction, separately as different stages of one of common process ---- interaction with the formation of a new material. To make this idea more concrete, the unique representations have been developed in work [13] about the role of directivity of the atomic interaction in the formation of structure and properties of molecular and crystalline compounds.

The role of each of these stages in definite processes can be interpreted in a different manner, the same as the definition of a limiting link of a process of interaction with participation of gas phase components. It was noted earlier in works [27, 36] that the division of the single physical-chemical process (and we see the interaction of melts with gases as such a process) into constituent parts is rather pictorial and convenient for the qualitative interpretation of its principle, however, it can become an insuperable barrier in attempts to describe the final results of the process at the numerical level.

2. Radically important in the developed methodology of physical-chemical modeling of processes, proceeding in metal and ion salt melts in dissolution of gases in them is the refusal of postulation of charge state of any components of phases participating in these processes. All the parameters of atomic interaction, used in the above-described investigation, were calculated as variable values, depending on composition of the medium in which the interaction is proceeding. Due to this, the calculated values Z of interstitial atoms (Tables 3, 5, 7, 12 in work [37]) are differed greatly from those accepted in literature on this problem in interpretation of their charge state in accordance with ion model of a chemical bond and theory of valency.

This difference is the consequence of conceptually different approaches to the problem of description of the atomic interaction. The need of revision of existing representations in this field, except the results of this work, is shown in particular by the results of foreign researchers [38], according to which the charge Z^* for carbon, nitrogen and oxygen in different metal is equal to:

Metals	Impurities		
	C	N	O
Cd	–(3.7–1.4)	–(2.6–6.4)	–(3.2–1.2)
Hf	–(1.9–1.2)	–(2.7–1.9)	–(1.5–1.6)
V	+2.2	+1.7	+1.2
Nb	+5.6	+1.7	+1.0
Ta	+(4.0–2.6)	+3.4	+(1.9–0.5)
α-Fe	+(3.7–1.4)	+4.3	–

3. Results of carried out investigations showed that the use of the developed physical-chemical model of structure of melts allows realization of a general thesis at the numerical level: solubility of a gas, as any other impurity, depends on the chemical nature of a solvent and elements being dissolved. Any intermediate stages of the dissolution process are associated in a limiting way with the information about parameters of structural and chemical state of the reagents. To reveal and to describe this relation, it is suggested

to consider the interaction of atoms by the methodology developed to be common for any combination of components, independently of the medium in which this interaction is realized.

1. Galaktinova, N.A. (1967) *Hydrogen in metals*. Moscow: Metallurgiya.
2. Geld, P.V., Ryabov, R.A. (1974) *Hydrogen in metals and alloys*. Moscow: Metallurgiya.
3. (1981) *Hydrogen in metals*. Vol. 1, 2. Moscow: Mir.
4. Shapovalov, V.I. (1982) *Effect of hydrogen on structure and properties of iron–carbon alloys*. Moscow: Metallurgiya.
5. Prikhodko, E.V. (1995) Procedure of determination of parameters of directed atomic interaction in molecular and crystalline compounds. *Metallofizika i Nov. Tekhnologii*, 17(**11**), 54–62.
6. Prikhodko, E.V., Petrov, A.F. (1995) Role of directed atomic interaction in formation of microheterogeneous structure of metal melts. *Izvestiya Vuzov. Chyorn. Metallurgiya*, **12**, 5–12.
7. Prikhodko, E.V., Petrov, A.F. (1998) Physico-chemical criteria for evaluation of microheterogeneity degree of metal melts. *Metallofizika i Nov. Tekhnologii*, 20(**7**), 64–74.
8. Prihodko, E.V., Petrov, A.F. (2000) Physico-chemical criteria for description of the composition effect on salt melt structure and properties. *Functional Materials*, **1**, 108–113.
9. Prikhodko, E.V., Belkova, A.I. (1998) Physico-chemical criteria for evaluation of effect of structure microheterogeneity of oxide melts on their properties. *Teoriya i Praktika Metallurgii*, **3**, 25–28.
10. Kulikov, I.S. (1990) *Isotopes and properties of elements*. Refer. book. Moscow: Metallurgiya.
11. Prikhodko, E.V., Moroz, V.F., Kuksa, O.V. (2002) Procedure of modeling of atomic interaction in hydrogen-containing compounds and alloys. In: *Fundamental and applied problems of ferrous metallurgy*. Issue 5. Kiev: Naukova Dumka.
12. Ivanovsky, A.A., Medvedeva, N.I., Medvedeva, Yu.E. (1999) Primary-principle studies of stability and electron properties of metal borides. *Metallofizika i Nov. Tekhnologii*, 21(**12**), 19–33.
13. Prihodko, E.V., Moroz, V.F. (2000) The role of the atomic interaction directionality in formation of structures and properties of compounds. *Functional Materials*, 2(**4**), 867–892.
14. Kolachev, B.A., Shomin, R.E., Iliin, A.A. (1975) *Alloys-hydrogen accumulating*. Moscow: Metallurgiya.
15. Prikhodko, E.V. (1991) About interaction of thermodynamic properties of compounds with electron structure parameters. *Izvestiya Vuzov. Chyorn. Metallurgiya*, **2**, 1–4.
16. Kuksa, O.V., Prikhodko, E.V. (2000) Effect of atomic interaction in intermetallics on their sorption capacity with respect to hydrogen. *Dopovidi NANU*, **7**, 96–100.
17. Ban, Ya.Sh., Fuva, T. (1973) Solubility of hydrogen in iron-base alloys. In: *Physico-chemical principles of metallurgical processes*. Moscow: Nauka.
18. Kurochkin, K.T., Nizhelsky, P.E., Umrikhin, P.V. (1957) Effect of carbon on hydrogen solubility in liquid iron–carbon alloys. Izvestiya AN SSSR. *Otd. Tekhn. Nauk*, **2**, 19–26.
19. Yakushev, A.M., Yavojsky, V.I. (1962) Effect of vanadium on solubility of hydrogen in liquid iron. *Izvestiya Vuzov. Chyorn. Metallurgiya*, **1**, 52–56.
20. Morozov, A.N., Danilovich, Yu.A. (1968) About effect of pressure on hydrogen solubility in liquid alloys of iron with titanium. *Izvestiya AN SSSR. Metally*, **6**, 220–222.
21. Abramycheva, L.E., Kostina, T.K. (1975) Hydrogen solubility in liquid alloys of iron with cobalt and nickel. In: *Physico-chemical investigations of metallurgical processes*. Issue 3.
22. Kurochkin, K.T., Yavojsky, V.I., Geld, P.V. (1952) Solubility of hydrogen in liquid iron alloys. *Stal*, **1**, 7–13.
23. Geld, P.V., Petrushevsky, M.S. (1973) Effect of short range ordering on hydrogen solubility in liquid metal alloys. In: *Physico-chemical investigations of metallurgical processes*. Moscow: Nauka.
24. Petrushevsky, M.S., Geld, P.V., Baum, B.A. et al. (1971) Calculation of hydrogen solubility in liquid alloys of chrome, nickel and cobalt with silicium. *Izvestiya AN SSSR. Metally*, **5**, 28–33.
25. Prikhodko, E.V., Moroz, F.V. (2002) Physico-chemical criteria for information «convolution» about melt composition and metal compounds. In: *Fundamental studies of physics-chemistry of metal melts*. Moscow: Akademkniga.
26. Prikhodko, E.V. (1998) Physico-chemical model of process of metal deoxidation. Report 1. *Problemy Spets. Elektrometallurgii*, **2**, 52–62; Report 2. *Ibid*., **3**, 46–56.
27. Prikhodko, E.V. (1995) *Metal chemistry of multicomponent systems*. Moscow: Metallurgiya.
28. Kulikov, I.S. (1986) *Thermodynamics of oxides*. Moscow: Metallurgiya.
29. Kulikov, I.S. (1975) *Metal deoxidation*. Moscow: Metallurgiya.
30. Elliot, D.F., Gleyser, M., Ramakrishna, V. (1969) *Thermochemistry of steelmaking processes*. Moscow: Metallurgiya.
31. Balkovoj, Yu.A., Aleev, R.A., Bakanov, V.G. (1984) *Parameters of first-order interaction in iron-base melts*. Moscow: Chermetinformatsiya.
32. Esin, O.A., Geld, P.V. (1966) *Physical chemistry of pyrometallurgical processes*. Part II. Moscow: Metallurgiya.
33. Averin, V.V., Revyakin, A.V. (1976) *Nitrogen in metals*. Moscow: Metallurgiya.
34. Luzgin, V.P., Yavojsky, V.I. (1983) *Gases in steels and quality of metal*. Moscow: Metallurgiya.
35. Grigoryan, V.F., Belyanchikov, L.N., Stomakhin, A.Ya. (1982) *Theoretical principles of electrical steelmaking processes*. Moscow: Metallurgiya.
36. Prikhodko, E.V. (1995) *Efficiency of complex alloying of steels and alloys*. Kiev: Naukova Dumka.
37. Prikhodko, E.V., Moroz, V.F. (2004) About effect of interatomic interaction in melts on solubility of gases and carbon in them. Part 1: Methodology of investigation. Solubility of carbon and nitrogen. *Advances in Electrometallurgy*, **2**, 32–41.
38. Fromm, E., Gebhardt, E. (1980) *Gases and carbon in metals*. Moscow: Metallurgiya.

ABOUT FEASIBILITY OF PRODUCING GASARS USING METHODS OF ELECTROMETALLURGY

V.V. KARPOV
National Metallurgical Academy of Ukraine, Dnepropetrovsk, Ukraine

Experiments have been carried out that confirm the feasibility of use of electric arc melting for producing composite materials such as gas-reinforced refractory metals (gasars). Effect of process parameters on arc stability and formation of structure of gasars was determined.

Keywords: *electric arc remelting, gas-eutectic transformation, gasar, gas phase, hydrogen*

The gas-eutectic transformation was discovered and studied more than twenty years ago when studying the metal–hydrogen systems [1–3]. Its principle is based on the fact that if the metal melt is saturated preliminary with hydrogen up to gas-eutectic concentration, then the liquid at its crystallization is decomposed into crystalline and gaseous phases. Moreover, during crystallization the geometrically-ordered structures, similar to eutectic colonies can form, where one of the forming phases is gaseous (hydrogen). This results in a cast metal matrix penetrated with pores. Bubbles are growing simultaneously with metal crystals, not tearing away from the crystallization front, thus forming the honey-comb, similar to eutectic, structure. This structure of metal was called gasarite, and material was called a gasar (from «gas-reinforced metal»).

The technological process is based on the fact that a preset material (metal, ceramics) is melted in the hydrogen atmosphere at a definite pressure (saturation pressure P_s). With some lapse of time the melt is saturated with hydrogen until required concentration, then it is poured to a mould, arranged in an autoclave. The proper pressure (crystallization pressure P_{cr}) is set depending on the task what structure and porosity are to be obtained.

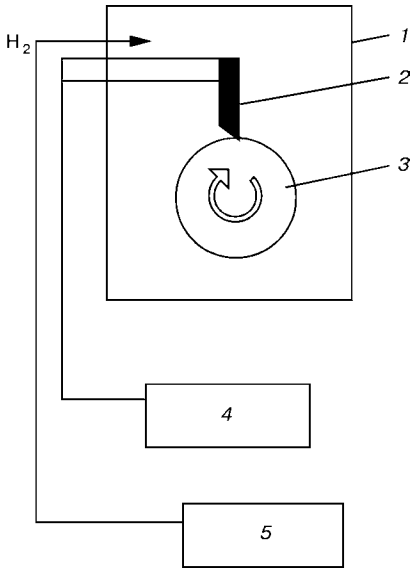

Figure 1. Scheme of experimental installation: *1* — autoclave; *2* — electrode; *3* — specimen; *4* — supply unit; *5* — system of gas phase control

Traditional methods of melting (gas heating, resistance furnaces, induction heating) of metals of a high melting temperature (chromium, molybdenum, tungsten and others) do not always give an opportunity to produce the sufficiently overheated melt for its saturation with hydrogen. This is explained by many reasons: from high chemical activity of metal to the absence of refractory metals capable to withstand the required temperature. The presence of the gaseous hydrogen in the furnace volume complicates greatly the problem of metal melting because of its quasi-high heat conductivity. At the same time a large number of metals form chemical compounds with it, namely hydrides, which differ radically from metals by the entire complex of physical-mechanical and chemical properties. All this narrows significantly the selection of methods of metallurgy for producing gasars from refractory metals and their alloys.

Analysis of existing methods shows that the most acceptable, in our opinion, is the method of electric arc remelting with a consumable electrode. When using the pure components (Me and hydrogen), the metal contamination is not occurred and the process is close to gas-eutectic. The main difference of this method from the traditional method is high rates of heating, melting and crystallization of metal. It was important to determine whether the metal will have a time to be saturated with hydrogen up to the necessary concentration for a short period. The estimations indicate the high degree of gas ionizing in electric arc, that makes the process of metal saturation with hydrogen sufficiently rapid. Difficulty may arise in a flexible control of hydrogen content in metal due to a very high rate and non-equilibrium of the process.

An experimental installation was designed and manufactured for experimental check-out of the above assumptions (Figure 1). A gaseous medium of hydrogen at up to 1 MPa pressure or vacuum up to 10^{-3} mm Hg

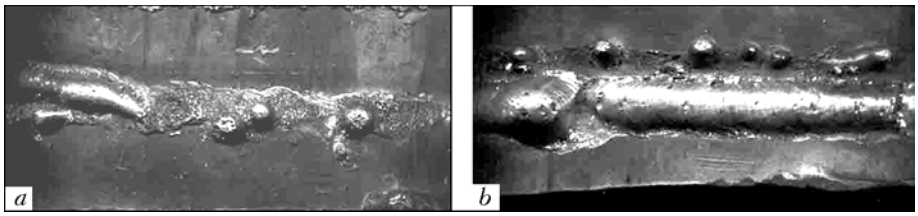

Figure 2. Appearance of specimen area melted by instable (*a*) and stable (*b*) arc in hydrogen medium

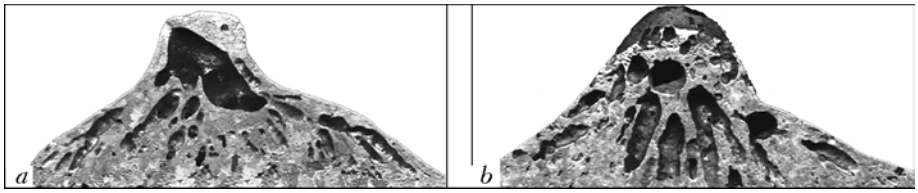

Figure 3. Microstructure of melting zone of copper specimen at a quick (*a*) and slow (*b*) rotation of billet

was created in a sealed autoclave using a system of the gas phase control. To simplify the scheme of experiment, tungsten was used as an electrode material.

The task of producing the gasar ingot was not put forward in the experiment. It was necessary to check the basic capabilities of this method. Specimen in the form of a disc was rotated inside the autoclave, and electrode from the specimen material was fed radially. Electric arc was ignited using an oscillator and supply unit and an area of metal was melted on the specimen surface.

It was established that in hydrogen introducing into the autoclave the stability of arc burning was abruptly deteriorated. However, it was possible to determine the hydrogen pressure, at which the arc was stable, and the hydrogen content, sufficient for the formation of the gasar structure.

Taking into account the low capacity of the experimental installation, we could not melt the large volume of metal and were limited by melting of an area on the surface of a monolithic specimen (Figure 2). It is seen in photos that instable arc burning leads of a break of melting regions (Figure 2, *a*). At high currents the melting of specimen is intensive and the arc is broken due to an increased gap between specimen and electrode. We have managed to obtain a stable arc and sufficiently uniform molten layer on the specimen surface (Figure 2, *b*).

Sections of specimen regions in the zone of arc burning show the feasibility of formation of structure of the gasar (Figure 3). The high rate crystallization due to specimen rotation has lead to the formation of large bubbles in the upper zone of the crystallizing metal. These bubbles almost disappeared at the reduction in rotation speed, that led to the higher heating of metal and reduction in crystallization rate. In our experiment, the slow rotation of the specimen led to molten metal flowing out from the specimen surface and to violation of the process stability. When the scanning movement of the arc was used on the surface of the flat specimen this drawback was not observed and we could produce a sufficiently uniform porous surface layer.

Analysis of obtained structures and experimental parameters show that even at low pressure of hydrogen it is possible to obtain the gasar structure owing to the ionizing action of arc and its high temperature. However, the high rates of process proceeding make it instable that is reflected on the structure of the gasar produced. Nevertheless, these experiments prove the feasibility of producing gasars from the metals of the highest refractoriness and require their continuation. It is more probable that this method will find practical application in case when necessary to produce a porous layer on the surface of billet or product.

These investigations resulted in confirmation of a fundamental feasibility of producing the gasar structure in melting metal using an electric arc. It was outlined that with growth of hydrogen pressure the stability the arc burning is abruptly decreased. Low hydrogen pressure and a short time of metal duration in a molten state are sufficient for its saturation with hydrogen up to the concentrations necessary for the gasar structure formation.

1. Shapovalov, V.I. (1985) Hydrogen as an alloying element. *MiTOM*, **8**, 13–17.
2. Shapovalov, V. *Method for manufacturing porous articles.* Pat. 5181549 USA. Publ. 1993.
3. Shapovalov, V. (2000) Formation of ordered gas-solid structures via gas eutectic reaction. In: *Proc. of Int. Conf.*, Dnepropetrovsk, Ukraine, June 12–14, 2000.

DEPENDENCE OF CONTACT ELECTRIC RESISTANCE OF THERMOANTHRACITE ON TEMPERATURE AND PRESSURE

V.I. LAKOMSKY and **V.A. LEBEDEV**
E.O. Paton Electric Welding Institute, NASU, Kiev, Ukraine

Constituents of contact electric resistance of thermoanthracite are studied. It is shown how great effect of adsorbed moisture can be exerted on contact resistance of a crushed thermoanthracite. Dependence of electric resistance of contact of thermoanthracite on pressure was obtained.

Keywords: *thermoanthracite, contact, surface and transition electric resistance, heating and pressure, electric contact properties*

The contact resistance R_c, which undergoes the electric current, passing from one piece of the thermoanthracite into another, is composed of two independent resistances such as surface R_s and transition resistance or, as it is called resistance of constriction, R_t. Let us describe these resistances in turn.

The surface resistance is occurred by the formation of very thin films of oxygen and moisture as a result of their adsorption on contact surfaces of thermoanthracite in air. Chemisorbed oxygen is retained at the thermoanthracite surface by powerful forces of a chemical bond between the oxygen atoms and surface atoms of carbon, while the moisture is retained by weak Van der Waals forces, moreover, the moisture film consists of several molecular layers of H_2O [1]. These films exert a great resistance to electric current, passing through the contact, at room temperature in particular.

It should be noted that the thermoanthracite in general is a good adsorbent. It was not without reason that it has found an application during recently at liqueur-vodka factories as an alternative to the widely-known adsorbent, such as a wood charcoal, for the high-quality treatment of water and ethyl alcohol [2].

As is known, the moisture, adsorbed on charcoal, can be removed largely by a low heating of the latter. In this case, the process of the moisture desorption will be developed intensively under the conditions of the atmospheric pressure even at 50–100 °C. By a slow heating the crushed anthracite, it is possible to remove almost all the physically-sorbed moisture. At a rapid heating up to 500–600 °C the part of moisture can react with coal, thus oxidizing it up to monoxide (CO) and carbonic acid gas (CO_2).

To evaluate the effect of adsorbed moisture on the contact resistance of thermoanthracite, we have performed the following experiments. The arbitrary selected small pieces of coal, close in sizes, were placed into a quartz tube so that they formed a single chain. At a vertical position of the tube the upper and lower pieces of coal of this chain contacted the copper electrodes whose edges were coated with a nickel layer to avoid copper oxidation at the experiment temperatures. The above-mentioned tube was mounted into a specially manufactured furnace.

Resistance of chain of coal grains was measured at different temperatures up to 150 °C and different pressure for all the chain of thermoanthracite grains. At a sufficient amount of coal grains the electric resistance of many intergranular contacts is so high that we neglected the thermoanthracite–nickel transition resistance and resistance of mass of grains.

Experiments showed (Figure) that even at heating up to 50 °C the contact resistance of the thermoanthracite was 1.86 times reduced as compared with resistance at room temperature, and at the next heating up to 150 °C, it goes without saying, it was 4.3 times reduced with holding in furnace for stabilizing the temperature field and low contact pressures P.

With increase in temperature, as is known [3], the specific electric resistance of the thermoanthracite is also decreased. In addition, at a total decrease of resistance of all the chain of thermoanthracite grains the share of a coal mass, as the calculations show, is negligible and equal to 1 % at 50 °C and 4 % at 150 °C.

In study the influence of the temperature factor on the contact resistance of the thermoanthracite, carried out in collaboration with German and Norwegian researchers [4], it was established that the value R_c of the thermoanthracite is reduced in a stable manner in

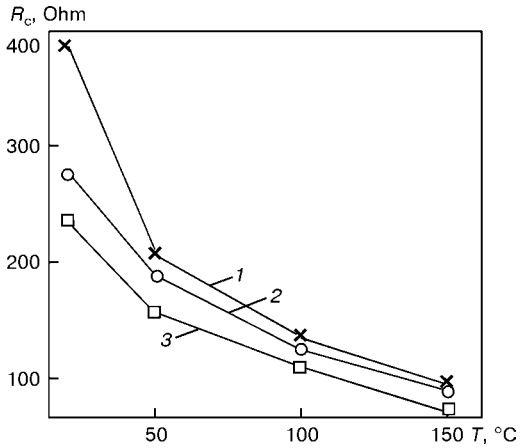

Dependence of contact resistance of thermoanthracite on temperature at P = 0.336 (*1*), 0.765 (*2*) and 1.195 (*3*) kg

heating of the latter, but only up to 950 °C. It should be supposed that the thermoanthracite surface during coal heating up to this temperature is cleaned completely not only from moisture, but also from oxygen.

The contact resistance of the thermoanthracite, caused by adsorbing films, is also decreased with increase in the force of pressing of two coal pieces. If to increase the contact pressure by 2.3 or 3.6 times, then R_c is decreased by 1.39 and 1.61 times, respectively, at room temperature. With increase in temperature up to 150 °C at the same change in pressing force the resistance is decreased, respectively, by 1.06 and 1.38 times (Figure). By comparing the effect of temperature and pressure on the contact resistance, it can be observed that the temperature effect prevails over the pressure effect.

These data confirm the assumption about the fact that the negligible increase in temperature and contact pressure leads to the increase in conductivity of the contact, because here the layers of physically-adsorbed moisture, having adhesion with the coal surface by weak Van der Waals forces, are destroyed. In this case even a low contact pressure is sufficient to change the contact resistance. If the moisture could be retained at the surface by chemisorption forces, then neither the slight heating of the coal, nor the increase in contact pressure up to thermoanthracite crushing could never lead to a significant change in the contact resistance.

The second constituent of the contact resistance is the transition resistance R_t. Unlike the surface resistance it is observed always even at a perfectly clean contact surface or at high temperatures when the surface resistance is too low or absent at all. R_t is stipulated by the existence of any solid body of microroughness on the contact surfaces. In these conditions the real contact surface of two grains of coal represents a sum of points of contact of this microroughness. When current is passing from one piece of thermoanthracite into another along these points of the real contact, the power lines of current have to be compressed in one coal piece up to current density 10^7 A / cm^2 and to be expanded in another piece consuming the certain energy, equivalent to R_t. The latter, according to R. Holm [5], is equal to $\rho_0 / 2a$, where ρ_0 is the internal specific resistance of the thermoanthracite; a is the radius of the given so-called a-spot, representing a sum of real sites (points) of current transition. According to a formal logic, the stronger pressing of two contacting solid bodies against each other, the larger their area of contact as a result of the solid body deformation. Theoretical and numerous experimental studies showed that, in general, the dependence of R_t on contact pressure is determined by formula $R_t = DP^{-n}$, where D and n are the coefficients depending on the type of a contact material; P is the contact pressure, kg. Our studies showed that for thermoanthracite $D = 251 \pm 6$, and $n = 0.36$. For comparison, the same coefficients for different contact materials were taken from work [6]. Thus, for example, in case of contact of aluminium with aluminium $D = 8.2 \cdot 10^{-4}$, $n = 0.7$, copper with copper $D = 2.4 \cdot 10^{-4}$, $n = 0.7$, for contacts of aluminium with copper $D = 3.0 \cdot 10^{-4}$, $n = 0.7$.

Generally speaking, the relation $R_c = f(P)$ is the characteristic of each pressing contact that indicates its quality. With the lower value D, the conductivity of the contact examined is higher, and with the higher value n the action of constriction force of elements of a pressed contact on its conductivity is more effective.

The comparison of parameters of electric contacts, given above, shows that thermoanthracite as a contact material, cannot be comparable with contacts of known tire materials. Electrical contact between the grains of thermoanthracite, whose surface was not subjected to mechanical treatment, is characterized as very poor. It is possible to improve this contact by increase in contact pressure only in rather limited ranges, as the thermoanthracite is very brittle material as compared with metals. Its strength in compression (from data of work [7]) is from 10 up to 20 MPa, and the microhardness, the more typical value for the contact phenomena, is 23.8–28.4 GPa. It is understandable that the material with these parameters of strength cannot be subjected to high forces at compression of a contacting pair to avoid its brittle fracture. Therefore, it should be recognized that the coal heating is the basic means of decrease in contact resistance of the thermoanthracite, as well as in its internal specific electric resistance [3].

Poor electric contacting properties of the thermoanthracite are used to the benefit of shaft furnaces for anthracite annealing, created more than a quarter of century ago. In these furnaces, the thermoanthracite serves as an active electric resistance and the coal charge is heated by the heat generated in the electric contacts of the thermoanthracite [8].

If in the light of statements about electric contact properties of thermoanthracite to consider the coal behavior in a shaft electric furnace-calcinator as regards to its contact resistance, then the conclusion can be made that the reduction in the latter should be expected on the furnace top, where the anthracite raw material is heated by hot top gases exhausting from the furnace. In this place of the furnace shaft during the anthracite heating not only the internal specific electric resistance of the coal is decreased, which, strictly speaking, is decreased very quickly by exponent, but also the contact resistance as a result of decrease in value R_s due to removal of the adsorbed moisture. When during the anthracite heating with hot gases of a dry coal distillation its R_s is decreased almost to zero, the R_c will be determined only by value R_t, and it will depend negligibly, as is seen from the above-said, on the contact pressure, and, consequently, will change negligibly with coal lowering in the direction from upper to the lower electrode of the furnace.

1. Esin, O.A., Geld, P.V. (1962) *Physical chemistry of pyrometallurgical processes*. Part 1. Sverdlovsk: Metallurgizdat.
2. Makhorin, K.E. (1998) Use of activated carbon in water treatment. *Khimiya i Tekhnologiya Vody*, XX(**1**), 53–57.
3. Bykovets, V.V., Lakomsky, V.I. (2003) Specific electric resistance of thermal anthracite. *Advances in Electrometallurgy*, **4**, 46–48.
4. Sorlie, M., Oye, H. (1998) *Cathodes in aluminium electrolysis.* Duesseldorf: Aluminium.
5. Holm, R. (1961) *Electric contacts.* Moscow: Inostr. Literatura.
6. Zajmovsky, A.S., Usov, V.V. (1949) *Metals and alloys in electrical engineering*. Moscow-Leningrad: Gosenergoizdat.
7. Fialkov, A.S. (1997) *Carbon, interlaminar bonds and composites on its base*. Moscow: Aspect Press.
8. Lakomsky, V.I., Bykovets, V.V. (2004) On problem of contact heating of thermoanthracite in electrical calcinator. *Tsvetnye Metally*, **1**, 52–54.

VOLT-AMPERE CHARACTERISTIC OF THERMOANTHRACITE CONTACTS

V.I. LAKOMSKY
E.O. Paton Electric Welding Institute, NASU, Kiev, Ukraine

Volt-ampere characteristics of contacts between grains of thermoanthracite under the conditions of pulsed and stationary electric supply of the latter were obtained for the first time. It is shown that VAC of thermoanthracite contacts in the isothermal conditions of measurements is straight-linear and passes through the origin of coordinates.

Keywords: *thermoanthracite, electric contact, electric heating, volt-ampere characteristic of contact, effect of pressure on contact resistance*

In electric shaft furnaces the loaded mass of coal for production of the thermoanthracite is firstly heated by a convective heat with gases of a dry coal distillation, exhausting from the furnace. During coal heating, its electric conductivity is growing exponentially. Then, when the electric conductivity of the coal reaches a definite value, and the coal layer lowers into the zone of action of electric current of the furnace, the coal grains will become the elements of electric circuit inside the furnace and electric current will pass along these elements from one electrode of the furnace into another.

Later on, the coal heating is realized by electric contact heating of those grains of the coal, which participate in the transfer of electric charges from one electrode of the furnace to another, and by heat transfer from the central zone of shaft, heated by electric current, to its periphery [1]. In other words, the high-temperature electric annealing of the anthracite in furnaces-calcinators is realized at the expense of Joule heat generated in electric contacts of the coal.

To analyze the processes of generation of heat energy in electric contacts of thermoanthracite–thermoanthracite, it is necessary to know the volt-ampere characteristics (VAC) of the mentioned contacts, except other contact characteristics and electric properties of the thermoanthracite itself [2–4].

Before definition of VAC contacts, let us evaluate the range of current and voltage in which the elementary thermoanthracite contacts in a coal shaft of industrial electric calcinator IET-10-UKhL-4 are operating. It spite of the fact that the evaluation will be rough, without allowance for non-uniformity of distribution of current density in a transverse section of electric calcinator shaft, it will give an opportunity to imagine the order of unknown values.

So, the above-mentioned calcinator is operating usually at 12–15 kA current in annealing of the «raw» anthracite. The voltage drop between furnace electrodes, locating at the 2 m distance from one another, does not exceed 60 V. The internal diameter of the calcinator shaft in lining is 1950 mm. Fractional composition of the coal charge is maintained at the level of 8–25 mm.

Now, after determining the mean arithmetic diameter of the coal charge grain and calculation of cross-section area of the furnace shaft, it is possible to find the statistic number of grains located in one layer of the mentioned section of the furnace. It is amounted to 10955 pieces. Assuming that each grain of the thermoanthracite has one spot contact with a neighboring grain in the direction of passing of electric current from electrode to electrode, it is possible, knowing the total current of the furnace, to evaluate the value of current falling at elementary contact. It amounts from $12000 / 10955 \approx 1.1$ up to $15000 / 10955 \approx 1.4$ A. To evaluate the electric voltage drop at each elementary contact we shall find in a similar way that the unknown value is ≈ 0.5 V.

Actually, as a result of non-uniform distribution of current density in cross-section of electric calcinator shaft the higher currents than calculated ones, will pass in the central zone of furnace through the elementary contacts of the thermoanthracite, while the lower current will pass in the periphery zones. The values of contact electric voltages will change by the same way. It is clear that with the higher mechanical action on the contact, exerted by the upper layers of the coal, the contact voltage will be lower and current will be higher.

Similarly, we shall find also that at the level of the lower end of the upper electrode of the furnace, each elementary contact between grains of the thermoanthracite in transfer of the electric energy is under the pressure of upper layers of coal ≈ 135 g, and at the level of the upper end of the lower electrode ---- 680 g.

Thus, the electrical range, within which the VAC of thermoanthracite contacts should be studied, will lie, evidently, in the range from tens of fractions up to several volts, while the current will be in the ranges from several to half-tens of amperes.

As was managed by us to establish in analyzing the available literature, VAC of contacts between the grains of thermoanthracite was not, unfortunately, studied earlier. Only one work of scientists from Sha-

khty Branch of Novo-Cherkassk Polytechnic Institute [5] is known, where VAC of anthracite itself as material was studied. The same investigations [6] studied the VAC of electric contact anthracite–nickel (we emphasize that of anthracite but not thermoanthracite). They established that under the isothermal conditions at a pulsed supply of the anthracite sample the VAC of anthracite has a linear nature to avoid the contact heating during its testing. If to perform the test under the conditions of a continuous condition of electric supply, when the current passing leads to the anthracite heating, its VAC with a current growth is distorted into the side of the current axis. Authors of works [5, 6] noted that the voltage drop at the contacts anthracite–metal leads to a significant change in electric voltage on the samples examined. Unfortunately, these works have no even one word about VAC of the thermoanthracite and its contacts. Nevertheless, these works are useful, because they allow us to state a priory that at much higher currents under the isothermal conditions of investigations the thermoanthracite contacts have straight-linear VAC, as the electric conductivity of the thermoanthracite is by several orders higher that that of raw materials from which it is produced.

In the present work the VAC was obtained in a simple equipment, whose scheme is presented in Figure 1. On 5 mm thick sheet of insulating material of 250 × 200 mm size, embedded into a rigid metallic frame, two copper rods *1* (upper) and *7* (lower) were fastened, where the lower rod was rigidly fixed to the sheet, while the upper rod was moved in a packing gland *2* in a vertical axis. Both copper rods had a blind hole in a head part, into which one grain of thermoanthracite was glued in by a carbon paste MUP. Grain *4* of a conical shape was glued into the upper rod, and a flat grain *6* was glued into the lower rod. After gluing, the rod with a grain of thermoanthracite was subjected to a low-temperature coking. Electric resistance of copper rod–thermoanthracite grain transition resulted in the fact that it was lower than 1 Ohm. Voltage drop on contacts between the theroanthracite grains was measured using the spring-loaded potentiometric probes *5* and *8*.

Equipment was operating as follows: electric load from special current source *10* was supplied on a closed contact between samples of thermoanthracite. Changes in values of voltage and current on a contact examined were recorded by instruments *3* and *9*, respectively, where the indications of voltage drop on thermoanthracite grains entered computer through the analog-digital converter for processing. At the same equipment the VAC of contact at different mechanical loads, changed by mass *P*, was determined.

Even the first experiments showed that, as also in the case of a monolithic anthracite [5], the VAC of a single thermoanthracite contact at a pulsed condition of current supply to the contact represents a straight line passing through the origin of the Cartesian coordinates. Typical VAC of thermoanthracite contact at mechanical load 110 g and at room temperature is shown in Figure 2. In this case the resistance of «as-assembled» contact is 1.16 Ohm. With increase in mechanical load the appearance of VAC, as was expected, is not changed, and the contact resistance is decreased. Thus, at 540 g pressure and the same temperature the resistance was reduced down to 0.46 Ohm (Figure 3). If to remove the increased mechanical load and to return to the previous load (110 g) then the value of a contact resistance is almost retained, which was observed under the conditions of 540 g. This is well seen in Figure 4. Here the calculated contact resistance is 0.44 Ohm.

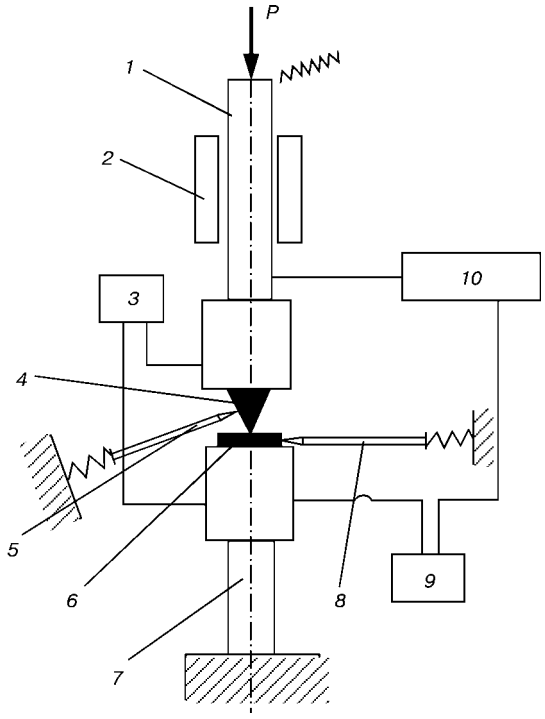

Figure 1. Scheme of equipment for determination of VAC of electric contacts (see designations in the text)

Analysis of presented Figures shows that, firstly, when testing such brittle material as thermoanthracite the phenomenon of hysterisis R_{con} is eliminated completely and, secondly, the increased load on contact of thermoanthracite particles compacts the contact surfaces, that is proved by much better reproducibility of separate measurements made after the preliminary loading (compare Figures 2 and 4).

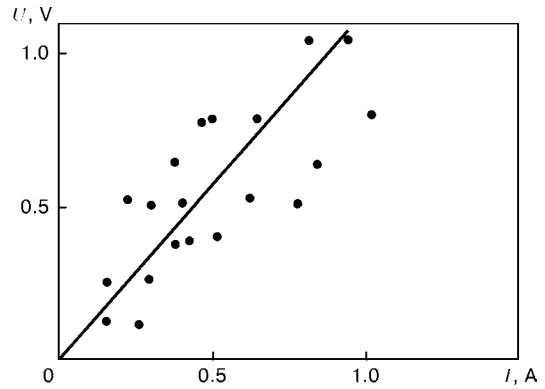

Figure 2. Typical VAC of thermoanthracite contact at room temperature and 110 g load

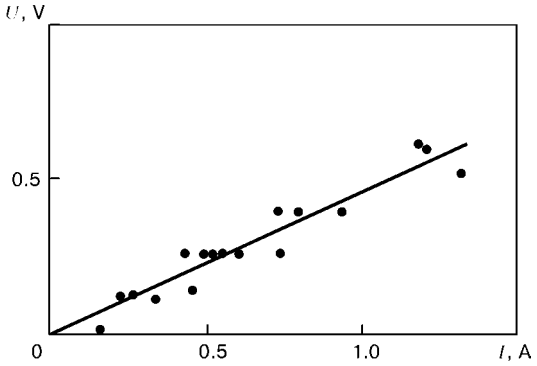

Figure 3. VAC of thermoanthracite contact at room temperature and 540 g load

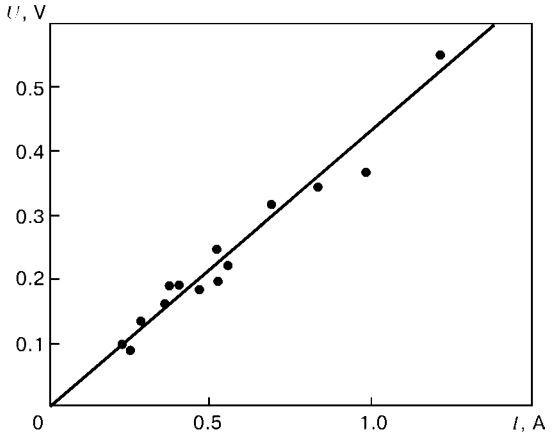

Figure 4. VAC of thermoanthracite contact at 110 g load after preliminary 540 g load

The observed phenomena, in our opinion, is useful for the practice of electric heating of a crushed thermoanthracite before preparation of mixture of charge of hearth units of aluminium electrolysers. It is sufficient to pack a layer of a crushed thermoanthracite in electric preheater at a force to make the coal layer more compact and, more important, to make its heating with electric current more uniform across the thickness of the layer.

At static condition of contact supply, its VAC is distorted into the side of current axis. Distortion of VAC is due, as is known, to the Joule heating of a contact material near *a*-spot of contact [4], therefore, the degree of distortion is defined by the temperature relationship of the specific electric resistance. As the resistance of the thermoanthracite depends on temperature linearly [5], then the considered VAC is distorted less intensively than VAC of anthracite for which the same relationship has an exponential nature.

Let us consider now in general the VAC of electric contacts of those materials which possess positive and negative temperature coefficient of specific resistance β. Hypothetic behavior of different VAC is presented in Figure 5. Here, position *1* indicates VAC of the contact at a pulsed condition of its supply when, for a short period of time of current passing through the contact, the material of the latter has no time to be heated. It is clear, that in this case the VAC will be presented by a straight line passing through the origin of coordinates. If the electric supply of the contact is

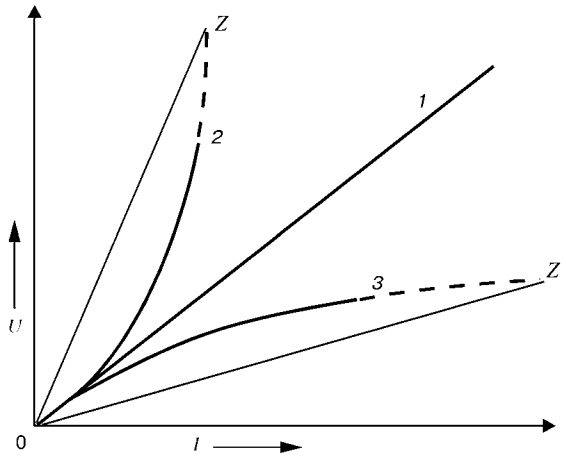

Figure 5. VAC of electric contact of conductors at pulsed (*1*) and static conditions of supply with a negative (*2*) and positive (*3*) temperature coefficient of specific resistance β

realized in a static condition that is more often observed in practice, then with a rise in current the VAC of contact will distort: for contact material with a positive value β (this refers to metals and, in principle, to all the metal alloys) ---- to the side of axes of stresses (position *2*), and for the material, possessing the negative β (this refers to thermoanthracite) ---- to the side of axes of currents (position *3*).

As the thermoanthracite is characterized by the negative value of the temperature coefficient of the specific electric resistance $-(3–4)\cdot10^{-4}$ T^{-1} [3], then with a growth of current in heating the contact material its contact resistance will decrease and, consequently, voltage drop at the contact will be lower. The higher current, passing through the contact, the higher temperature of heating the contact material and lower the voltage drop. As the electric power dissipated on the contact depends on I^2, the growth in temperature of contact material will be obligatory ahead the growth of current passing through the contact. It is evident, that it cannot be long even under conditions of the controllable reduction atmosphere. The increase in temperature for the metallic contacts leads, finally, to the fusion of contact surfaces and contact failure. The moment of degradation should appear for the thermoanthracite contact, in spite of a rather high temperature of the coal melting. Probably, this is associated with carbon sublimation. In Figure 5 the failure of contact is shown by a thin straight vanishing line.

1. Lakomsky, V.I., Bykovets, V.V. (2004) On problem of contact heating of thermoanthracite in electrical calcinator. *Tsvetnye Metally*, **1**, 52–54.
2. Lakomsky, V.I. (2003) Mathematical model of calculation of specific electrical resistance of grained thermoanthracite depending on its fractional composition. *Advances in Electrometallurgy*, **3**, 44–47.
3. Bykovets, V.V., Lakomsky, V.I. (2003) Specific electric resistance of thermal anthracite. *Ibid.*, **4**, 46–48.
4. Bykovets, V.V., Lakomsky, V.I., Kirilenko, V.P. (2004) Specific electric resistance of lumpy thermoanthracite in thin layer. *Ibid.*, **1**, 44–45.
5. Okorochkov, A.I., Pavlinov, A.B., Posylny, V.Ya. (1980) On nonlinearity of volt-ampere characteristics of anthracites. *Khimiya Tvyord. Topliva*, **3**, 52–54.
6. Okorochkov, A.I., Pavlinov, A.B., Posylny, V.Ya. (1983) Properties of metal–anthracite contacts at in high density of current. *Ibid.*, **4**, 103–105.

INDEX OF ARTICLES FOR AEM'2004, Nos.1–4

LIST OF AUTHORS